NASA CR 134922
ASRL TR 154-11

EXPERIMENTAL TRANSIENT AND PERMANENT DEFORMATION STUDIES OF STEEL-SPHERE-IMPACTED OR IMPULSIVELY-LOADED ALUMINUM BEAMS WITH CLAMPED ENDS

Emmett A. Witmer
Fred Merlis
Robert L. Spilker

Aeroelastic and Structures Research Laboratory
Department of Aeronautics and Astronautics
Massachusetts Institute of Technology
Cambridge, Massachusetts 02139

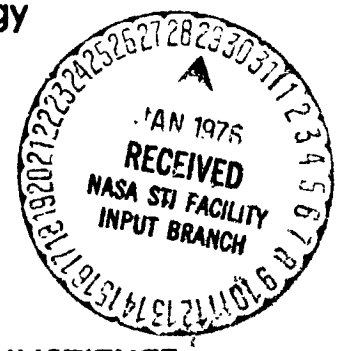

October 1975

Prepared for
AEROSPACE SAFETY RESEARCH AND DATA INSTITUTE
LEWIS RESEARCH CENTER
NATIONAL AERONAUTICS AND SPACE ADMINISTRATION
CLEVELAND, OHIO 44135

NASA Grant NGR 22-009-339

1 Report No. NASA CR-134922	2. Government Accession No.	3. Recipient's Catalog No.
4 Title and Subtitle Experimental Transient and Permanent Deformation Studies of Steel-Sphere-Impacted or Impulsively-Loaded Aluminum Beams with Clamped End-		5. Report Date October 1975 6 Performing Organization Code
7 Author(s) Emmett A. Witmer Fred Merlis Robert L. Spilker		8. Performing Organization Report No. ASRL TR 154-11 10. Work Unit No
9 Performing Organization Name and Address Aeroelastic and Structures Research Laboratory Department of Aeronautics and Astronautics Massachusetts Institute of Technology Cambridge, Massachusetts 02139		11. Contract or Grant No NGR 22-009-339
12. Sponsoring Agency Name and Address National Aeronautics and Space Administration Washington, D.C. 20546		13. Type of Report and Period Covered Contractor Report 14. Sponsoring Agency Code

15. Supplementary Notes

Technical Monitors: Solomon Weiss and Robert D. Siewert
Aerospace Safety Research and Data Institute
NASA Lewis Research Center

16. Abstract

The sheet explosive loading technique (SELT) has been employed to obtain elastic-plastic, large-deflection transient and/or permanent strain data or simple well-defined structural specimens and materials: initially-flat 6061-T651 aluminum beams with both ends ideally clamped via integral construction. The SELT loading technique was chosen since it is both convenient and provides "forcing function information" of small uncertainty. These data will be useful for evaluating pertinent structural response prediction methods.

A second objective of the present study was to obtain high-quality transient-strain data for a well-defined structural/material model subjected to impact by a "rigid body" of known mass, impact velocity, and geometry; large-deflection, elastic-plastic transient response conditions are of primary interest. Accordingly, the aforementioned beam with both ends clamped and a steel sphere as the impacting body were chosen. The steel sphere was launched vertically by explosive propulsion to achieve various desired impact velocities. The sphere/beam impact tests conducted resulted in producing a wide range of structural responses and permanent deformations, including rupture of the beam from excessive structural response in two cases. The transient and permanent strain data as well as the permanent deflection data obtained are of high quality and should be quite useful for checking and evaluating methods for predicting the responses of simple 2-d structures to fragment (sphere) impact. Unfortunately, however, transient strain data very close to the point of impact were not obtained over as long a time as desirable because the gage(s) in that region became detached during the transient response. Alternate schemes to obtain such data would be worth exploring.

Both of these types of experimental structural response data will be valuable for checking structural response prediction methods. In particular, the present impact-induced structural response data will be employed to evaluate the adequacy and accuracy of methods developed to predict the responses of protective structures subjected to impact by aircraft engine rotor fragments.

17. Key Words (Suggested by Author(s))		18. Distribution Statement
Structural Response Experiments Impact Loading Impulsive Loading Elastic-Plastic Behavior Large Deflections Transient Strain Data	Permanent Deformations Structural Failure Aircraft Hazards Aircraft Safety	Unclassified, Unlimited

19. Security Classif. (of this report)	20. Security Classif. (of this page)	21. No. of Pages	22. Price*
Unclassified	Unclassified	110	

* For sale by the National Technical Information Service, Springfield, Virginia 22151

NASA-C-168 (Rev. 6-71)

FOREWORD

This research was carried cut by the Aeroelastic and Structures Research Laboratory, Department of Aeronautics and Astronautics, Massachusetts Institute of Technology, Cambridge, Massachusetts under NASA Grant No. NGR 22-009-339 from the Lewis Research Center, National Aeronautics and Space Administration, Cleveland, Ohio 44135, as a part of the NASA Rotor Burst Protection Program. Mr. Solomon Weiss and Mr. Robert D. Siewert of NASA-LeRC served as technical monitors. The valuable advice and cooperation from these individuals is acknowledged gratefully.

The authors are indebted to Earle Wassmouth, Thomas R. Stagliano, and José J.A. Rodal of the MIT-ASRL for much assistance in model and test-fixture preparation and in data reduction and analysis. Also Joseph Marksteiner of the MIT Aerophysics Laboratory machined some of the test specimens, and still others were machined by the Whitman Tool and Die Co., Whitman, Massachusetts.

The use of SI units (NASA Policy Directive NPD 2220.4, September 14, 1970) was waived for the present document in accordance with provisions of paragraph 5d of that Directive by the authority of the Director of the Lewis Research Center.

CONTENTS

LIST OF ILLUSTRATIONS

LIST OF ILLUSTRATIONS (Continued)

LIST OF ILLUSTRATIONS (Concluded)

LIST OF TABLES

SUMMARY

The sheet explosive loading technique (SELT) has been employed to obtain elastic-plastic, large-deflection transient and/or permanent strain data on simple well-defined structural specimens and materials: initially-flat 6061-T651 aluminum beams with both ends ideally clamped via integral construction. The SELT loading technique was chosen since it is both convenient and provides "forcing function information" of small uncertainty. These data will be useful for evaluating pertinent structural response prediction methods.

A second objective of the present study was to obtain high-quality transient-strain data for a well-defined structural/material model subjected to impact by a "rigid body" of known mass, impact velocity, and geometry; large-deflection, elastic-plastic transient response conditions are of primary interest. Accordingly, the aforementioned beam with both ends clamped and a steel sphere as the impacting body were chosen. The steel sphere was launched vertically by explosive propulsion to achieve various desired impact velocities. The sphere/beam impact tests conducted resulted in producing a wide range of structural responses and permanent deformations, including rupture of the beam from excessive structural response in two cases. The transient and permanent strain data as well as the permanent deflection data obtained are of high quality and should be quite useful for checking and evaluating methods for predicting the responses of simple 2-d structures to fragment (sphere) impact. Unfortunately, however, transient strain data very close to the point of impact were not obtained over as long a time as desirable because the gage(s) in that region became detached during the transient response. Alternate schemes to obtain such data would be worth exploring.

Both of these types of experimental structural response data will be valuable for checking structural response prediction methods. In particular, the present impact-induced structural response data will be employed to evaluate the adequacy and accuracy of methods developed to predict the responses of protective structures subjected to impact by aircraft engine rotor fragments.

SECTION 1

INTRODUCTION

In order to determine whether or not methods for predicting the large-deflection elastic-plastic transient responses of structures provide reliable and accurate predictions, it is essential that they be evaluated by carrying out detailed comparisons of predictions against pertinent well-defined experimental data. It is for this purpose that the present experiments have been performed.

In particular experimental data are sought to provide detailed transient strain data on simple structures which undergo principally planar deformations when subjected to low-velocity impact of a well-defined fragment. Accordingly, 6061-T651 aluminum beam models with both ends "ideally clamped" were prepared and were subjected to steel-sphere impact near the midspan location on the lower surface of the beam. Nominally on each specimen, 16 high-elongation strain gages were affixed at various spanwise stations along the upper and the lower surface of each specimen; usually transient strain records were recorded for 8 of these gages, and permanent strain was recorded for all surviving gages. Since measurements were made also to define the location and the instant of initial impact of the steel sphere against the beam specimen, the resulting transient strain data have high resolution in both space and common time. It is intended, therefore, that these data will be used to make a critical evaluation of computer codes which are designed to predict the large-deflection elastic-plastic transient responses of simple structures subjected to aircraft engine rotor fragment impact; the development and verification of prediction methods of this type constitute an important part of the NASA Rotor Burst Protection Program. Typically these codes (see Refs. 1 and 2, for example) include an approximate impact-interaction model whose adequacy has not been definitively evaluated. By employing the present transient strain data to compare with predictions, it is intended to assess whether or not the approximate impact-interaction model being used is adequate and, if not, to gain indications of aspects requiring improvement so that appropriate modifications and improvements can be carried out.

A second theoretical-analysis aspect requiring further study and appropriate evaluative experimental data, is the adequacy, accuracy, and efficiency

of the finite-element structural-response analysis itself -- quite apart from the impact-interaction model questions noted previously. Assumed-displacement finite-element models for straight beams and curved rings have been developed [3, for example]* and are utilized in the computer codes described in Refs. 1, 2, and 4. These elements employ 4 degrees of freedom (DOF) per node and have been shown [3,5] to provide reasonably accurate predictions of transient deflections and strains; however, these lower-order elements exhibit bending-strain discontinuity but membrane-strain continuity at their nodes. Continuity in both contributions to the strain throughout the element would represent an improvement which can be achieved readily by utilizing higher-order elements. It is expected that these higher-order elements with 5, 6, 7, or 8 DOF per node will exhibit greater efficiency in the sense that for the same total number of DOF for the entire structure, more accurate strain predictions should be provided. Some well-defined transient-strain data for large-deflection elastic-plastic planar structural response conditions will be valuable for assessing these elements. Accordingly, 6061-T651 beam specimens were prepared, instrumented with strain gages, and subjected to impulsive loading over a short spanwise portion centered at the midspan station by the sheet-explosive loading technique (SELT). This technique provides an accurately-known impulse applied to the structure and hence a well-defined initial-condition problem is established; this type of problem is very convenient for use in testing finite-element analysis adequacy and accuracy for application to large-deflection, elastic-plastic transient response problems.

Section 2 is devoted to describing the test specimens, instrumentation, test procedure, and results for the impulsively-loaded beams. Section 3 contains a similar description for the beams subjected to steel sphere impact. Summary observations are given in Section 4. Finally, supplementary data on beam specimen stress-strain properties and on strain gage installation details are given in appendices.

---

*Numbers in square brackets [ ] indicate references which are listed in the text immediately after Section 4.

SECTION 2

SHEET HE LOADING AND RESPONSE TESTS OF 6061-T651 ALUMINUM BEAMS WITH CLAMPED ENDS

2.1 Objectives

Sought were both transient response and permanent deformation experimental data of high quality for use in evaluating the reliability and accuracy of methods for predicting the large-deflection elastic-plastic transient and permanent deformations of a well-defined structure, including the following desired structural, material property, forcing function, and deformation features:

(1) Structural Features: The structure shall be an initially-straight beam with ideally-clamped ends.

(2) Material Properties: The material shall exhibit well-defined mechanical properties -- initially-isotropic, very little strain hardening, and with little to moderate strain rate sensitivity.

(3) Forcing Function: The externally-applied forces which produce the structural response shall be well-defined and repeatable with minimum uncertainty.

(4) Deformation Features: Large structural deformations with strains ranging to moderate levels shall be included.

To meet these objectives, an initially-flat beam model of 6061-T651 aluminum with clamped ends and impulse loading provided by the sheet explosive loading technique were chosen. In view of the instrumentation available at the MIT Aeroelastic and Structures Research Laboratory, it was decided to attempt to make measurements of transient strains, permanent strains, and permanent deformations.

In the following subsections of Section 2, discussed are: (a) the beam models and mounts, (b) the experimental arrangement and procedure, and (c) the experimental results obtained.

2.2 Beam Models and Mounts

To circumvent the difficulties that experimenters have had repeatedly in trying to achieve an ideally-clamped edge of a structure by utilizing a variety

of clamping arrangements (massive serrated clamps, hardened faces, massive bolts, etc.) most of which unfortunately revealed post-test evidence of slippage, an "integral-edge arrangement" was tried in the present test program. This consisted, as shown in Fig. 1, of integrally machining the beam specimen (of nominal 8-in span, 1.5-in width, and 0.100-in thickness) from a solid bar (1.55 by 3.60 by 13.0-in) of 6061-T651 aluminum. Although the "integral support collar" provided a reasonably rigid restraint to simulate ideally-clamped ends, this collar was securely bolted to a heavy flat-ground steel channel support structure with 1/2"-13 Holo-Krome socket head shoulder screws with nuts torqued to a uniform 651 inch-pounds, producing an axial load of about 38,000 pounds per bolt. Note in Fig. 1 that to reduce the hazard of undesired or "premature" cracking at the boundary because of stress concentrations at a sharp re-entrant corner, all "inside corners" were machined to a radius of about 0.125 in, which is somewhat larger than the nominal beam thickness.

Four specimens ("clamped beam models" CB-1, CB-2, CB-3, and CB-4) were prepared and subjected to impulse loading. The dimensions of these specimens are given in Table 1. Post-fabrication measurements of beam thickness h were made at 0.5 in intervals along the span along lines defined by y = -0.5, 0, and 0.5 in (see Fig. 2); beam width was also measured at 0.5 in intervals along the span. It was found that these dimensions were uniform: at the values shown with a standard deviation within 0.5 per cent for thickness, and within about $\pm$ 0.001 in for width. The top and bottom faces of the "support collar" portion of the specimens were flat and parallel to within $\pm$ 0.0005 inch.

2.3 Experimental Arrangement and Procedure

2.3.1 Test Procedure

Shown in Fig 3 is a schematic of the test arrangement. The beam specimen bolted to the heavy steel support channel has a portion of its lower surface midspan region covered with a 0.25-in thick by 2-in wide by 2.30-in spanwise layer of polyester-type polyurethane foam[+] weighing 3 lb/ft^3; this

[+] Attached with du Pont 4684 cement; the HE sheet was similarly attached to the buffer.

"buffer" material (provided to prevent stress-wave-induced spall fracture of the beam by sheet HE detonation) is overlaid by a uniform-thickness layer of du Pont Detasheet D (sometimes called EL 506D) covering the entire beam width, having a spanwise length of 1.80 in centered at midspan, and weighting 1.45 gm/cc. The Detasheet leader, nominally 43-in long, 0.25-in wide, and 0.016-in thick is attached to the main HE beam-patch by a 0.25-in by 0.25-in by 0.016-in thick "end region" centered at the midwidth-midspan point; the Detasheet leader is detonated by firing a Hercules No. 6 detonator. The detonation then proceeds along the leader and initiates the detonation of the HE patch on the beam specimen. A detonation wave then proceeds radially from this "initiation point", resulting in progressive detonation of the HE beam patch; since according to the manufacturer [6] the detonation front travels at 7200 meters/sec (283,464 in/sec), the entire HE-covered region becomes loaded almost simultaneously (within about 3.5 microseconds of simultaneity).

Beam specimen CB-1 and CB-2 were loaded impulsively by the detonation of an HE layer of nominal 0.015-in thickness; two such layers were used for model CB-3; and model CB-4 employed a 0.025-in thick layer composed of the superposition of 0.015 and 0.010-in thick layers obtained from large sheets of Detasheet D from the same HE batch but with nominal thicknesses of 0.010 and 0.015 in. To improve the intimacy of contact between layers, these two-layer HE sheets were placed on "separator paper" and upon firm cardboard, and a pattern of thin-needle punctures was applied to effect some "mechanical knitting". Since the Detasheet is supplied in sizes 10-in wide by a 20-in long in various "uniform" thicknesses, sheets of nominal 0.010 and 0.015-in thickness were measured to determine the thickness distribution over the entire sheet. Only uniform-thickness regions were employed in constructing each loading patch for each beam specimen.

The resulting HE weight per square inch for each beam specimen is given in Table 2. Shown also in Table 2 is the "initial velocity" imparted impulsively to the HE-covered portion of each beam specimen, where the specific impulse from calibration tests [7] is taken to be 18.1×10^4 dyne-sec/gm of HE or 0.407 lb-sec/gm of HE, and a beam material weight of 0.098 lb/in^3 is used.

2.3.2 Strain Measurements

In an effort to measure transient strains, type EP-08-031DE-120 high elongation annealed constantan foil-type polyimide-backed strain gages* were oriented spanwise and were attached at various spanwise locations along the midwidth station y=0 on the upper and the lower surface, as listed in Table 3. These gages were attached with Micro-Measurements AE-15 cement and cured at 175°F for 120 minutes as advised by the manufacturer; according to the manufacturer, this system should permit one to measure strains (relative elongations) reliably up to about 10 per cent. One-foot long varnish-covered copper leads, type AWG 36, were attached to each transient-strain gage, fed via a shielded cable to a standard Wheatstone bridge, and the strain signal was recorded on a dual-beam Tektronix oscilloscope. As indicated in Fig. 3, the scope sweeps were triggered by passage of the detonation front at a station along the HE leader 15 inches from the HE beam-load patch; hence, impulse loading to the beam is initiated about 53 microseconds after this instant (also the instant of scope sweep initiation). Each scope trace was set to sweep at a known rate; thus, all transient strains are correlatable to a common time. These strain traces were recorded on Polaroid type 47 film with a Tektronix 196A scope camera.

In addition to measuring transient strain (on nominally, 8 gages on each beam specimen), 8 additional gages were used to obtain only permanent strain. Permanent strain data were obtained on all surviving gages. Summarized in Table 3 are the strain gage locations, the gages used for transient strain measurements, and the permanent strain indicated on all surviving strain gages.

2.3.3 Deflection Measurements

Since appropriate photographic or other equipment for measuring or recording transient deformations of structures is not available at the MIT-ASRL, only pre-test and post-test configuration measurements have been obtained for these specimens. Since each beam model had its upper and lower

*Manufactured by Micro-Measurements Corp. 38905 Chase Road, Romulus, Michigan 48174.

"collar support" surfaces machined flat and parallel, each specimen was clamped securely to the moveable carriage of a Model H Milwaukee universal milling machine. The vertical location of the surface of each beam specimen was determined as the specimen was traversed by a station monitored by an Ames dial-gage indicator with 0.001-inch divisions readable to the nearest 0.0002 inch. This arrangement is shown in Fig. 4. These vertical locations z_ℓ (see Fig. 2 and Table 4) were measured along lines y = -0.5, 0, and 0.5 in from x = -4.50 to +4.50 in.

2.4 Test Results

The beam specimens identified in Table 1 as CB-1, CB-2, CB-3, and CB-4 were tested by impulsive loading in this sequence. The test arrangement used is indicated schematically in Fig. 3. The weight per unit area of explosive covering each specimen and the attendant impulsively-imparted (initial) velocity are shown in Table 2; essentially identical buffers were used in all cases. The "initial velocity" values are based upon a specific impulse for this Detasheet D batch and HE/buffer system of 0.407 lb-sec/gm (=18.1×10^4 dyne-sec/gm of HE); this impulse calibration procedure and information are given in Ref. 7.

Specimens CB-1 and CB-2 were loaded such that their initial velocities were of the order of 6500 in/sec; this resulted in a moderate degree of permanent deflection, the midspan permanent deflection being about 0.59 in (compared with an initial beam thickness of 0.102 in). Specimen CB-3 was tested next by doubling the impulse loading; this was too severe and resulted in shear failure at each "clamped end" of the specimen. Model CB-4 was then subjected to an impulse level about 50 per cent greater than applied to models CB-1 and CB-2; this resulted in a large degree of permanent deformation, the midspan permanent deflection being about 0.97 in.

Post-test photographs of these four models are shown in Fig. 5.

2.4.1 Deformed Beam Data

Table 4 lists the post-test lower-surface vertical location z_ℓ data measured along y = -0.5, 0, and +0.5 in for x = -4.50 to +4.50 in for specimens CB-1, CB-2, and CB-4. Note that the pre-test dimensions of these specimens are given in Table 1; the nominal beam dimensions are: span = 8 in,

width = 1.5 in, and thickness 0.102 in. Since Model CB-3 sheared off at both ends, no "permanent deformation" data are included for this specimen.

Models CB-1 and CB-2 were subjected to essentially the same impulse loading, and exhibit very nearly the same permanent deformation z_ℓ vs x for fixed y. These measurements indicate that the beam deflections are nearly planar, but one can detect the existence of a small amount of "twist" and some anticlastic deformation. On these specimens there is no indication of stress-wave-induced spalling in the HE-covered region or of cracking or shear deformation at the two clamped ends of each model. It appears that the integral-edge arrangement does provide a very good simulation of ideally-clamped ends.

Model CB-4 has undergone considerably greater permanent deformation than specimens CB-1 and CB-2 but the general character of its deformation is similar: far from the impulsively-loaded region, the deflection appears to be nearly planar; however, near the region of applied impulse, there is evidence of a small amount of twist and a slight amount of anticlastic deformation. At both clamped ends, one can see on the lower surface about an eighth-inch spanwise region extending entirely across the width of the beam in which very severe plastic deformation and some necking has occurred. Shear fracture, however, appears not to have commenced, although shear deformation is clearly evident in these cited eighth-inch spanwise regions.

2.4.2 Transient and Permanent Strain Data

The locations of each of the strain gages for which transient strain measurements were attempted are denoted by an asterisk (*) in Table 3. Transient strain traces (some very good throughout, some good for a part of the time span, and others of questionable value) were obtained for the following models and gages, and are shown in the indicated figures:

Model	Gages	Figure
CB-1	1 2 3 4 5 8 11 13	6
CB-2	1 2 3 4 5 8 11 13	7
CB-3	2 4 7 8	8
CB-4	2 3 4 5 7 8 11 13	9

For each of these strain traces, the sweep speed (time scale) and the

as-read or nominal relative elongation E_x in per cent are given on each figure. For sufficiently large "strain" values, a nonlinear correction must be applied to obtain the "corrected relative elongation"; Fig. 10 is a graph relating the nominal relative elongation E_x to the corrected relative elongation E_{xc} for both tension and compression. The relation betweeen these quantitites is given by [8]:

$$E_{xc} = \frac{\Delta R}{R(GF \pm E_x)} \equiv \frac{GF\ E_x}{GF \pm E_x} \qquad (2.1)$$

where

ΔR = change of resistance of the strain gage because of its elongating

R = original strain gage resistance (nominally 120 ohms $\pm$ 0.2%)

GF = gage factor of the strain gage (2.06 $\pm$ 1%)

E_x = strain reading on the oscilloscope picture based on a linear scale used for calibration convenience during a test; plus (+) denotes tension and minus (-) indicates compression; units of in/in

It is emphasized that the strain traces shown in Figs. 6-9 represent the nominal relative elongation E_x with the linear scale indicated. If desired, one can convert these nominal (uncorrected) values E_x to corrected relative elongations E_{xc} by using Fig. 10 which represents Eq. 2.1, or Eq. 2.1 itself.

Note that, in general, two strain traces appear on each photograph. Identified for each trace are the strain gage number, the pre-test zero strain position, and the "instant" of HE beam-patch detonation (which may be interpreted as zero time at which the specimen is subjected to a uniform initial velocity over the HE-covered region). Unless noted explicitly to the contrary, both traces have the same sweep speed (in microseconds per division).

Certain strain traces appear to be valid throughout the recorded time history, while others vanish after a short time (probably because of broken lead wires), and still others drop rapidly to essentially zero strain after apparently behaving in a plausible fashion for an initial period. In this latter case, it is likely that the strain gage became detached from the specimen (hence a drop in indicated strain) after a short time; in all cases,

post-test observations confirmed that such a gage had become detached from the beam specimen.

The strain traces for models CB-1, CB-2, and CB-4 should be useful to the analyst throughout the recorded time period since all of these models survived in the sense of exhibiting substantial permanent deformation but no fracture of the beam specimen. Since model CB-3 sheared off at both ends at an unknown time during the response, one must interpret its strain traces with care; some early portion of each trace will apply to an "intact" specimen.

SECTION 3

BEAMS SUBJECTED TO STEEL SPHERE IMPACT

3.1 Objective

In this part of the investigation, high-quality transient-strain data are sought for a well-defined structural specimen undergoing principally planar (2-d) large elastic-plastic deformation when impacted by an essentially non-deformable body of well-defined geometry, known mass, and known impact velocity. These data are intended to be used to evaluate prediction methods such as those of Refs. 1 and 2. especially the adequacy of the approximate impact-interaction portion of the analysis employed in Refs. 1 and 2. Accordingly, simple initially-straight beams of 6061-T651 aluminum with both ends ideally clamped were chosen, each to be impacted by a steel sphere of one-inch diameter.

In the following subsections of Section 3, discussed are: (a) the beam models and mounts, (b) the experimental arrangement and procedure, (c) the experimental results obtained, and (d) the sphere velocity calibration procedure.

3.2 Beam Models and Mounts

The 6061-T651 aluminum beam models employed were essentially the same as those described in Subsection 2.2. The specimens subjected to steel-sphere impact are identified as clamped-beam models CB-8 through CB-18 in Table 1; the dimensions of these models are given in Table 1 and were determined as described in Subsection 2.2.

In most cases the beam specimen's "support collar" was bolted directly to a flat-ground heavy steel support channel; in other cases, steel spacer blocks were inserted between the support channel and the beam model for additional clearance between the deformed beam specimen and the support channel. These mounting arrangements are shown in Fig. 11.

3.3 Experimental Arrangement and Procedure

A schematic of the test arrangement is shown in Fig. 12. The steel sphere is launched vertically by "explosive propulsion" and is intended to impact the beam specimen at its midspan/midwidth position. At sphere/beam impact, an "impact switch" provides an electrical signal which starts the sweeps of the

oscilloscopes employed to measure transient strain at various spanwise locations on the midwidth line on the upper and the lower surface. This impact switch consists of heavy-duty aluminum foil separated from the aluminum beam by a polyurethane foam pad insulator (2.5-in spanwise by 1.5-in wide by 0.5-in thick) of 6 lb/ft^3 density with a 0.5-in diameter hole (in the pad) at the location of intended impact. The sphere causes the aluminum foil to contact the aluminum-beam specimen at the "instant of impact", thereby closing a circuit and causing an electrical signal which initiates the sweeping of the oscilloscopes.

In order to produce beam responses ranging from moderate to very large permanent deformation (including specimen rupture), various steel-sphere velocities were used in testing specimens CB-8 through CB-18; these values and the associated results are described in Subsection 3.4.

In an effort to measure transient strains, type EP-08-031DE-120 high elongation annealed constantan foil-type polyimide-backed strain gages were oriented spanwise and were attached at various spanwise locations along the midwidth station (y=0; see Fig. 2) on the upper and the lower surface, as listed in Table 5. These gages were attached with Micro-Measurements AE-15 cement and cured at $175^{\circ}F$ for 120 minutes as advised by the manufacturer; according to the manufacturer, this system should permit one to measure strains (relative elongations) reliably up to about 10 per cent. One-foot long varnish-covered copper leads, type AWG36, were attached to each transient-strain gage, fed via shielded cable to a standard Wheatstone bridge, and the strain signal was recorded on a dual-beam Tektronix oscilloscope. As noted earlier, each scope sweep was initiated at the "instant of initial impact" by an electrical signal generated upon "closing of the impact switch". Each scope trace was set to sweep at a known rate; thus, all transient strains are correlatable to a common time. These strain traces were recorded on Polaroid type 47 film with a Tektronix 196A scope camera. In addition to measuring transient strain (attempted on 8 gages on each beam specimen), 8 additional gages were used to obtain permanent strain data. Permanent strain data were obtained on all surviving gages. Summarized in Table 5 are the strain gage locations, the gages used for transient strain measurements, and the permanent strain data on all surviving strain gages.

It should be noted that a circuit was designed so that upon closing of the "impact switch" a short-duration pulse would be applied to each transient strain channel as a "marker pulse" as indicated in Fig. 12. This design was tested and modified so that this impact pulse would have a duration of about 3 microseconds or less; in some cases this pulse persists up to 8 microseconds, depending on the response of the oscilloscope. Accordingly, only about the initial 8 microseconds or less of each transient strain pulse represents a "false strain reading"; thereafter, it is believed that valid transient strain data were obtained until effects such as lead wire breakage, gage detachment, etc. occur.

Post-test configuration measurements were made on typical models in this test series by mounting the specimen on a milling machine and employing a dial gage arrangement (see Fig. 4) to determine the vertical location z_ℓ of the lower surface along lines y = -0.5, 0, and +0.5 in, from x = -4.50 to +4.50 in (see Fig. 2); this procedure was the same as described in Subsection 2.3.3.

3.4 Beam Response Results

3.4.1 Deflection Data

The beam specimens identified in Table 1 as CB-8 through CB-18 were tested under steel-sphere impact in this sequence. Models CB-8 through CB-13 were mounted as indicated in Fig. 11a, while models CB-14 through CB-18 were mounted on spacer blocks as shown in Fig. 11b in order to provide more room for the beam model to deflect before being in danger of contacting the steel support channel. Also, to improve the prospects of sphere impact occurring at the midspan/midwidth position of the beam model, each test specimen was mounted about 11-5/8 in vertically above the to-be-launched sphere. This short distance of travel from sphere launch to sphere/beam impact was reasonably successful in producing impact near the desired point. Summarized in Table 7 are: (a) the observed x,y coordinates (see Fig. 2) of the point of initial impact, (b) the impact velocity and (c) the weight of explosive used to launch the sphere. The listed impact velocity was determined from velocity-calibration tests as described in Subsection 3.5.

Post-test photographs of the impacted beam specimens are shown in the figures listed below in groupings with the same nominal sphere impact velocity;

concisely indicated also are the observed effects on the specimens:

Specimen	Figure	Nominal Impact Velocity (in/sec)	Comments
CB-8, -9, -10, -11	13	1900	Small permanent deformation
CB-12, -13	14	2500	Moderate permanent deformation
CB-14	15	3075	Well beyond threshold rupture
CB-15, -16	16	2870	Near threshold rupture One ruptured; other intact
CB-17, -18	17	2800	Large permanent deformation

As indicated in Table 7 and in the above tabulation, models CB-8 through CB-11 were subjected to steel sphere impact at a nominal velocity of 1900 in/sec; this resulted in small permanent deformation of each specimen -- with a midspan permanent deflection of about 0.38 in. The second group (specimens CB-12 and CB-13) were subjected to a higher sphere impact velocity ($\tilde{}$ 2500 in/sec) which produced moderate permanent deflections -- about 0.63 in near midspan. Next, in an effort to produce substantially larger deformation, specimen CB-14 was impacted at 3075 in/sec which turned out to be well beyond the threshold rupture condition. Hence, models CB-15 and CB-16 were subjected to lower-velocity impact ($\tilde{}$ 2870 in/sec); this turned out to be very close to the threshold rupture condition. Specimen CB-15 experienced impact about 0.15 in from its midwidth line (y=0) and underwent large bending-stretching deformations with pronounced twisting and distinct necking widthwise at the impact station but did not rupture. The next specimen, CB-16, impacted under essentially the same conditions but with impact occurring at y=.035 in (much closer to the midwidth y=0 line), resulted in large bending-stretching deformations with almost no twisting, but shear-type rupture occurred across the entire width of the beam and was accompanied by considerable necking. The final set of models, CB-17 and CB-18, was tested at a slightly smaller impact

velocity 2800 in/sec in an attempt to obtain very large transient and permanent deformations and strains but to avoid rupture. These tests were successful.

An examination of the intact but permanently-deformed specimens revealed that in the case of impact near the midwidth line (y=0), the beam specimens exhibited nearly planar deformation (that is, essentially the same z-direction displacements occur over the entire width of the beam) except near the impact point itself. At and near the impact point, a three-dimensional deformation state (bulge) exists; the photographs of the post-test specimen in Figs. 13-17 show this situation reasonably clearly. Representative permanent deflection data from each of the three nominal impact velocity groups 1900, 2500, and 2800 in/sec are given in Table 6 for models CB-9, CB-13, and CB-18, respectively. Shown for each of these models is the vertical location z_ℓ of the impacted surface along lines y = -0.5, 0, and +0.5 in for x = -4.50 to +4.50 in. By comparing these Table 6 deflection values with the Table 7 data indicating the point of initial impact, one can note readily the bulge that occurs at and surrounding the impact location.

3.4.2 Transient and Permanent Strain Data

For sphere-impacted specimens CB-8 through CB-18, attempts were made to measure transient and permanent strains at various locations on the upper and the lower (impacted) surface as indicated in Table 5.

Permanent strain data for all surviving strain gages are given in Table 5; in all cases, these strains are the corrected relative elongations E_{xc} as determined from Eq. 2.1. It is seen that at the locations sensed, these permanent strains ranged from a fraction of a per cent to more than 4 per cent. Much larger strains clearly occurred near the impact point but midwidth-midspan gage 1 which was intended to provide some data in that vicinity became detached in every case despite diligent gage installation and protective measures. However, it is believed that the permanent strain data obtained will be of value to the analyst.

Of greater interest are the transient strain data. The gages for which transient strain measurements were attempted are denoted by an asterisk (*) in Table 5; transient strain data were obtained successfully on all specimens except CB-8. Although transient strain data for the three nominal

impact velocity groups CB-8 through CB-11 (1900 in/sec), CB-12 and CB-13 (2500 in/sec), and CB-17 and CB-18 (2800 in/sec) will be of primary interest since these specimens were permanently deformed but not ruptured, transient strain data are also included in this report for the more severely impacted specimens CB-14, CB-15, and CB-16; it is believed that the latter data will also be of value to the analyst.

Transient strain traces (some very good throughout, some good for a part of the time span, and others of questionable value) were obtained for the following models and gages, and are shown on the indicated figures:

Specimen	Nominal Impact Velocity (in/sec)	Gages	Figure
CB-9	1900	1,2,3,5,7,8,9,12	18
CB-10		2,3,8,9,	19
CB-11		1,2,5,7,8,12	20
CB-12	2500	1,2,3,5,7,8,9,12	21
CB-13		1,2,3,5,7,8,9,12	22
CB-14	3075	3,4,5,6,7,9,10,12	23
CB-15	2870	3,4,5,6,7,9,10,12	24
CB-16		3,4,5,6,7,10,12	25
CB-17	2800	3,4,5,6,7,9,10,12	26
CB-18		3,4,5,9,10,12	27

For each of these strain traces, the sweep speed (time scale) and the as-read or nominal relative elongation E_x in per cent with linear scales are given on each figure. If desired, one can convert these nominal (uncorrected) values E_x to corrected relative elongations E_{xc} by using Eq. 2.1 or Fig. 10 which represents Eq. 2.1.

Note that, in general, two strain traces appear on each photograph. Identified for each strain trace are the strain gage number, the pre-test zero strain position, and the "instant of impact". Unless noted explicitly to the contrary, both traces have the same sweep speed (in microseconds per division).

Certain strain traces appear to be valid throughout the recorded time history, while others vanish after a short time (probably because of broken lead wires), and still others drop rapidly to essentially zero strain after apparently behaving in a plausible fashion for an initial period. In the latter case, it is likely that the strain gage became detached from the specimen after a short time, thus resulting in a drop in indicated strain; in all cases, post-test observations confirmed that such a gage had become detached from the beam specimen.

The strain traces for models CB-9, -10, -11, -12, -13, -15, -17, and -18 should be useful to the analyst throughout the recorded time period (except for the previously cited types of "defective" traces) since all of these models survived in the sense of exhibiting substantial permanent deformation but no fracture. Since specimens CB-14 and CB-16 ruptured at an unknown time during the response, one must interpret these strain traces with care; some early portion of each trace will apply to an "intact" specimen.

3.5 Sphere Velocity Calibration Procedure and Results

As noted earlier, the steel sphere was launched vertically, for convenience, by an explosive technique shown schematically in Fig. 28, parts a and b. The one-inch diameter steel sphere rested in a beveled hole of a steel support plate as depicted in Fig. 28b. Cemented to the sphere is a 3/4-in diameter by 1-in long cylinder of 6 pcf polyurethane foam buffer material; cemented on the other end of this buffer-material cylinder is a 3/4-in diameter stack of 0.025-in thick Detasheet D layers sufficient to provide a selected total weight of explosive. A Detasheet leader is attached to this HE stack and is led to a No. 6 Hercules electric detonator. As Fig. 28b shows, a steel "confinement barrel" is used to confine the high-pressure gas produced following HE stack detonation from unhindered expansion and hence, to subject the sphere to a longer duration of "high pressure propulsion" than would otherwise be achieved; this increases the "propulsion efficiency". The foam buffer is employed to protect the steel sphere against stress-wave-induced fracturing following HE stack detonation (a high-pressure, short-duration event).

The objective is to launch an intact (undamaged) steel sphere with a selected velocity. In order to determine the velocity achieved by the sphere

for a given weight of the HE stack, a series of launchings was carried out under carefully-controlled conditions, and sphere position versus time measurements were made with a Fastax camera as indicated in Fig. 28a. In this procedure, an event-initiation switch was closed; this sent a signal (a) to start the camera and (b) to a delay timer which sent out a signal to fire the detonator after the Fastax camera had achieved "full speed". The sphere subsequently was launched vertically, passed through slit-mylar sheets which cover "portholes" in the two smoke (control) shields located about 14 and 21 inches above the launch table, and then proceeded vertically into the (now smoke-free) field of view of the Fastax camera; the center of this field of view was about 30 in above the launch base. Near its flight path in the view of the camera, a vertical steel scale with 0.5-inch graduations was positioned. Since 1000 cps timing marks from an accurate time-mark generator were applied to the edge of the Fastax film, one can then determine position versus time information for each sphere photographed.

In carrying out these sphere-velocity-measurement tests, care was exercised to insure that the HE (Detasheet) used was from the same lot or batch as that used to launch the spheres for specimens CB-8 through CB-18. Summarized in Table 8 are the pertinent data for a series of velocity calibration tests in three groups of nominal HE stack weight: 2.3, 3.2, and 4.2 grams. Included are the run identification numbers, buffer weight, HE stack weight, post-test sphere weight, sphere velocity V, and the associated kinetic energy and momentum. Tabulated also for each is the ratio of the imparted momentum* mV to the weight of the HE stack employed; note that this ratio clearly depends on the launch configuration employed and the geometry (at the pressure-loaded region) of the launched body, and would be very different if a cylindrical rod rather than a sphere were launched.

It should be noted that position vs. time data for each sphere was obtained over about an 8 to 12-in distance centered about 30 inches above the launch platform. For specimens CB-8 through CB-18, however, the beam specimen was located about 11-5/8 in above the pre-launched sphere. Hence, in applying the Table 8 data to deduce the appropriate sphere velocities for specimens

*The mass of the sphere is denoted by m.

CB-8 through CB-18, one should in principle, make a "gravity" and "drag" correction. However, as the gravity and drag correction studies in Section 5 of Ref. 9 show, the drag correction for a circular flat plate is quite small and for a sphere would be even smaller (negligible) because of its smaller drag coefficient; the gravity correction is even smaller. Thus, the Table 8 data are used herein without any drag or gravity correction. Accordingly, a plot of the Table 8 data for mV vs W_{HW} was employed to determine V for specimens CB-8 through CB-18 as listed in Table 7 since the mass of the sphere used in each of these tests is known.

SECTION 4

SUMMARY AND COMMENTS

The sheet explosive loading technique (SELT) has been employed to obtain elastic-plastic, large-deflection transient and/or permanent strain data on simple well-defined structural specimens and materials: initially-flat 6061-T651 aluminum beams with both ends ideally clamped via integral construction. The SELT loading technique was chosen since it is both convenient and provides "forcing function information" of small uncertainty. These data will be useful for evaluating pertinent structural response prediction methods.

A second objective of the present study was to obtain high-quality transient-strain data for a well-defined structural/material model subjected to impact by a "rigid body" of known mass, impact velocity, and geometry; large-deflection, elastic-plastic transient response conditions are of primary interest. Accordingly, the aforementioned beam with both ends clamped and a steel sphere as the impacting body were chosen. The steel sphere was launched vertically by explosive propulsion to achieve various desired impact velocities. The sphere/beam impact tests conducted resulted in producing a wide range of structural responses and permanent deformations, including rupture of the beam from excessive structural response in two cases. The transient and permanent strain data as well as the permanent deflection data obtained are of high quality and should be quite useful for checking and evaluating methods for predicting the responses of simple 2-d structures to fragment (sphere) impact. Unfortunately, however, transient strain data very close to the point of impact were not obtained over as long a time as desirable because the gage(s) in that region became detached during the transient response. Alternate schemes to obtain such data would be worth exploring.

Both of these types of experimental structural response data will be valuable for checking structural response prediction methods. In particular, the present impact-induced structural response data will be employed to evaluate the adequacy and accuracy of methods developed to predict the responses of protective structures subjected to impact by aircraft engine rotor fragments.

REFERENCES

1. Stagliano, T.R., Spilker, R.L., and Witmer, E.A., "User's Guide to Computer Program CIVM-JET 4B to Calculate the Transient Structural Responses of Partial and/or Complete Structural Rings to Engine-Rotor Fragment Impact", ASRL TR 154-9, Aeroelastic and Structures Research Laboratory, Massachusetts Institute of Technology, September 1975. (Available as NASA CR-134907).

2. Wu, Richard, W-H, Spilker, R.L., Stagliano, T.R., and Witmer, E.A., "User's Guide to Computer Programs JET 5A and CIVM-JET 5B to Calculate the Large Elastic-Plastic Dynamically-Induced Deformations of Multilayer Partial and/or Complete Structural Rings", ASRL TR 154-10, Aeroelastic and Structures Research Laboratory, Massachusetts Institute of Technology, December 1975. (Available as NASA CR-

3. Wu, Richard, W-H and Witmer, E.A., "Finite Element Analysis of Large Transient and Elastic-Plastic Deformations of Simple Structures, with Application to the Engine Rotor Fragment Containment/Deflection Problem", ASRL TR 154-4, Aeroelastic and Structures Research Laboratory, Massachusetts Institute of Technology, January 1972. (Available as NASA CR-120886).

4. Wu, Richard W-H and Witmer, E.A., "Computer Program - JET 3 - To Calculate the Large Elastic-Plastic Dynamically-Induced Deformations of Free and Restrained, Partial and/or Complete Structural Rings", ASRL TR 154-7, Aeroelastic and Structures Research Laboratory, Massachusetts Institute of Technology, August 1972. (Available as NASA CR-120993).

5. Wu, Richard, W-H and Witmer, E.A., "Finite Element Predictions of Transient Elastic-Plastic Large Deflections of Stiffened and/or Unstiffened Rings and Cylindrical Shells", ASRL TR 171-4, Aeroelastic and Structures Research Laboratory, Massachusetts Institute of Technology, April 1974. (Available as AMMRC CTR 74-31).

6. Anon., "Du Pont Detasheet Flexible Explosive", E.I. du Pont de Nemours & Co., Inc., Wilmington, Delaware, 1971.

7. Witmer, E.A., Wu, R. W-H, and Merlis, F., "Experimental Transient and Permanent Deformation Studies of Impulsively-Loaded Rings and Cylindrical Panels, both Stiffened and Unstiffened", ASRL TR 171-3, Aeroelastic and Structures Research Laboratory, Massachusetts Institute of Technology, April 1974. (Available as AMMRC CTR 74-29).

8. Murray, W.M. "Fundamental Concepts for Strain Gages", Department of Mechanical Engineering, Massachusetts Institue of Technology, 1973.

9. Witmer, E.A., Merlis, F., and Pirotin, S.D., "Experimental Studies of Explosively-Induced Large Deformations of Flat Circular 2024-0 Aluminum Plates with Clamped Edges and of Free Thin Cylindrical 6061-T6 Shells", ASRL TR 152-5, Aeroelastic and Structures Research Laboratory, Massachusetts Institute of Technology, January 1974. (Available as BRL CR 134).

10. Private communication 4-20-73 from J.F. Raudenbush, Senior Applications Engineer, Micro-Measurements, Inc., Romulus, Michigan; also, M-M Technical Note 137.

TABLE 1

PRE-TEST DIMENSIONS OF THE 6061-T651 BEAM SPECIMENS

Spec. No.	Beam Region (in)			Support "Collar" (in)				
	h	w	L	h_1	h_2	w_1	w_2	L_c
CB-1	.102	1.493	8.006	1.501	1.501	3.500	.948	1.997
CB-2	.102	1.509	8.011	1.474	1.474	3.499	.946	1.994
CB-3	.102	1.501	8.006	1.475	1.475	3.499	.946	1.998
CB-4	.102	1.497	8.005	1.476	1.476	3.499	.948	1.998
CB-8	.100	1.508	8.004	1.501	.752	2.469	.435	2.491
CB-9	.101	1.482	8.001	1.501	.752	2.469	.434	2.494
CB-10	.101	1.488	8.000	1.502	.753	2.469	.434	2.491
CB-11	.099	1.506	8.000	1.501	1.005	2.469	.435	2.493
CB-12	.101	1.492	8.000	1.502	1.004	2.468	.434	2.490
CB-13	.100	1.501	8.002	1.502	1.004	2.468	.436	2.490
CB-14	.099	1.506	8.002	1.501	1.004	2.468	.434	2.490
CB-15	.098	1.506	8.017	1.501	1.501	2.522	.456	2.480
CB-16	.098	1.495	8.002	1.500	1.500	2.535	.467	2.490
CB-17	.097	1.497	8.005	1.502	1.502	2.537	.468	2.488
CB-18	.097	1.498	8.002	1.501	1.501	2.535	.466	2.490

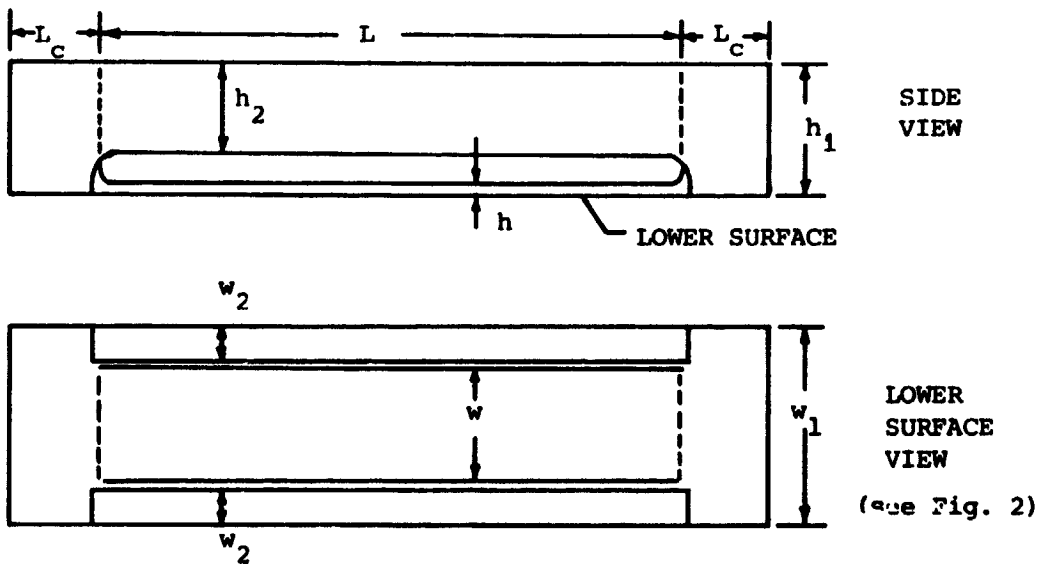

TABLE 2

SHEET HE WEIGHT PER UNIT AREA AND INITIAL LATERAL VELOCITY IMPARTED TO EACH 6061-T651 IMPULSIVELY-LOADED BEAM

Specimen	CB-1	CB-2	CB-3	CB-4
HE Sheet Weight per Unit Area (gm/in^2)	.4235	.4164	.8424	.6736
Initial Velocity* (in/sec)	6,657	6,546	13,243	10,589

*Based upon a specific impulse of 0.407 lb-sec/gm = 18.1×10^4 dyne-sec/gm and 6061-T651 aluminum material weight of 0.098 lb/in^3.

TABLE 3

STRAIN GAGE LOCATION AND PERMANENT STRAIN

DATA FOR IMPULSIVELY-LOADED BEAMS

Strain Gage Identif. Number	Location		Permanent Strain[a] (per cent)			
	x(in)	Surface (Upper(U) or Lower (L))	Model CB-1	Model CB-2	Model CB-3	Model CB-4
1	0	U	*[b]	--*	--	--
2	+1.40	U	0.51*	0.55*	--*	--*
3	+2.20	U	0.77*	0.87*	--*	--*
4	+3.00	U	1.35*	1.39*	--*	--*
5	+3.80	U	0.16*	0.02*	2.83*	1.78*
6	-1.40	U	0.59	0.57	3.22	2.55
7	-2.20	U	0.75	1.07	4.72*	--*
8	-3.00	U	1.67*	1.68*	--*	--*
9	-3.80	U	1.22	0.02	1.41	2.36
10	+1.40	L	1.30	1.07	4.65	--
11	+2.20	L	1.36*	1.12*	--*	--*
12	+3.00	L	0.02	0.14	1.76	0.89
13	+3.80	L	0.02*	0.47*	--*	1.27*
14	2.20	L	1.32	1.29	4.81	--
15	-3.00	L	0.35	0.24	--	1.57
16	-3.80	L	0.18	0.28	--	1.15

a: This permanent strain is actually the relative elongation E_1 defined by $E_1 = \sqrt{1+2\gamma_{11}} - 1$ where γ_{11} is the extensional strain tensor component in the spanwise direction; all values listed are tension (+).

b: A dash (-) indicates that the strain gage was found to be detached after the test.

*: Denotes that transient strain measurements were attempted.

TABLE 4

POST-TEST VERTICAL LOCATION OF THE LOWER SURFACES OF THE IMPULSIVELY-LOADED BEAMS

Spanwise Location x(in)	Vertical Location, z_ℓ (in)								
	Model CB-1			Model CB-2			Model CB-4		
	Along y=-0.5	Along y=0 in	Along y=0.5	Along y=-0.5	Along y=0 in	Along y=0.5	Along y=-0.5	Along y=0 in	Along y=0.5
-4.50	0	0	0	0	0	0	0	0	0
-4.20	-.001	-.0005	0	0	0	0	0	0	0
-4.10	-.001	-.001	0	0	0	0	0	0	.001
-4.00	.002	.003	.004	.003	.003	.003	.012	.016	.012
-3.90	.014	.014	.015	.015	.014	.014	.048	.048	.048
-3.80	.033	.034	.035	.033	.033	.030	.100	.096	.099
-3.60	.081	.082	.083	.081	.081	.078	.210	.209	.210
-3.40	.125	.128	.128	.128	.126	.123	.307	.305	.306
-3.00	.205	.208	.211	.208	.204	.199	.460	.459	.459
-2.50	.273	.276	.281	.276	.271	.264	.595	.594	.593
-2.00	.324	.330	.335	.327	.321	.311	.706	.705	.698
-1.50	.397	.404	.411	.402	.394	.381	.808	.803	.795
-1.25	.438	.445	.453	.445	.437	.424	.847	.845	.834
-1.00	.479	.487	.496	.489	.480	.466	.883	.882	.866
-0.80	.509	.518	.527	.523	.513	.498	.908	.910	.891
-0.60	.536	.546	.555	.554	.544	.528	.930	.936	.913
-0.40	.557	.567	.575	.577	.567	.550	.947	.955	.928
-0.20	.570	.581	.588	.592	.581	.565	.958	.967	.938
0	.575	.585	.592	.598	.588	.572	.962	.971	.941

TABLE 4 CONCLUDED

Spanwise Location x(in)	Vertical Location, z_ℓ (in)								
	Model CB-1			Model CB-2			Model CB-4		
	Along y=-0.5	Along y=0 in	Along y=0.5	Along y=-0.5	Along y=0 in	Along y=0.5	Along y=-0.5	Along y=0 in	Along y=0.5
0.20	.568	.579	.584	.593	.582	.567	.957	.966	.936
0.40	.552	.563	.567	.578	.568	.553	.946	.954	.926
0.60	.529	.539	.544	.556	.548	.533	.930	.934	.911
0.80	.498	.506	.512	.527	.518	.505	.906	.906	.889
1.00	.465	.472	.478	.495	.487	.474	.882	.880	.865
1.25	.421	.428	.432	.453	.445	.434	.849	.844	.833
1.50	.377	.385	.390	.411	.405	.394	.808	.803	.794
2.00	.308	.314	.317	.338	.334	.325	.705	.702	.693
2.50	.262	.264	.269	.284	.280	.275	.595	.592	.586
3.00	.196	.198	.201	.209	.207	.205	.455	.449	.447
3.40	.119	.120	.122	.125	.125	.123	.295	.289	.288
3.60	.075	.074	.076	.078	.077	.077	.195	.188	.188
3.80	.027	.027	.028	.028	.030	.030	.080	.076	.076
3.90	.011	.012	.012	.012	.012	.012	.040	.037	.037
4.00	.002	.001	.002	.001	.001	.002	.005	.005	.004
4.10	-.001	-.001	0	-.001	-.001	-.001	-.001	-.002	-.001
4.20	0	-.001	0	-.001	-.001	-.001	-.001	-.002	-.001
4.50	0	-.001	0	0	0	0	0	-.002	-.001

TABLE 5

STRAIN GAGE LOCATIONS AND PERMANENT STRAIN DATA FOR THE STEEL-SPHERE-IMPACTED BEAMS

Strain Gage Identif. Number	Location		Permanent Strain[a] (per cent)										
	x(in)	Surface (Upper(U) or Lower (L))	Model CB-8	CB-9	CB-10	CB-11	CB-12	CB-13	CB-14	CB-15	CB-16	CB-17	CB-18
1	0	U	b*	--*	--*	--*	--*	--*	--	--	--	--	--
2	+.30	U	0.88*	1.84*	--*	0.38	--*	--*	-0.47	--	--	--	--
3	+.60	U	0.08*	-0.24*	0.10*	-0.08*	--*	0.40*	-0.29*	--*	0.32*	2.35*	2.24*
4	+1.20	U	0	-0.12	-0.06	0.06	0.38	0.64	-0.26*	1.37*	1.02*	1.08*	1.13*
5	+1.50	U	0.06*	0*	0.06*	0.04*	0.46*	0.73*	-0.34*	1.03*	0.75*	1.28*	1.48*
6	+3.00	U	0.24	0.24	0.16	1.60	0.85	0.66	-0.98*	1.44*	0.52*	1.33*	1.34*
7	+3.70	U	0.24*	0.14*	0.18*	0.04*	0.42*	0.35*	-3.13*	0.95*	0.38*	0.66*	0.56*
8	-.30	U	1.00*	0*	--*	1.26*	1.22*	--*	--	2.49	0.49	2.45	4.02
9	-.60	U	0.18*	-0.16*	-0.26*	0.08*	0.39*	0.69*	-0.77*	1.51*	0.46*	1.46*	2.36*
10	-1.50	U	0.08	0	0.08	0.08	0.94	0.56	-0.45*	1.35*	0.89*	1.19*	1.13*
11	-3.70	U	0.24	0.08	0.28	0.20	0.25	0.48	-4.29	1.09	0.06	0.69	0.68
12	+1.50	L	0.26*	0.22*	0.10*	0.02*	0.79*	0.60*	0.58*	1.55*	0.89*	1.27*	1.31*
13	+3.00	L	0.16	0.02	0.14	0.12	0.59	0.49	0.74	1.47	1.31	1.19	1.23
14	+3.70	L	0.02	0.06	0.06	0.32	0.22	0.26	--	0.76	1.47	0.55	1.07
15	-1.50	L	0.24	0.24	0.22	0.24	0.90	0.74	0.79	1.29	0.97	1.67	1.27
16	-3.70	L	0.26	0.16	0.08	0.18	0.32	0.20	--	1.07	1.11	0.57	0.47

a: This permanent strain is the relative elongation; tension is (+), compression is (-).

b: a dash (-) indicates that the strain gage was lost.

*: Denotes that transient strain measurements were attempted.

TABLE 6

POST-TEST VERTICAL LOCATION OF THE LOWER SURFACES OF THE STEEL-SPHERE-IMPACTED BEAMS

Spanwise Location x(in)	Vertical Location, z_ℓ (in)								
	Model CB-9			Model CB-13			Model CB-18		
	Along y=-0.5	Along y=0 in	Along y=0.5	Along y=-0.5	Along y=0 in	Along y=0.5	Along y=-0.5	Along y=0 in	Along y=0.5
-4.50	0	0	0	0	0	0	0	0	0
-4.20	0	0	0	0	-.001	0	0	0	0
-4.10	0	0	0	0	0	0	0	0	0
-4.00	0	0	0	.001	.001	0	.002	.003	.004
-3.90	.003	.004	.004	.005	.006	.006	.012	.015	.017
-3.80	.009	.010	.010	.014	.010	.015	.026	.032	.036
-3.60	.026	.027	.027	.043	.045	.044	.065	.075	.084
-3.40	.043	.045	.045	.074	.076	.076	.103	.117	.131
-3.00	.077	.078	.080	.132	.133	.135	.177	.200	.224
-2.50	.116	.118	.120	.201	.204	.206	.267	.300	.334
-2.00	.154	.157	.160	.269	.274	.276	.354	.399	.442
-1.50	.192	.197	.200	.337	.344	.345	.442	.503	.550
-1.00	.233	.241	.244	.407	.420	.412	.533	.613	.657
-0.80	.251	.261	.262	.435	.454	.446	.568	.660	.698
-0.60	.269	.283	.282	.463	.490	.475	.600	.711	.736
-0.40	.286	.306	.301	.489	.534	.502	.628	.769	.770
-0.20	.301	.335	.318	.510	.587	.524	.646	.840	.796
0	.310	.376	.330	.521	.633	.534	.654	.865	.804

TABLE 6 CONCLUDED

Spanwise Location x(in)	Vertical Location, z_ℓ (in)								
	Model CB-9			Model CB-13			Model CB-18		
	Along y=-0.5	Along y=0 in	Along y=0.5	Along y=-0.5	Along y=0 in	Along y=0.5	Along y=-0.5	Along y=0 in	Along y=0.5
0.20	.308	.376	.328	.515	.604	.527	.647	.813	.788
0.40	.296	.332	.313	.495	.544	.506	.624	.750	.759
0.60	.279	.299	.292	.469	.499	.480	.596	.697	.724
0.80	.259	.273	.270	.441	.462	.451	.563	.650	.686
1.00	.239	.250	.249	.413	.42[illegible]	.422	.529	.605	.645
1.50	.192	.199	.201	.343	.349	.350	.441	.499	.543
2.00	.150	.155	.157	.276	.280	.282	.356	.399	.440
2.50	.111	.114	.111	.209	.211	.214	.272	.302	.335
3.00	.074	.076	.078	.140	.141	.143	.181	.203	.227
3.40	.042	.044	.044	.082	.083	.084	.105	.119	.134
3.60	.025	.026	.027	.051	.053	.052	.067	.077	.085
3.80	.009	.010	.010	.020	.022	.021	.028	.033	.038
3.90	.003	.004	.004	.009	.009	.009	.013	.015	.017
4.00	0	0	0	.001	.002	.001	.003	.003	.005
4.10	0	0	0	0	-.001	-.001	0	0	0
4.20	0	0	0	-.001	-.001	-.001	0	0	0
4.50	0	0	0	0	-.001	-.001	0	0	0

TABLE 7

IMPACT LOCATION, IMPACT VELOCITY, AND WEIGHT OF LAUNCHING EXPLOSIVE FOR THE STEEL-SPHERE-IMPACTED BEAM SPECIMENS

Model	Impact Location x(in)	Impact Location y(in)	Sphere Weight (gm)	Impact Velocity (in/sec)	HE Weight (gm)	Remarks
CB-8	+.046	+.174	66.753	1941	2.279	Small permanent deformation
CB-9	+.106	+.037	66.779	1896	2.229	
CB-10	-.047	-.087	66.806	1893	2.227	
CB-11	-.041	-.126	66.809	1898	2.231	
CB-12	+.168	-.022	66.745	2485	3.210	Moderate permanent deformation
CB-13	+.023	0	66.738	2490	3.225	
CB-14	-.180	+.092	66.799	3075	5.501	Too fast; model ruptured
CB-15	+.308	+.152	66.800	2865	4.498	Large permanent deformation
CB-16	+.024	+.035	66.809	2868	4.501	Barely beyond rupture threshold
CB-17	+.194	+.135	66.820	2796	4.198	Large permanent deformation
CB-18	-.019	+.057	66.810	2794	4.189	

TABLE 8

STEEL SPHERE VELOCITY CALIBRATION DATA

Run I.D. No.	Weights (grams)			Deduced Data for Sphere			
	Post-Test Sphere	Buffer	HE W_{HE}	Velocity in/sec	Kinetic Energy (in-lb)	mV (lb-sec)	mV/W_{HE} (lb-sec)/gm
CB-5	66.755	.709	2.231	1972	741.4	.7514	.3368
CB-6	66.752	.711	2.379	1908	694.1	.7274	.3058
CB-7	66.740	.590	2.223	1886	677.3	.7186	.3233
CB-T22	66.731	.629	2.489	2090	832.4	.7965	.3200
CB-T29	66.729	.570	2.227	1913	697.2	.7289	.3273
CB-T30	66.733	.561	2.320	1823	632.9	.6944	.2993
						Group Average:	.3188
CB-T32	66.738	.578	3.152	2496	1186.6	.9510	.3017
CB-T33	66.732	.579	3.195	2407	1104.1	.9173	.2871
CB-T34	66.735	.580	3.210	2474	1165.7	.9425	.2936
CB-T35	66.736	.595	3.179	2472	1164.7	.9421	.2964
CB-T36	66.745	.581	3.149	2470	1162.4	.9413	.2989
						Group Average:	.2955
CB-T45	66.788	.635	4.195	2676	1366.0	1.0208	.2433
CB-T46	66.798	.628	4.202	2876	1578.3	1.0974	.2612
CB-T47	66.800	.633	4.198	2786	1480.6	1.0629	.2532
CB-T48	66.821	.631	4.203	2811	1508.1	1.0729	.2553
						Group Average:	.2532

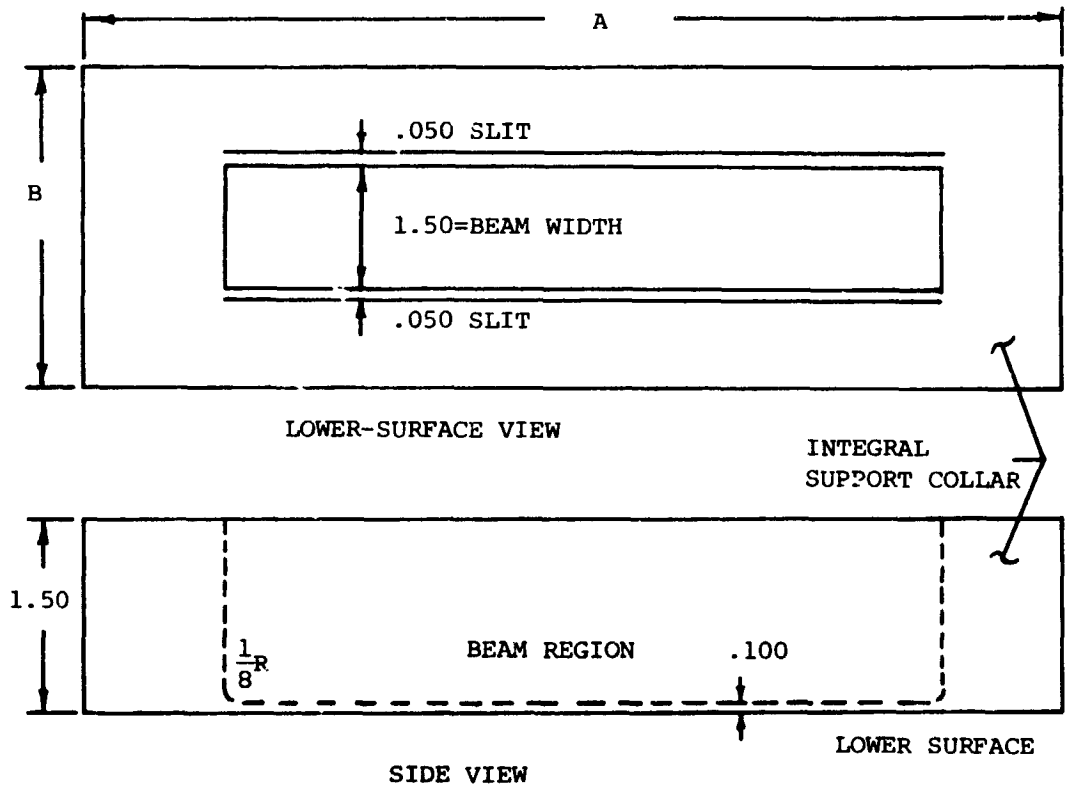

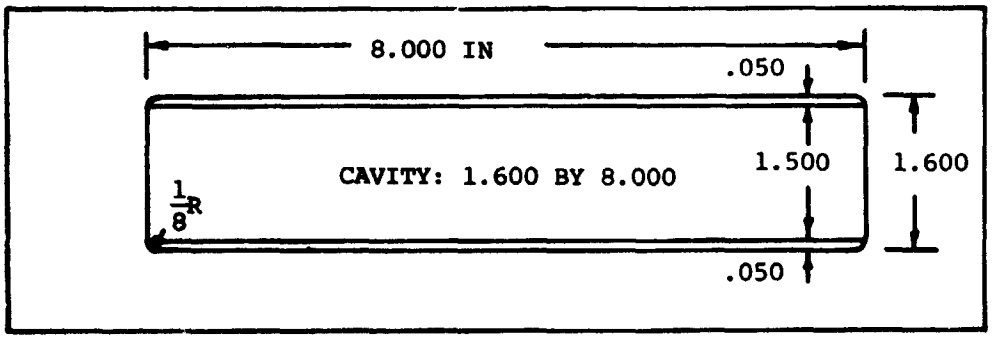

FOR MODELS CB-1,-2,-3,AND -4	A=12.00 IN B=3.50 IN
FOR MODELS CB-8,-9,...,-18	A=13.00 IN B=2.55 IN

FIG. 1 NOMINAL DIMENSIONS FOR THE 6061-T651 ALUMINUM CLAMPED-BEAM MODELS

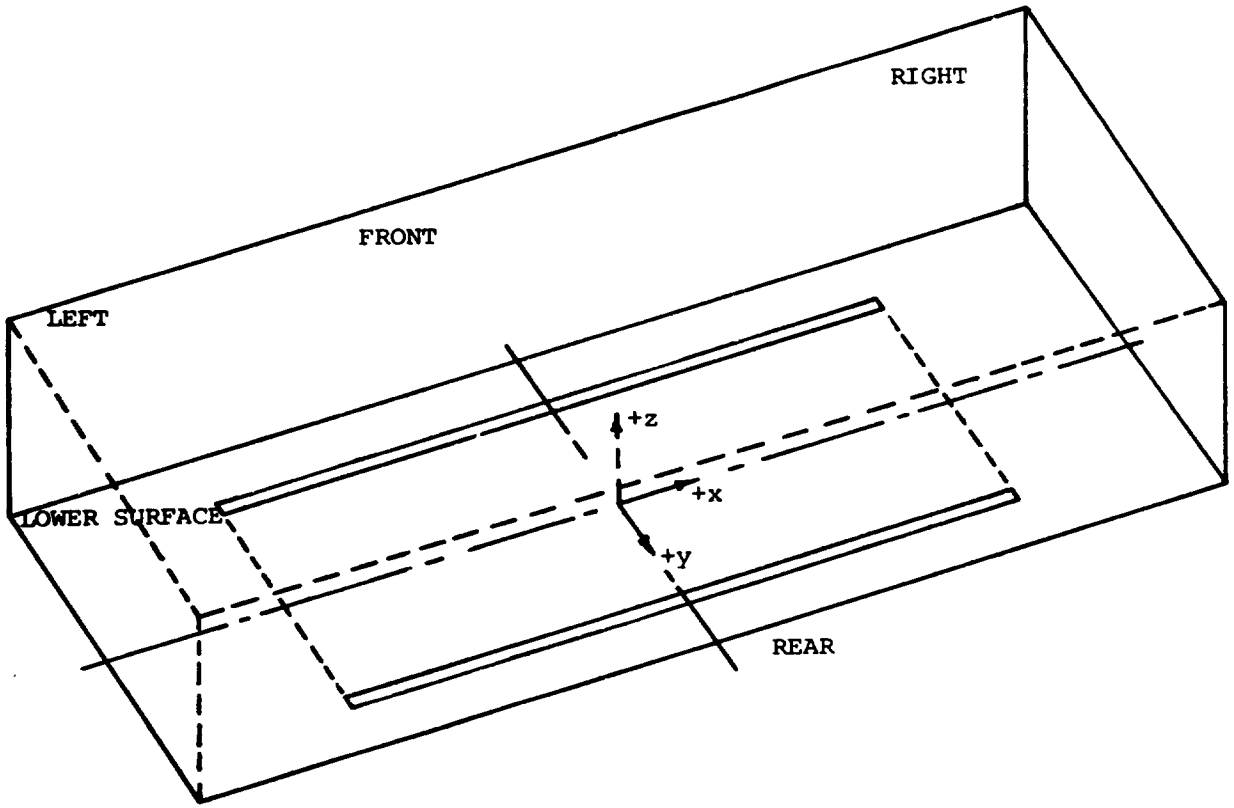

FIG. 2 CLAMPED BEAM MODEL COORDINATES AND NOMENCLATURE

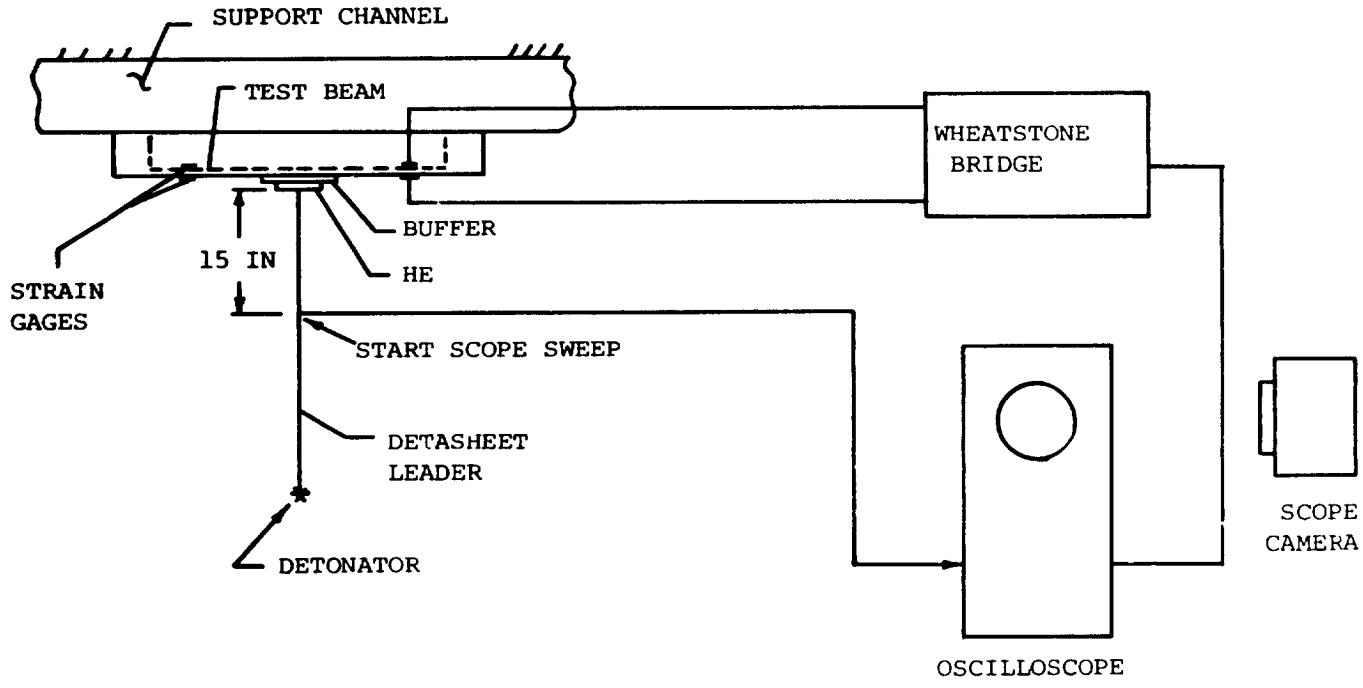

FIG. 3 SCHEMATIC OF IMPULSIVE-LOADING TESTS ON 6061-T651 BEAMS WITH CLAMPED ENDS

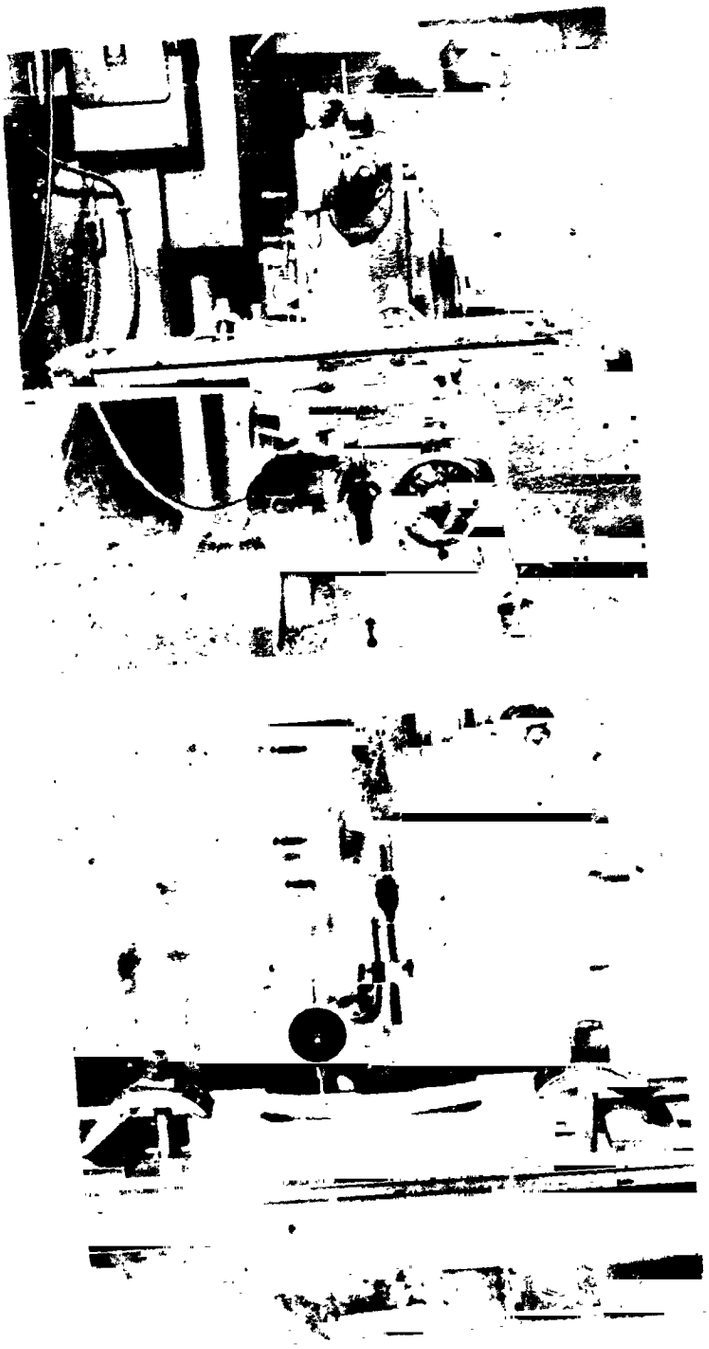

FIG. 4 MILLING MACHINE TRAVERSE AND DIAL GAGE ARRANGEMENT FOR MEASURING THE VERTICAL LOCATION z OF THE MODFL SURFACES AT SELECTED x,y LOCATIONS

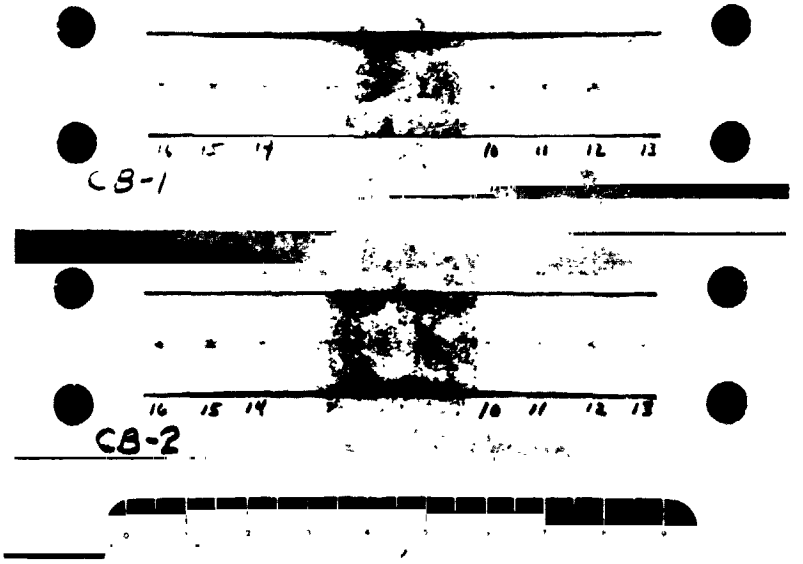

LOWER SURFACE VIEW

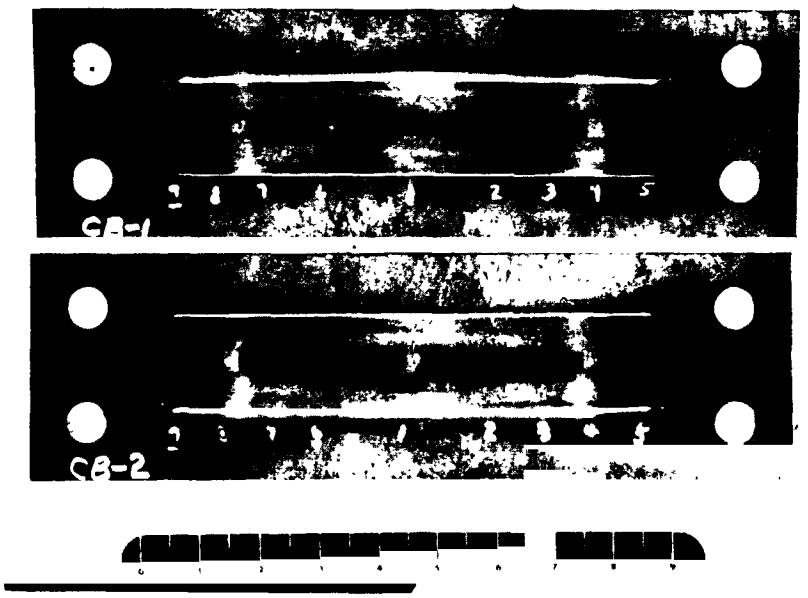

UPPER SURFACE VIEW (INTO CAVITY)

(a) Models CB-1 and CB-2

FIG. 5 POST TEST PHOTOGRAPHS OF THE IMPULSIVELY-LOADED 6061-T651 BEAM MODELS

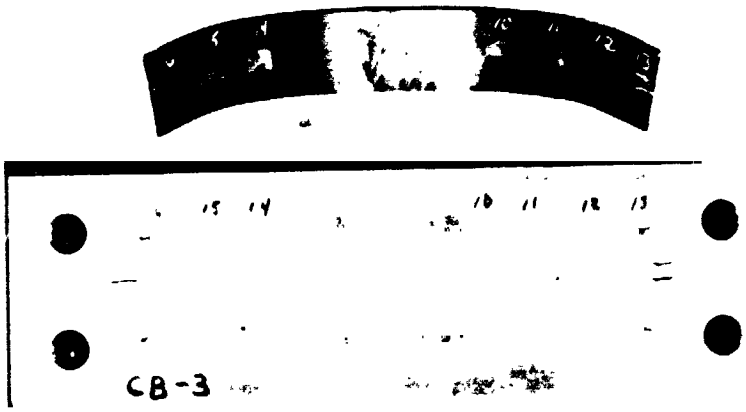

LOWER SURFACE VIEW

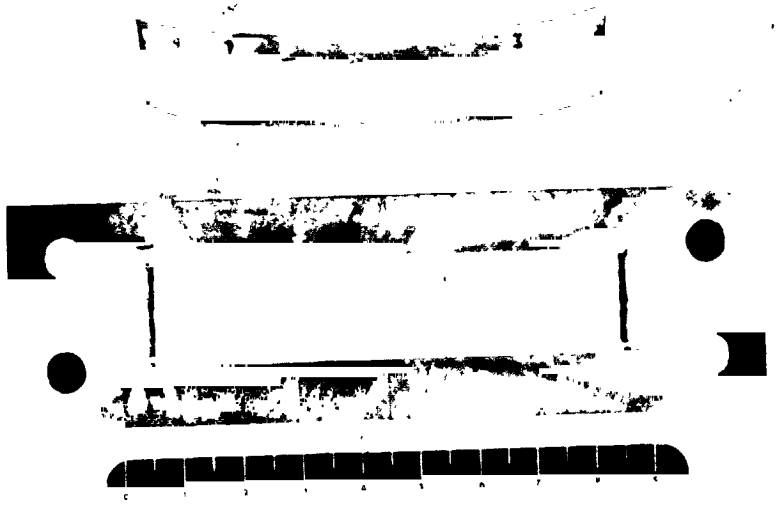

UPPER SURFACE VIEW (INTO CAVITY)

(b) Model CB-3

FIG. 5 CONTINUED

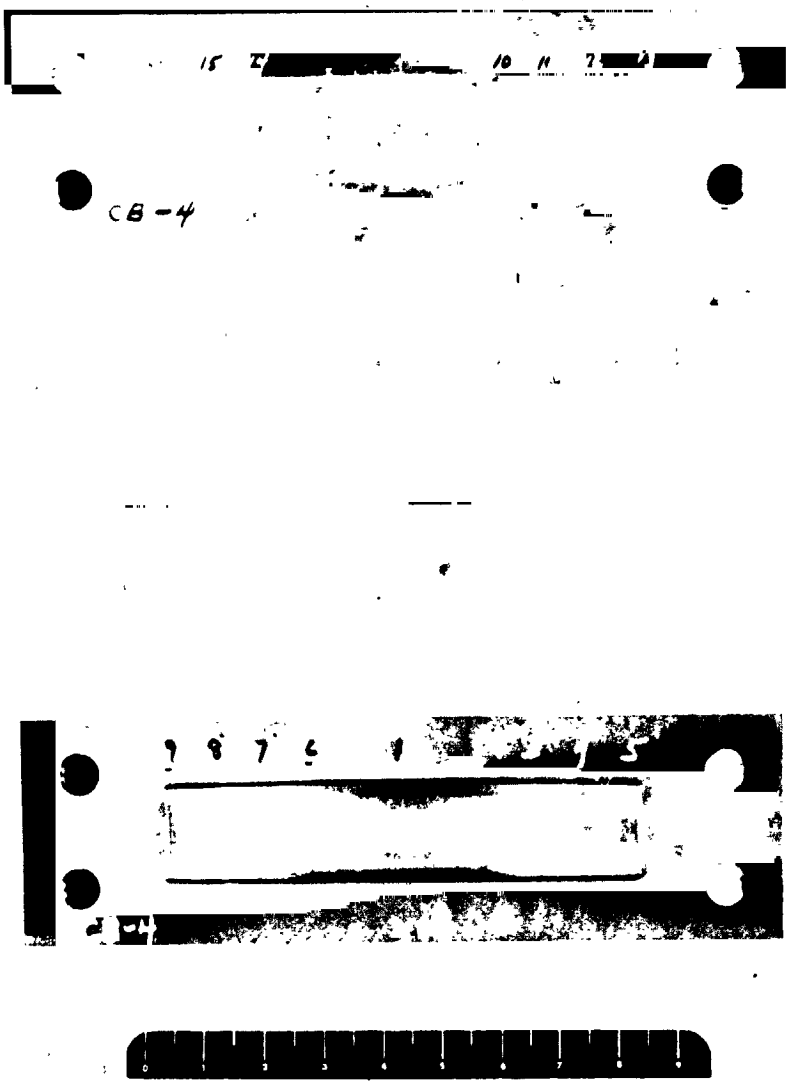

LOWER SURFACE VIEW

UPPER SURFACE VIEW (INTO CAVITY)

(c) Model CB-4

FIG. 5 CONCLUDED

ABSCISSA: TIME, 50 μSEC/DIV
ORDINATE: UNCORRECTED RELATIVE ELONGATION E_x IN PER CENT
+ = TENSION (UP)
- = COMPRESSION (DOWN)
▽: TIME = 0

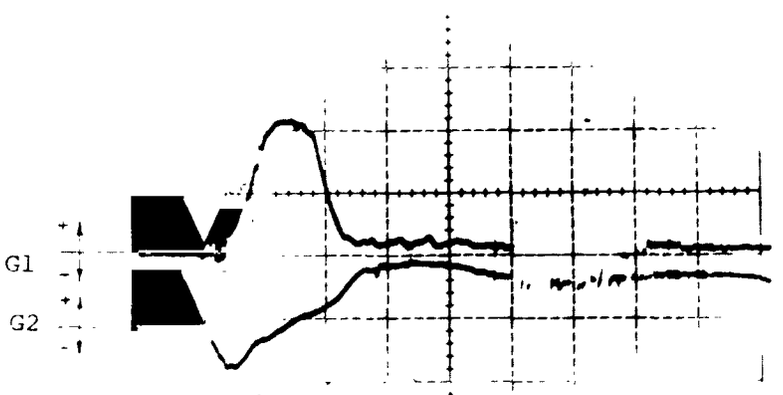

GAGE 1
E_x: 3%/DIV

GAGE 2
E_x: 2%/DIV

GAGE 4
E_x: 2%/DIV

GAGE 8
E_x: 2%/DIV

FIG. 6 UNCORRECTED TRANSIENT STRAIN RECORDS FOR IMPULSIVELY-LOADED 6061-T651 BEAM MODEL CB-1 WITH CLAMPED ENDS

ABSCISSA: TIME, 100 μSEC/DIV
ORDINATE: UNCORRECTED RELATIVE
ELONGATION E_x IN PER CENT
+ = TENSION (UP)
- = COMPRESSION (DOWN)
∇: TIME = 0

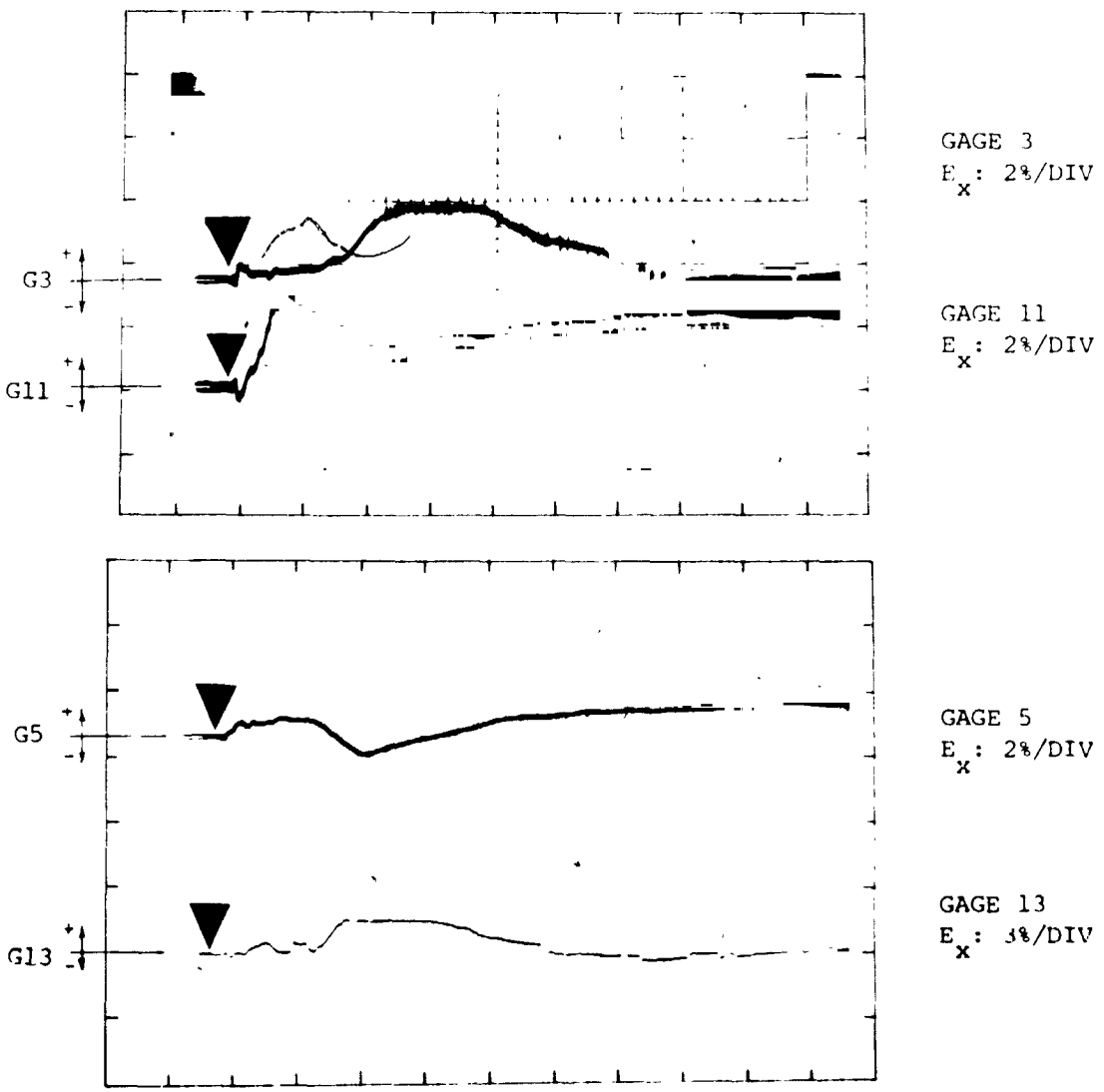

FIG. 6 CONCLUDED (CB-1)

ABSCISSA: TIME, 50 μSEC/DIV
ORDINATE: UNCORRECTED RELATIVE ELONGATION E_x IN PER CENT
+ = TENSION (UP)
- = COMPRESSION (DOWN)
▽: TIME = 0

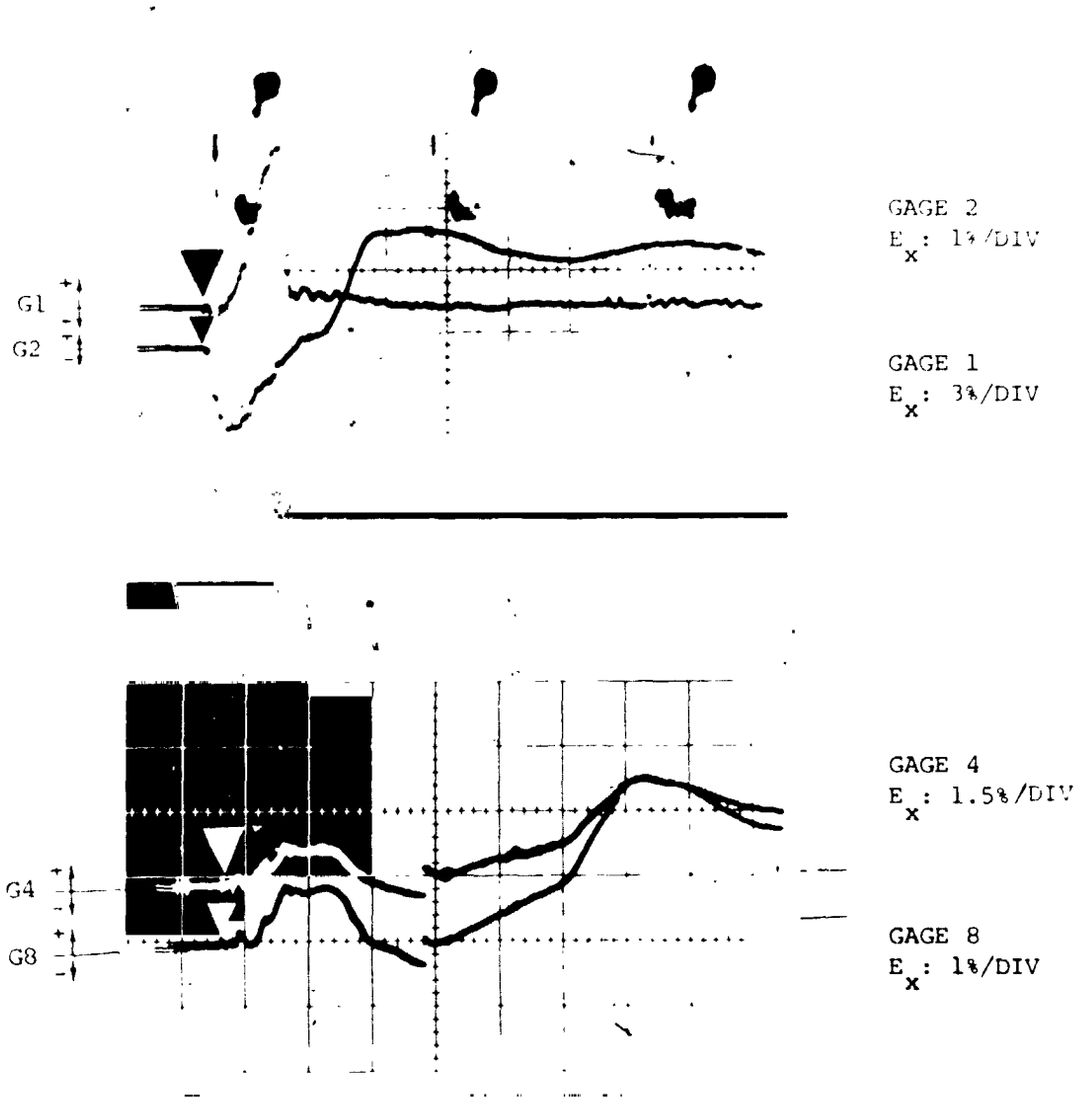

FIG. 7 UNCORRECTED TRANSIENT STRAIN RECORDS FOR IMPULSIVELY-LOADED 6061-T651 BEAM MODEL CB-2 WITH CLAMPED ENDS

ABSCISSA: TIME, 100 μSEC/DIV
ORDINATE: UNCORRECTED RELATIVE
ELONGATION E_x IN PER CENT
+ = TENSION (UP)
- = COMPRESSION (DOWN)
V: TIME = 0

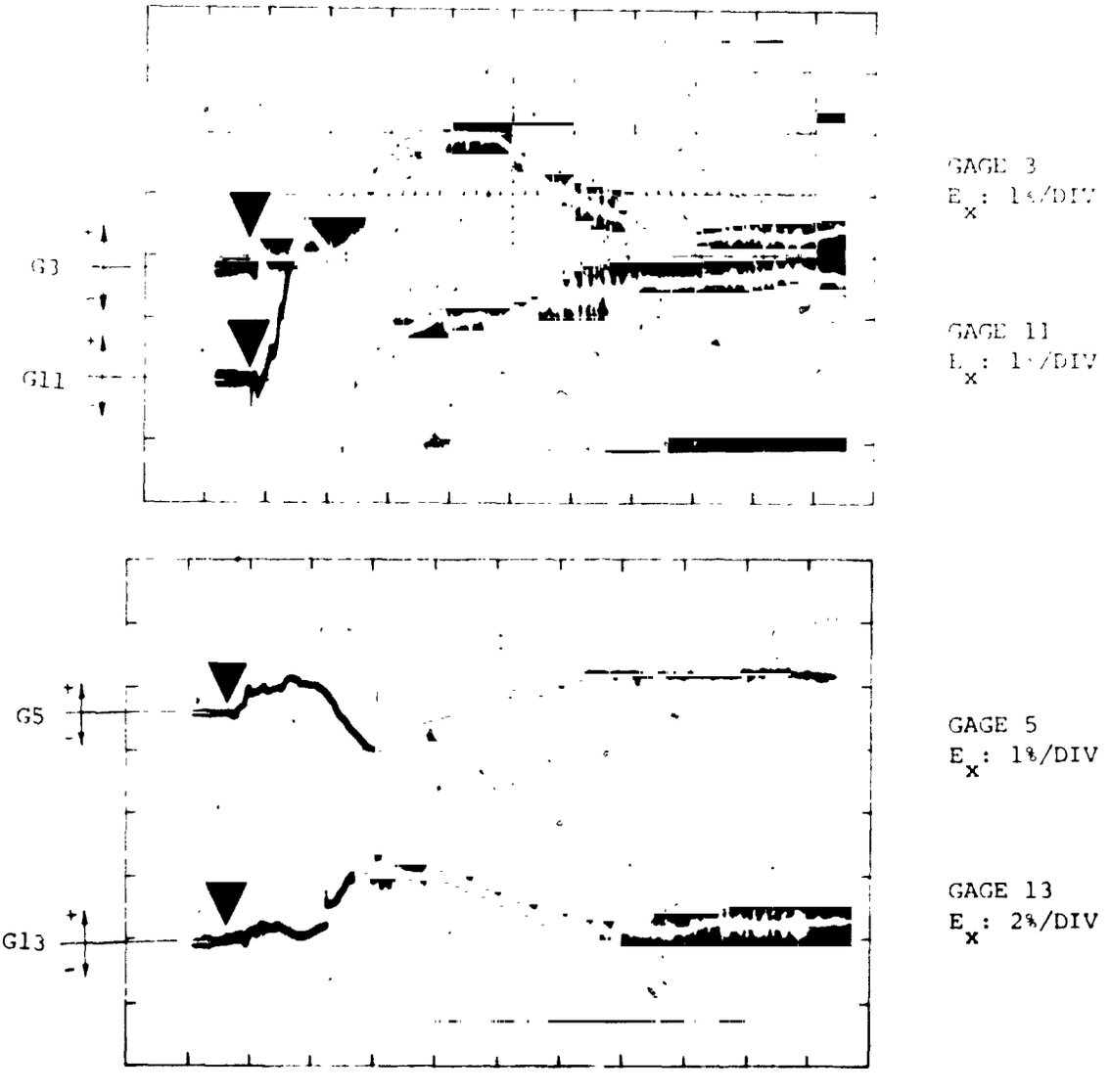

FIG. 7 CONCLUDED (CB-2)

ABSCISSA: TIME, 50 μSEC/DIV
ORDINATE: UNCORRECTED RELATIVE ELONGATION E_x IN PER CENT
+ = TENSION (UP)
- = COMPRESSION (DOWN)
▽: TIME = 0

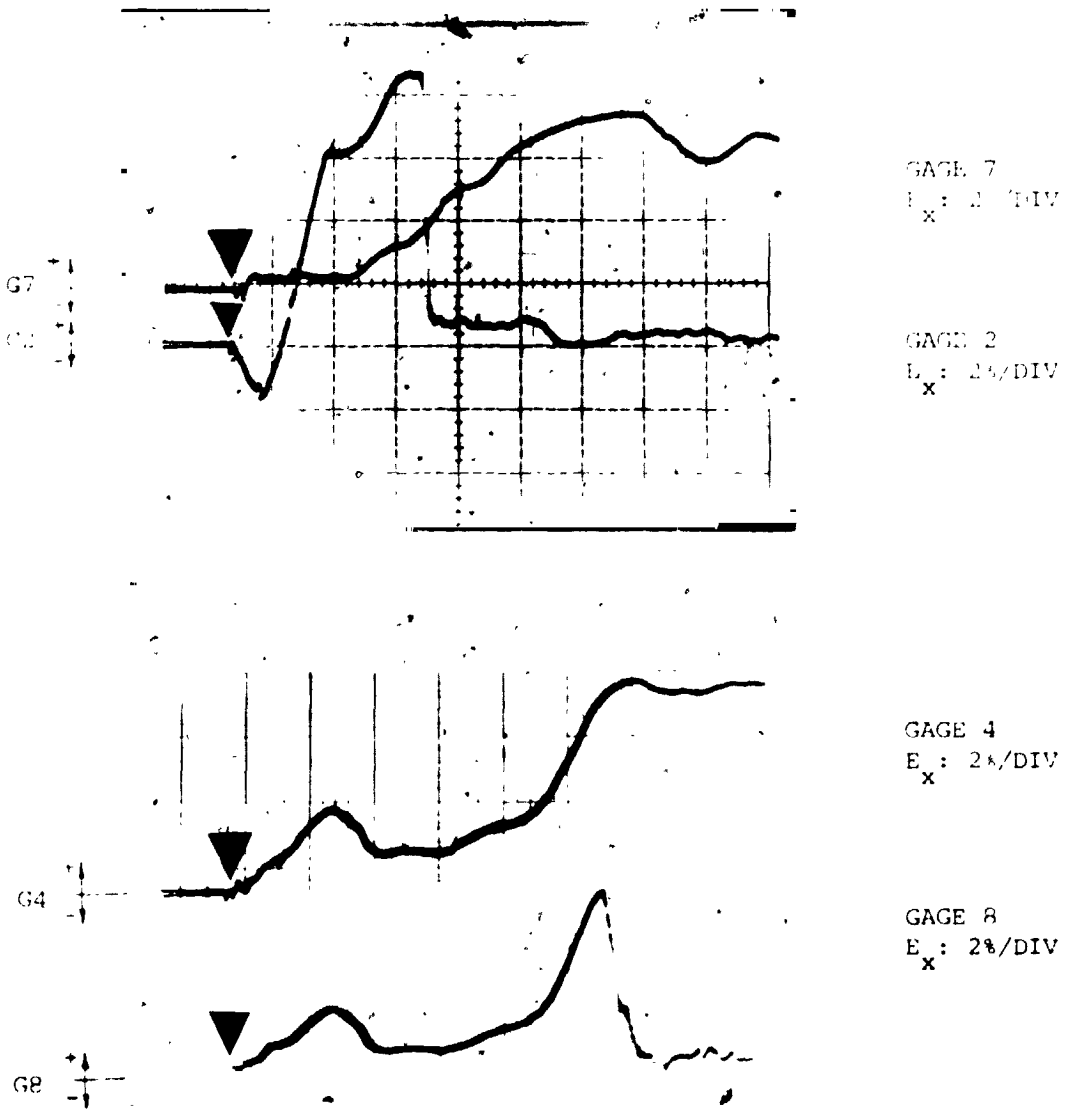

FIG. 8 UNCORRECTED TRANSIENT STRAIN RECORDS FOR IMPULSIVELY-LOADED 6061-T651 BEAM MODEL CB-3 WITH CLAMPED ENDS

ABSCISSA: TIME, 50 μSEC/DIV
ORDINATE: UNCORRECTED RELATIVE ELONGATION E_x IN PER CENT
+ = TENSION (UP)
- = COMPRESSION (DOWN)
▽: TIME = 0

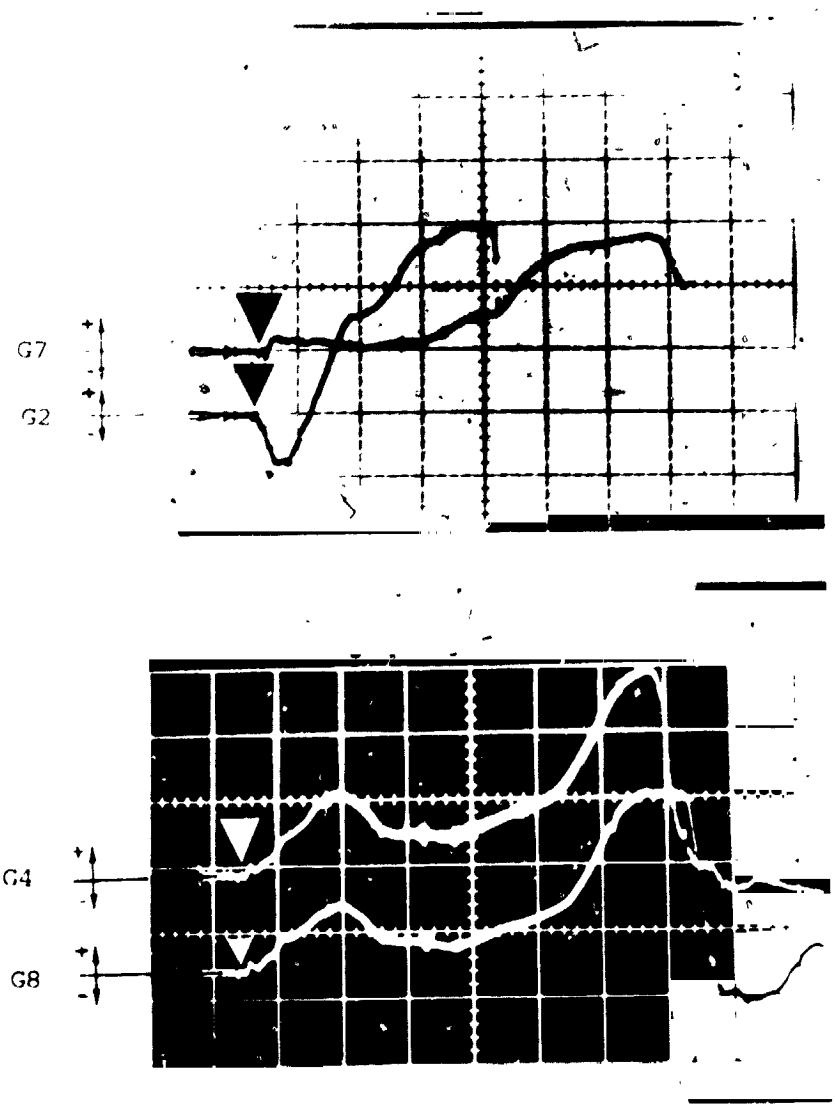

FIG. 9 UNCORRECTED TRANSIENT STRAIN RECORDS FOR IMPULSIVELY-LOADED 6061-T651 BEAM MODEL CB-4 WITH CLAMPED ENDS

ABSCISSA: TIME, 100 μSEC/DIV
ORDINATE: UNCORRECTED RELATIVE ELONGATION E_x IN PER CENT
+ = TENSION (UP)
- = COMPRESSION (DOWN)
V: TIME = 0

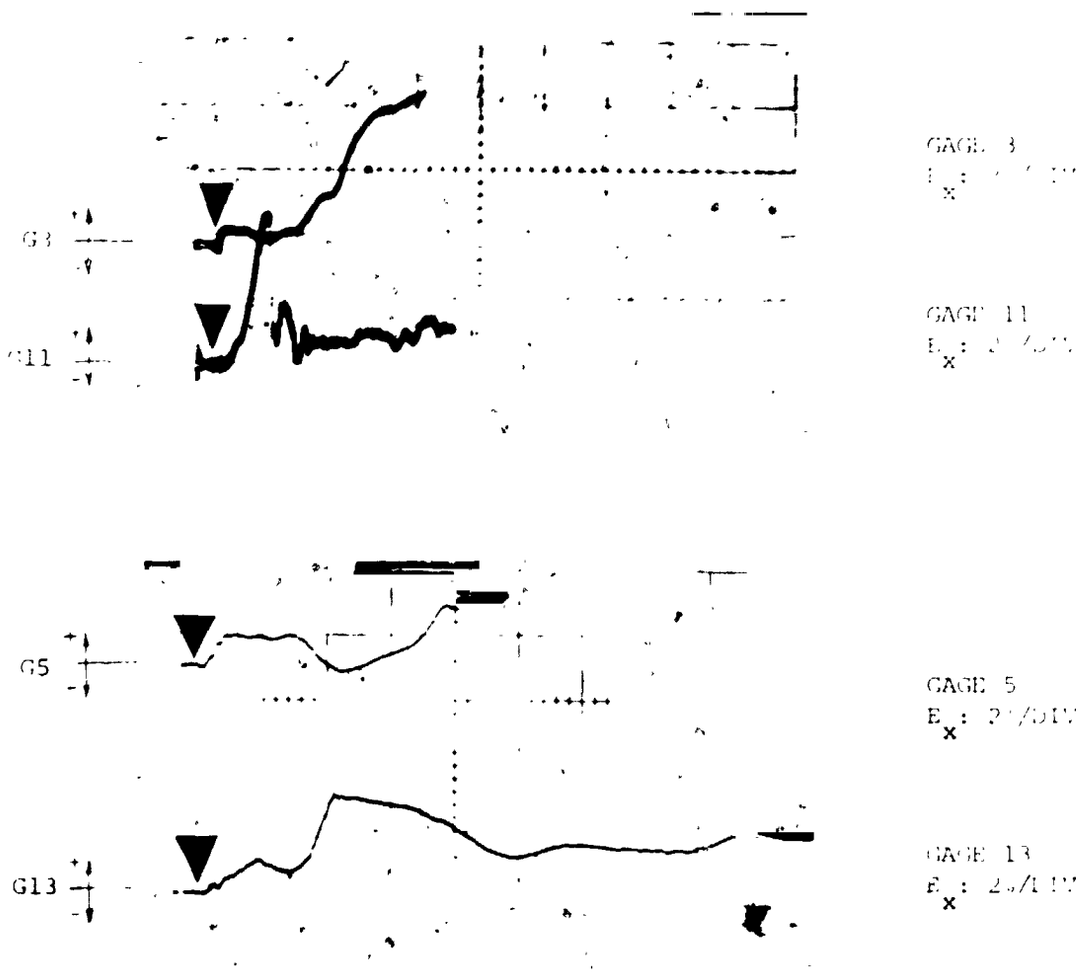

FIG. 9 CONCLUDED (CB-4)

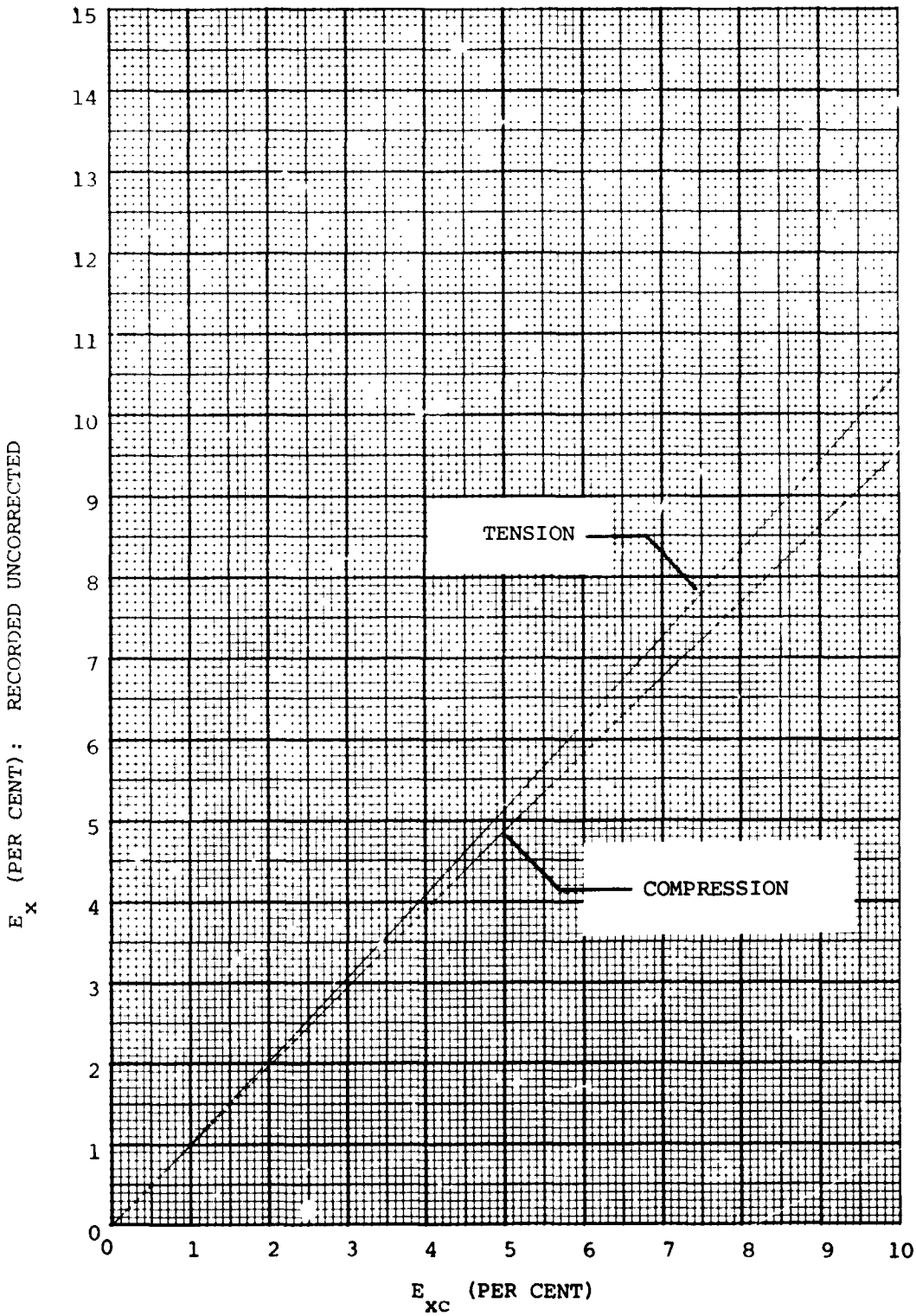

FIG. 10 RELATION BETWEEN RELATIVE ELONGATIONS E_x AS RECORDED (UNCORRECTED) AND E_{xc} CORRECTED

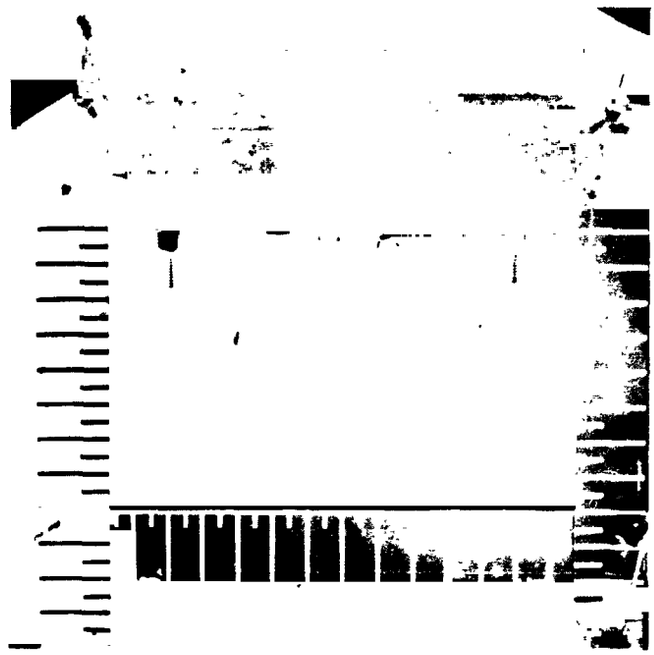

(a) Model Bolted Directly to Steel Support Channel

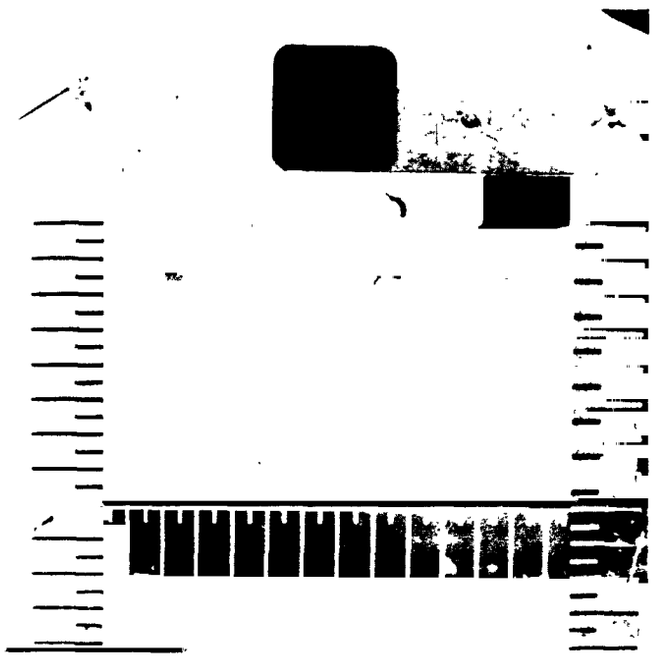

(b) Model on Spacer Blocks

FIG. 11 ARRANGEMENTS FOR MOUNTING THE BEAM MODELS ON THE HEAVY STEEL SUPPORT CHANNEL

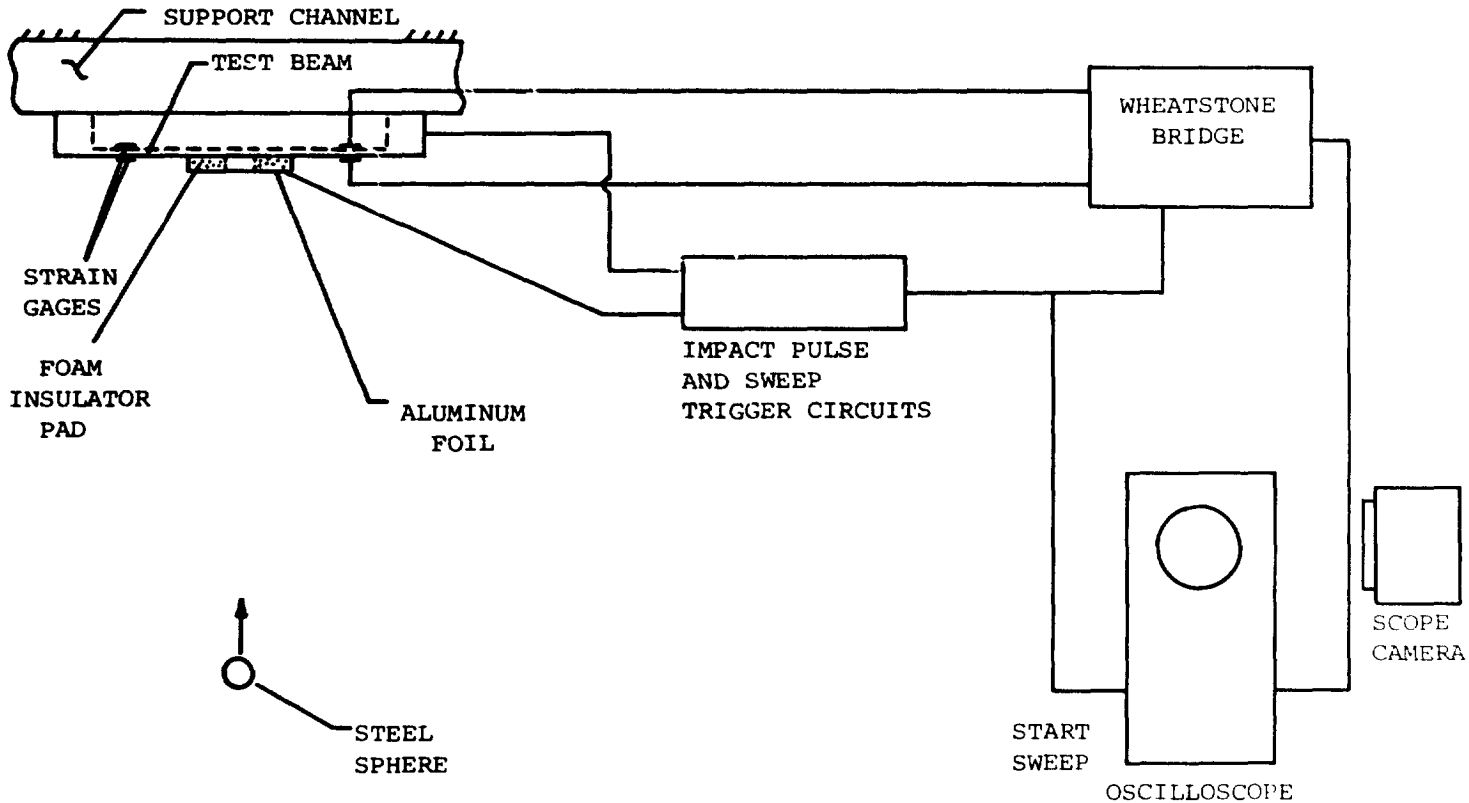

FIG. 12 TEST SCEHMATIC FOR STEEL-SPHERE-IMPACTED 6061-T651 ALUMINUM BEAMS WITH CLAMPED ENDS

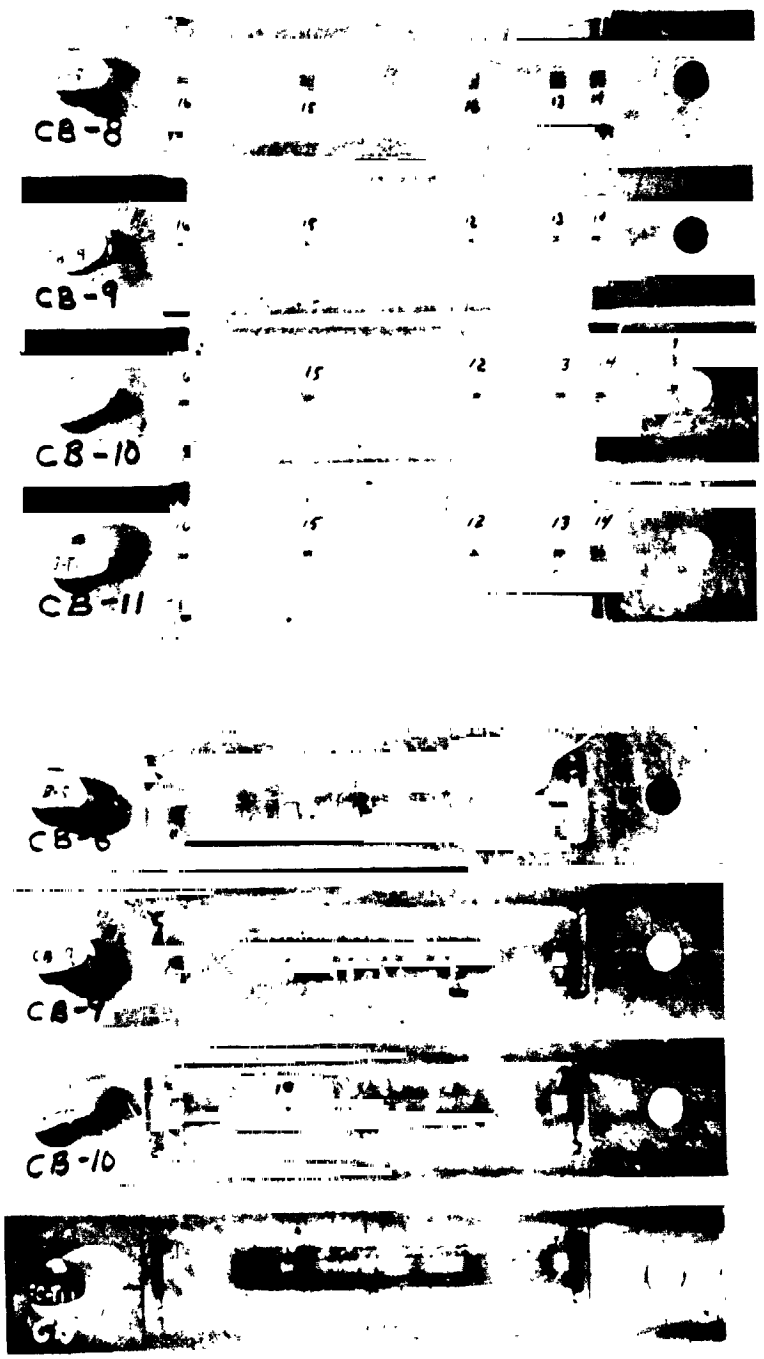

FIG. 13 POST-TEST VIEWS OF STEEL-SPHERE-IMPACTED BEAM SPECIMENS CB-8, CB-9, CB-10, AND CB-11 (NOMINAL IMPACT VELOCITY: 1900 IN/SEC)

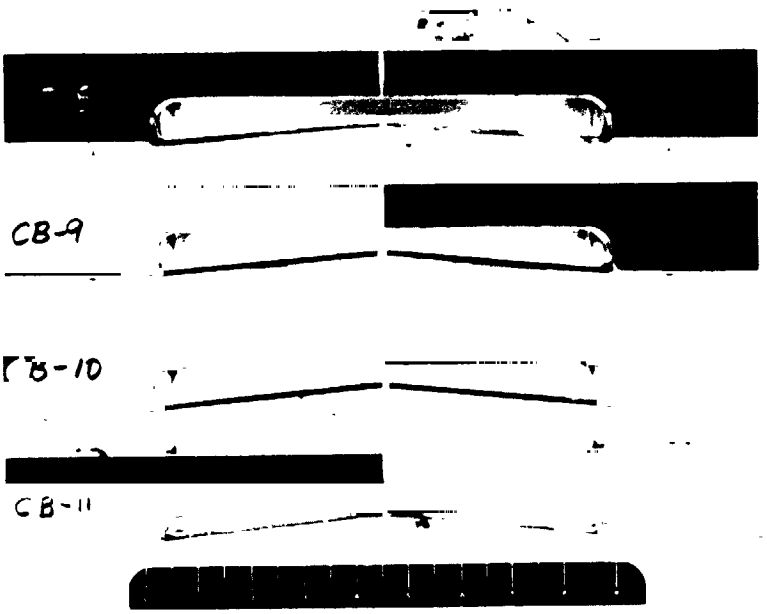

SIDE
VIEW

FIG. 13 CONCLUDED

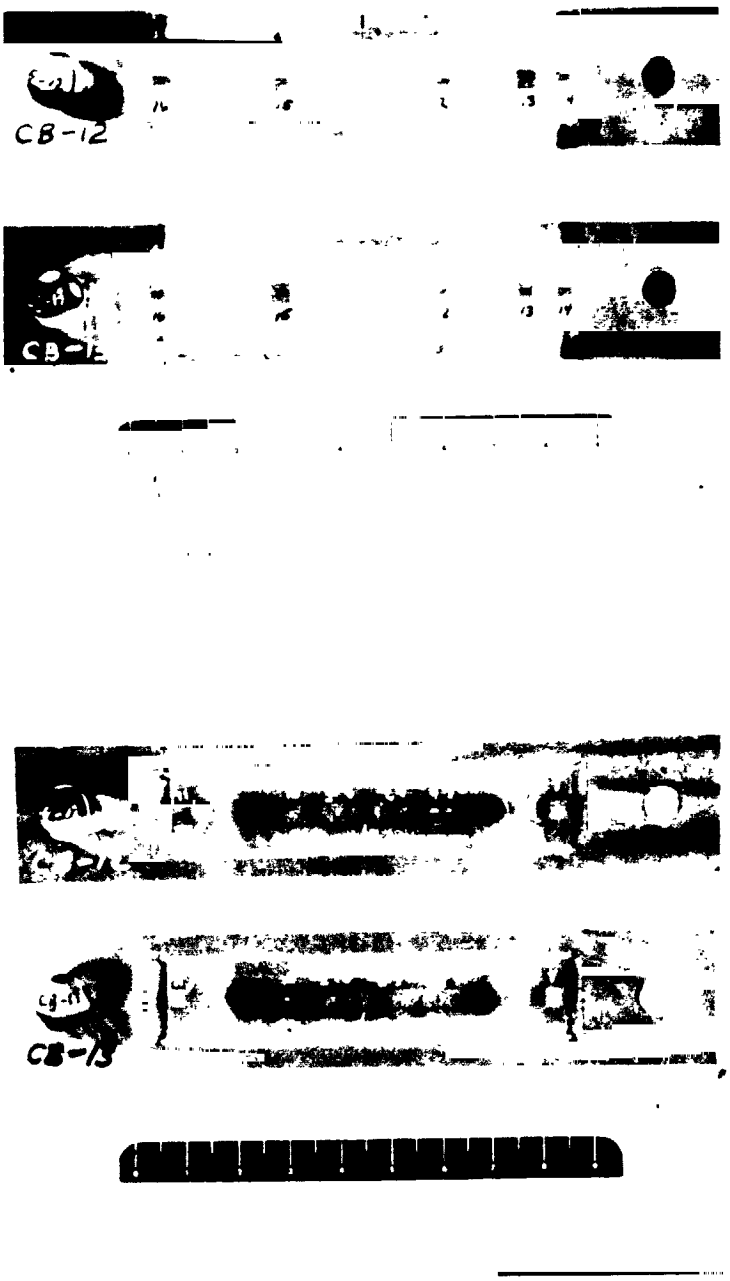

FIG. 14 POST-TEST VIEWS OF STEEL-SPHERE-IMPACTED BEAM SPECIMENS CB-12 AND CB-13 (NOMINAL IMPACT VELOCITY: 2500 IN/SEC)

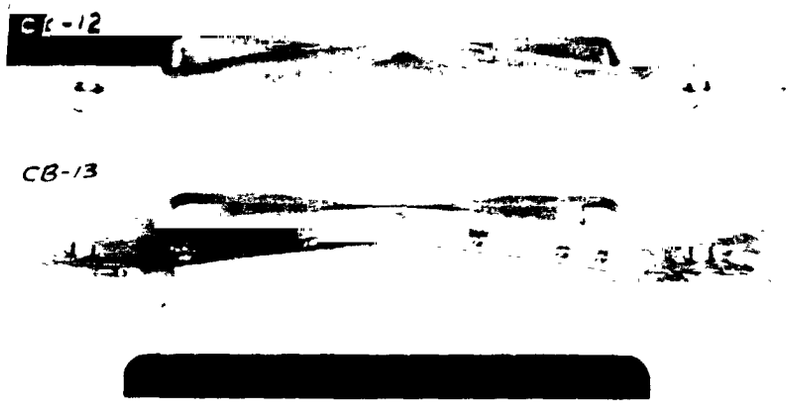

SIDE
VIEW

FIG. 14 CONCLUDED

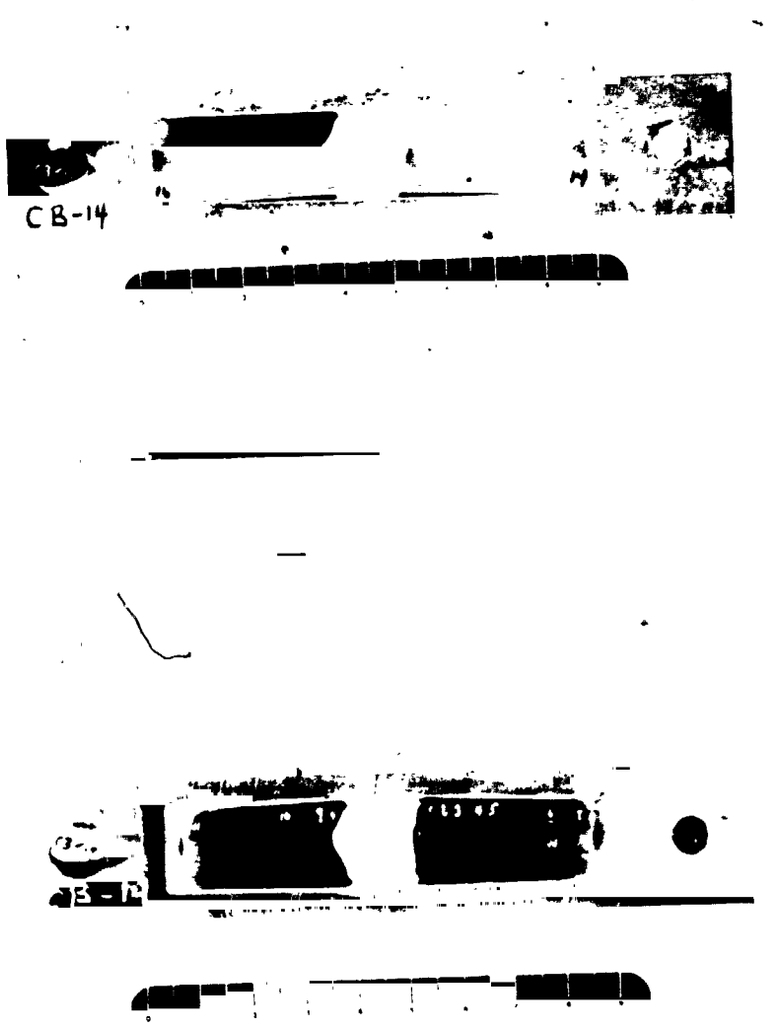

FIG. 15 POST-TEST VIEWS OF STEEL-SPHERE-IMPACTED BEAM SPECIMEN CB-14
(NOMINAL IMPACT VELOCITY: 3075 IN/SEC)

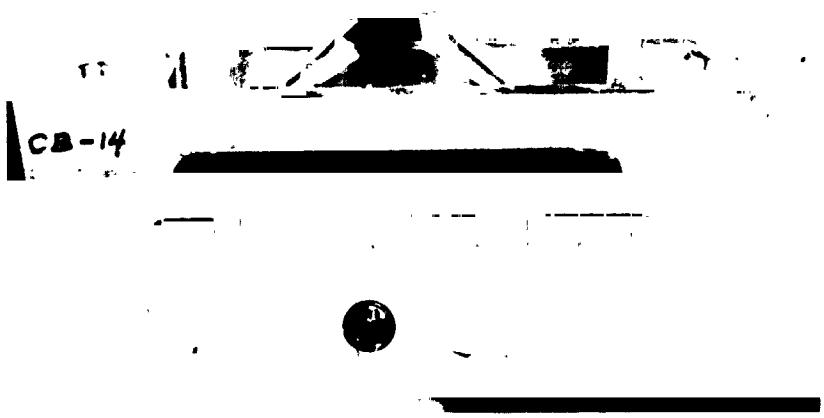

SIDE
VIEW

FIG. 15 CONCLUDED

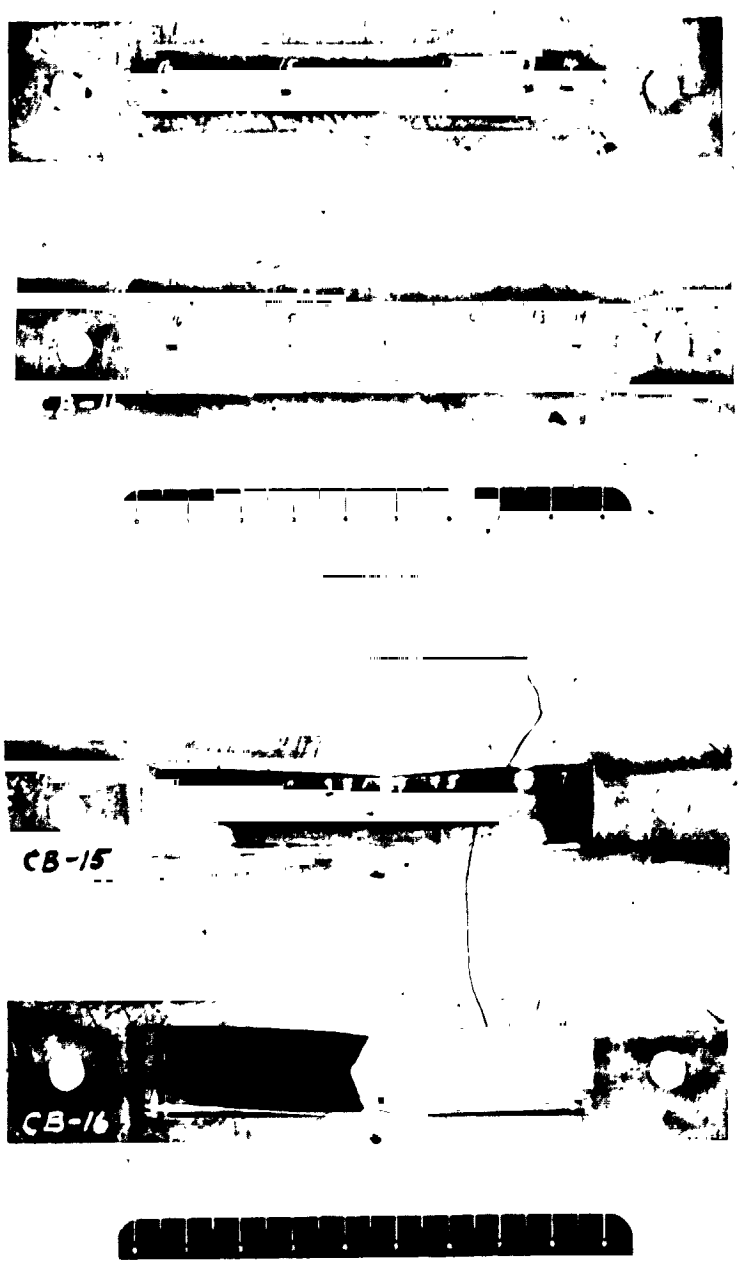

LOWER SURFACE VIEW

UPPER SURFACE VIEW (INTO CAVITY)

FIG. 16 POST-TEST VIEWS OF STEEL-SPHERE-IMPACTED BEAM SPECIMENS CB-15 AND CB-16 (NOMINAL IMPACT VELOCITY: 2870 IN/SEC)

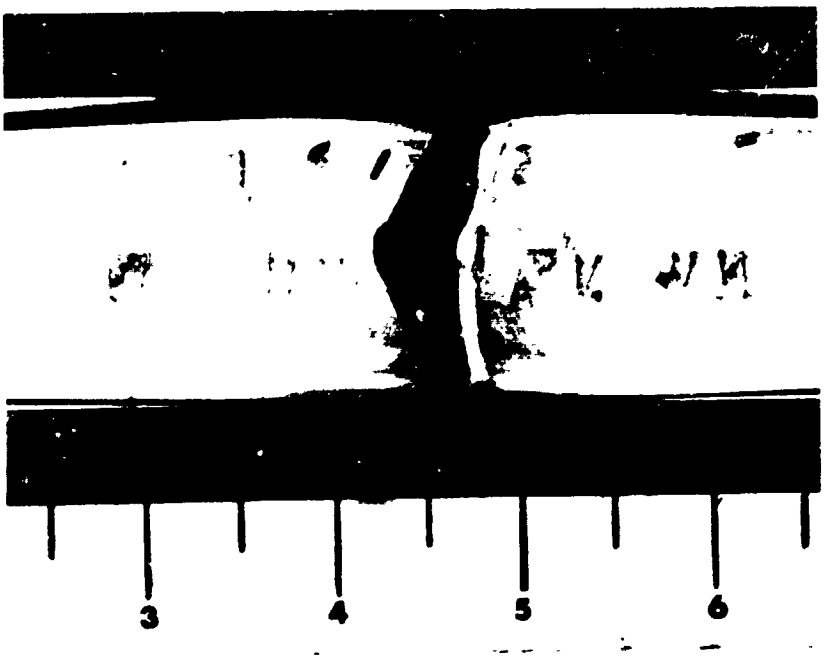

CLOSEUP
UPPER
SURFACE
VIEW
(INTO
CAVITY)

CB-16

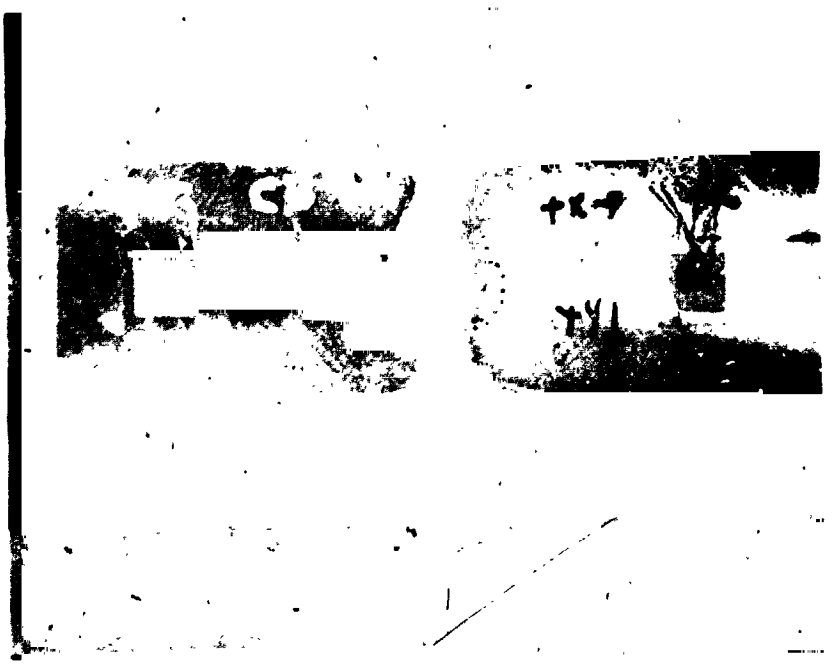

CLOSEUP
LOWER
SURFACE
VIEW

CB-16

FIG. 16 CONCLUDED

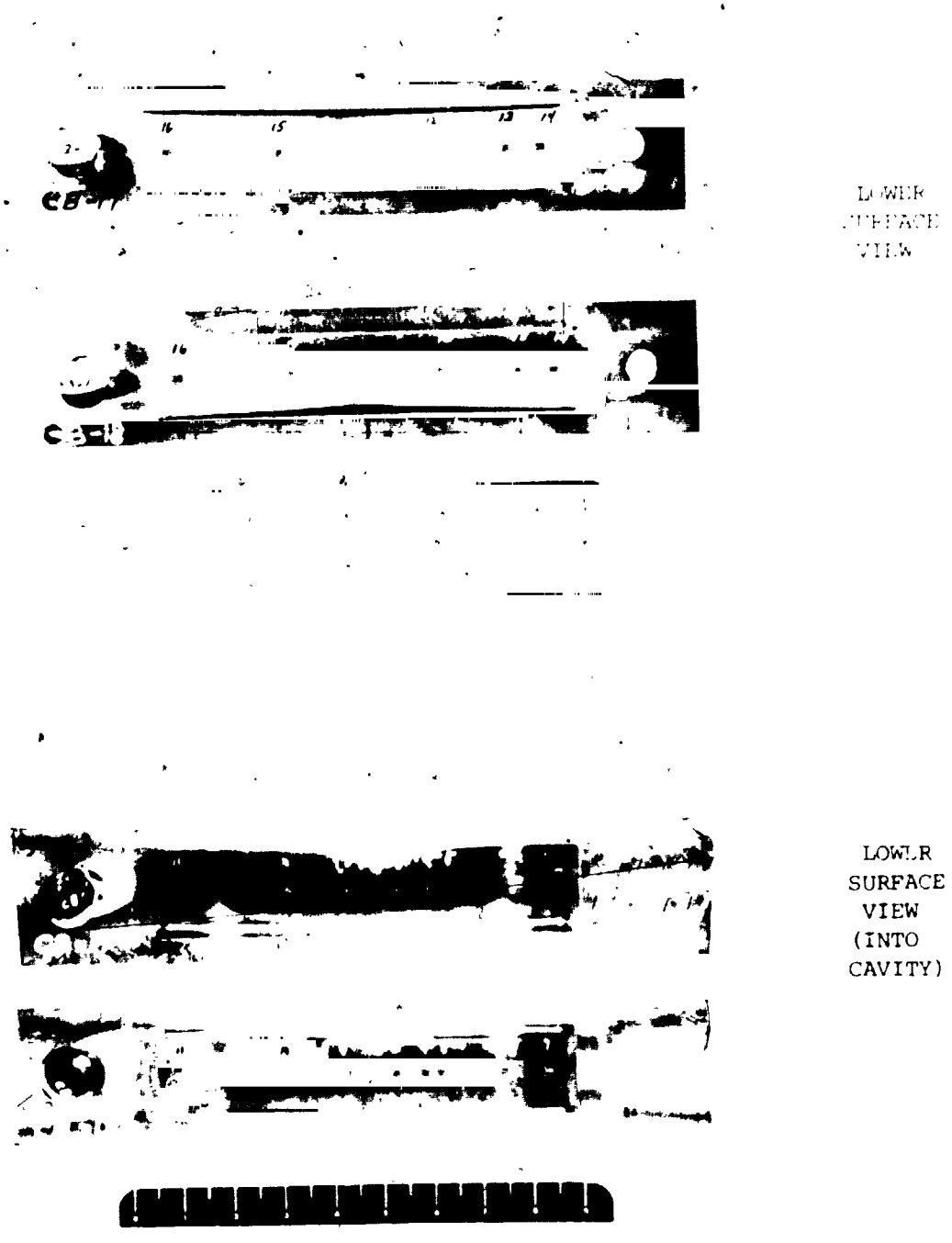

FIG. 17 POST-TEST VIEWS OF STEEL-SPHERE-IMPACTED BEAM SPECIMENS CB-17 AND CB-18 (NOMINAL IMPACT VELOCITY: 2800 IN/SEC)

ABSCISSA: TIME, 50 μSEC/DIV
ORDINATE: UNCORRECTED RELATIVE ELONGATION E_x IN PER CENT
+ = TENSION
- = COMPRESSION
▽: INSTANT OF IMPACT

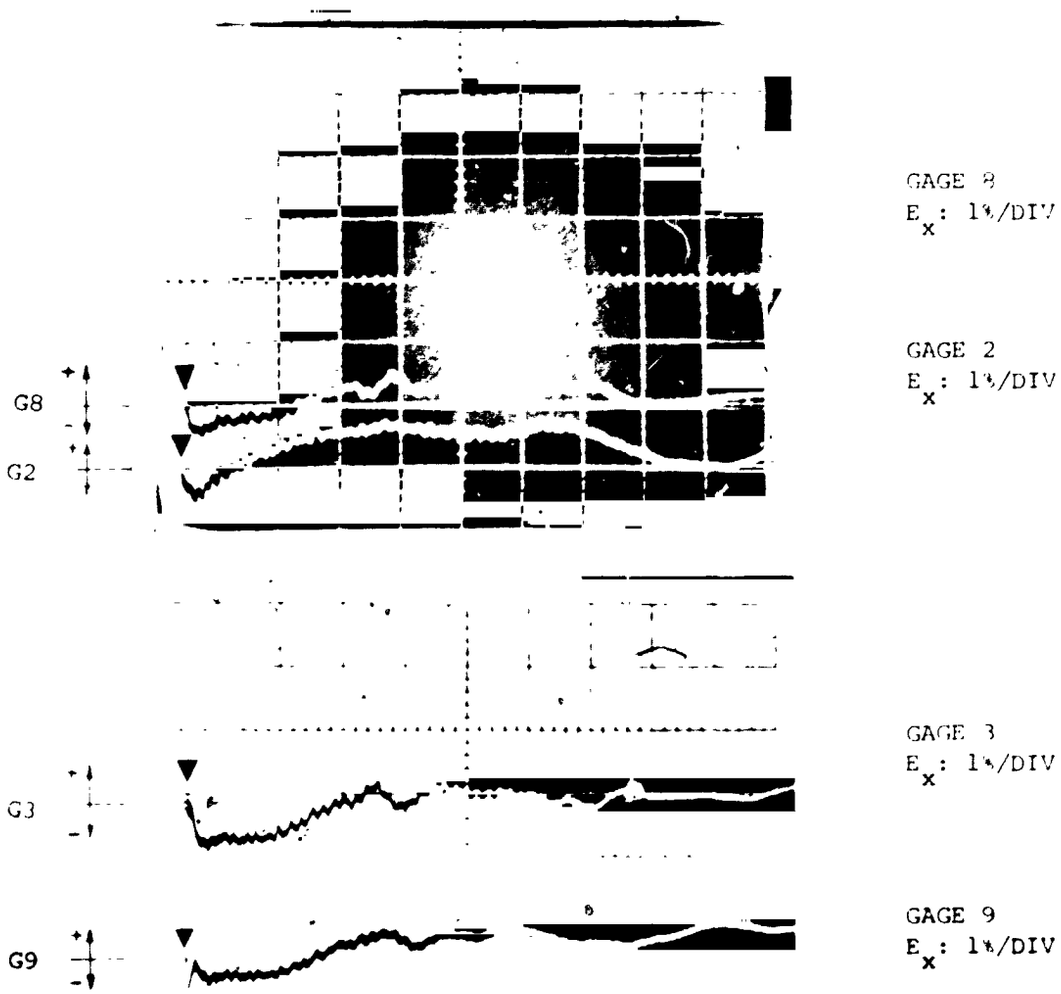

FIG. 18 UNCORRECTED TRANSIENT STRAIN RECORDS FOR STEEL-SPHERE IMPACTED 6061-T651 ALUMINUM BEAM MODEL CB-9

ABSCISSA: TIME
ORDINATE: UNCORRECTED RELATIVE ELONGATION E_x IN PER CENT
+ = TENSION
- = COMPRESSION
V: INSTANT OF IMPACT

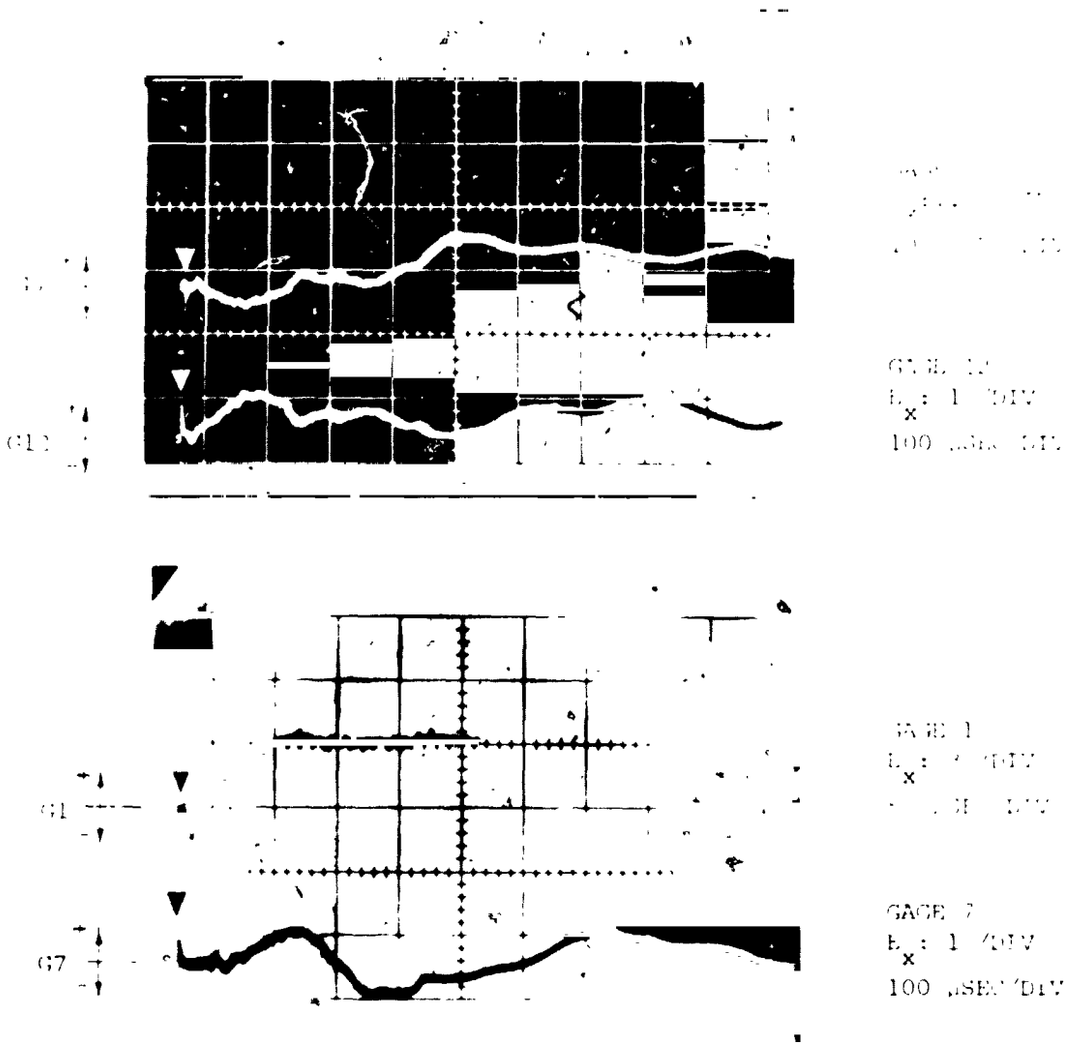

FIG. 18 CONCLUDED (CB-9)

ABSCISSA: TIME, 50 μSEC/DIV
ORDINATE: UNCORRECTED RELATIVE ELONGATION E_x IN PER CENT
+ = TENSION
- = COMPRESSION
∇: INSTANT OF IMPACT

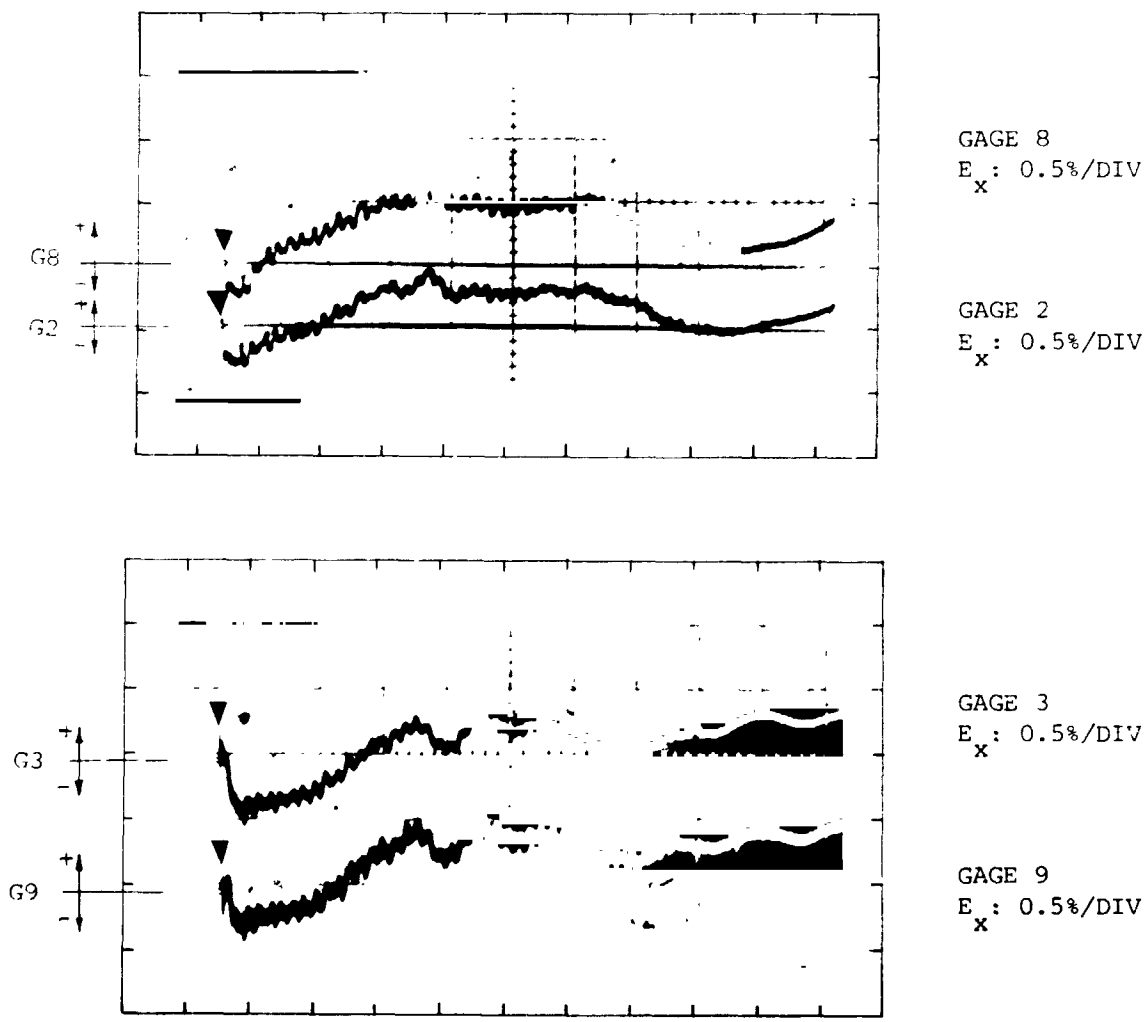

FIG. 19 UNCORRECTED TRANSIENT STRAIN RECORDS FOR STEEL-SPHERE IMPACTED 6061-T651 ALUMINUM BEAM MODEL CB-10

ABSCISSA: TIME, 50 μSEC/DIV
ORDINATE: UNCORRECTED RELATIVE ELONGATION E_x IN PER CENT
+ = TENSION
- = COMPRESSION
∇: INSTANT OF IMPACT

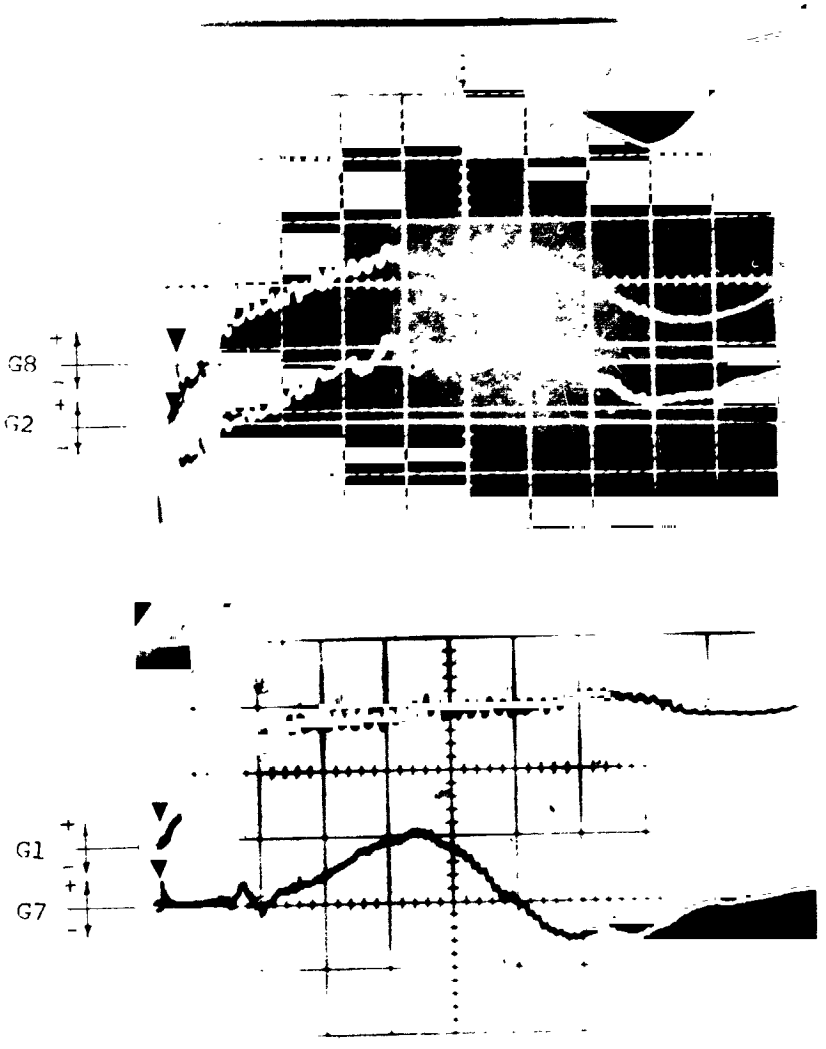

GAGE 8
E_x: 0.5%/DIV

GAGE 2
E_x: 0.5%/DIV

GAGE 1
E_x: 3%/DIV

GAGE 7
E_x: 0.5%/DIV

FIG. 20 UNCORRECTED TRANSIENT STRAIN RECORDS FOR STEEL-SPHERE IMPACTED 6061-T651 ALUMINUM BEAM MODEL CB-11

ABSCISSA: TIME, 100 μSEC/DIV
ORDINATE: UNCORRECTED RELATIVE ELONGATION E_x IN PER CENT
+ = TENSION
- = COMPRESSION
V: INSTANT OF IMPACT

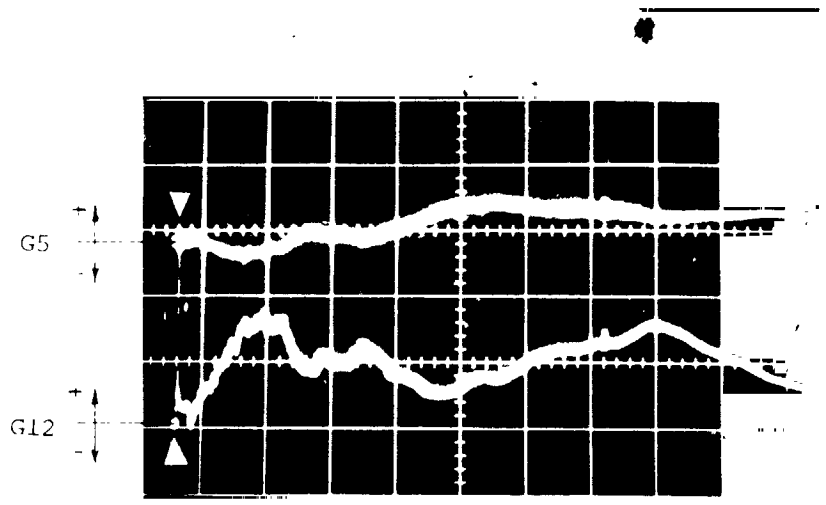

GAGE 5
E_x: 1.5%/DIV

GAGE 12
E_x: 0.5%/DIV

FIG. 20 CONCLUDED (CB-11)

ABSCISSA: TIME, 50 μSEC/DIV
ORDINATE: UNCORRECTED RELATIVE ELONGATION E_x IN PER CENT
+ = TENSION
- = COMPRESSION
▽: INSTANT OF IMPACT

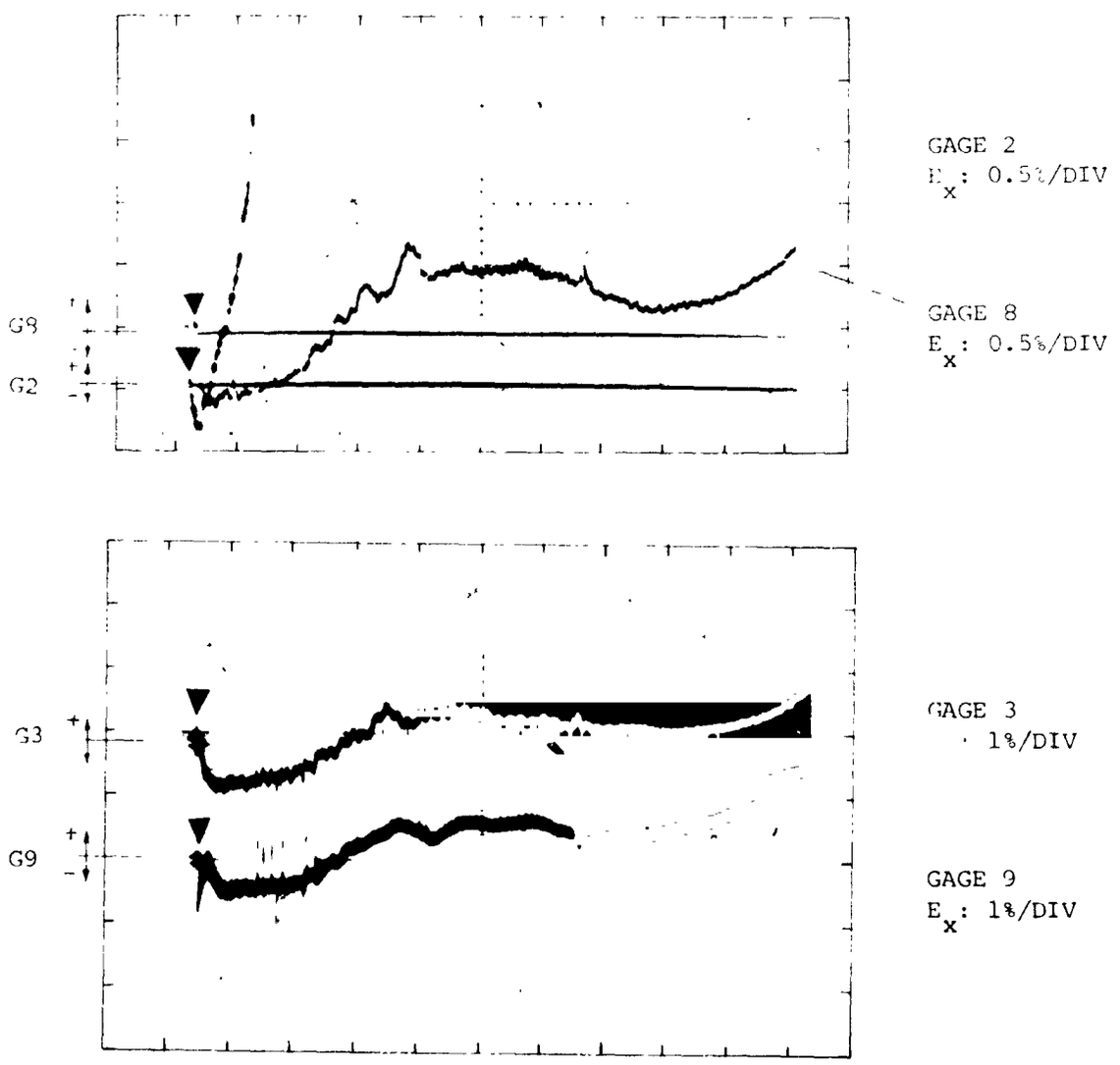

FIG. 21 UNCORRECTED TRANSIENT STRAIN RECORDS FOR STEEL-SPHERE IMPACTED 6061-T651 ALUMINUM BEAM MODEL CB-12

ABSCISS: TIME
ORDINATE: UNCORRECTED RELATIVE ELONGATION E_x IN PER CENT
+ = TENSION
- = COMPRESSION
▽: INSTANT OF IMPACT

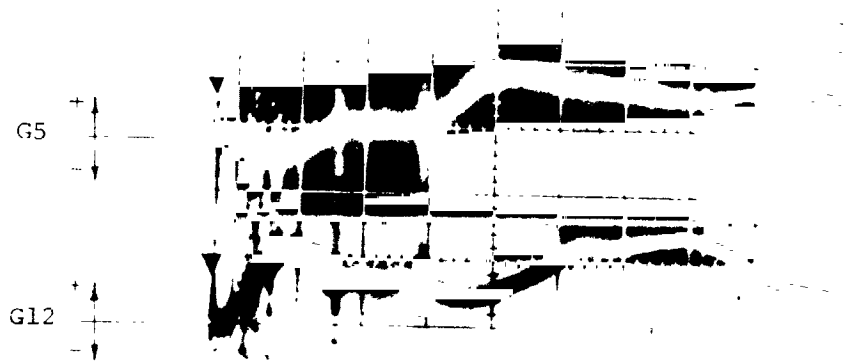

GAGE 5
E_x: 1.5%/DIV
100 μSEC/DIV

GAGE 12
E_x: 1%/DIV
100 μSEC/DIV

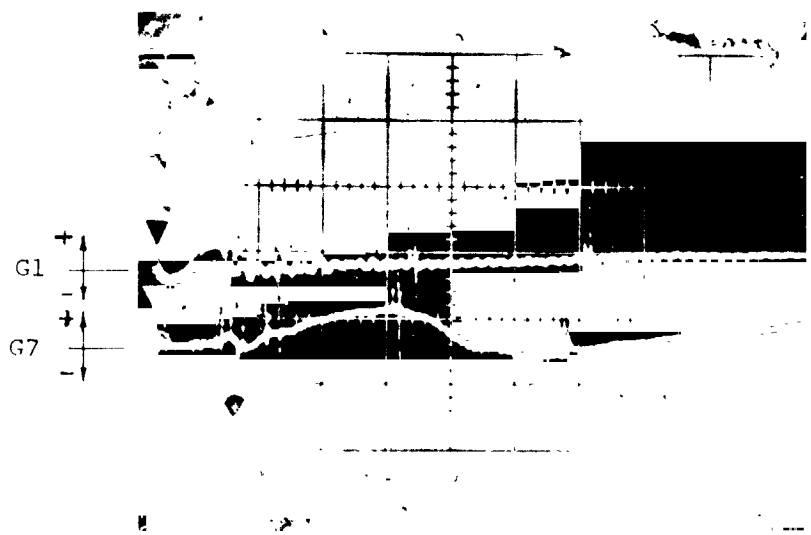

GAGE 1
E_x: 3%/DIV
50 μSEC/DIV

GAGE 7
E_x: 1%/DIV
50 μSEC/DIV

FIG. 21 CONCLUDED (CB-12)

ABSCISSA: TIME, 50 μSEC/DIV
ORDINATE: UNCORRECTED RELATIVE ELONGATION E_x IN PER CENT
+ = TENSION
- = COMPRESSION
∇: INSTANT OF IMPACT

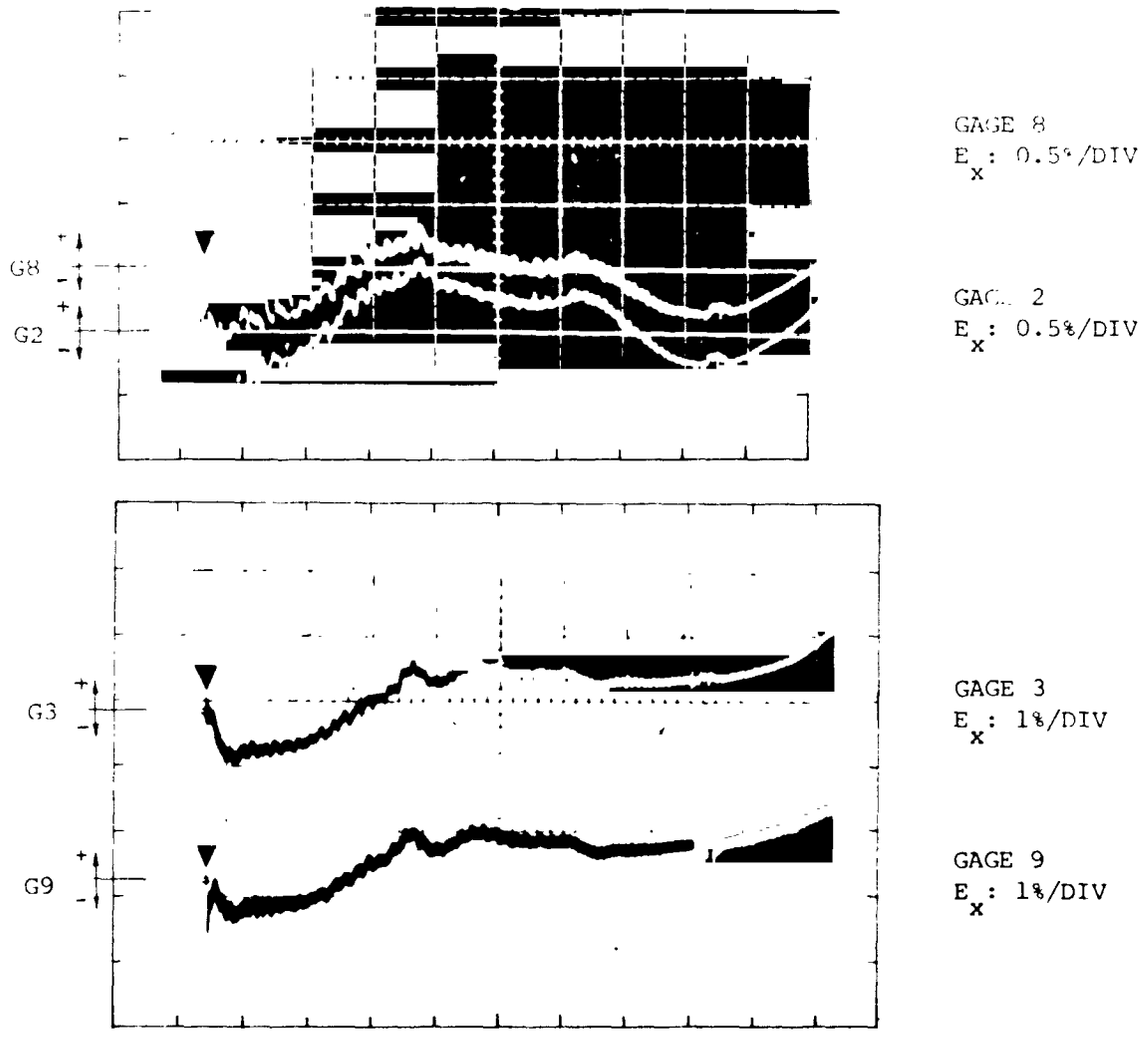

FIG. 22 UNCORRECTED TRANSIENT STRAIN RECORDS FOR STEEL-SPHERE IMPACTED 6061-T651 ALUMINUM BEAM MODEL CB-13

ABSCISSA: TIME
ORDINATE: UNCORRECTED RELATIVE ELONGATION E_x IN PER CENT
+ = TENSION
- = COMPRESSION
▽: INSTANT OF IMPACT

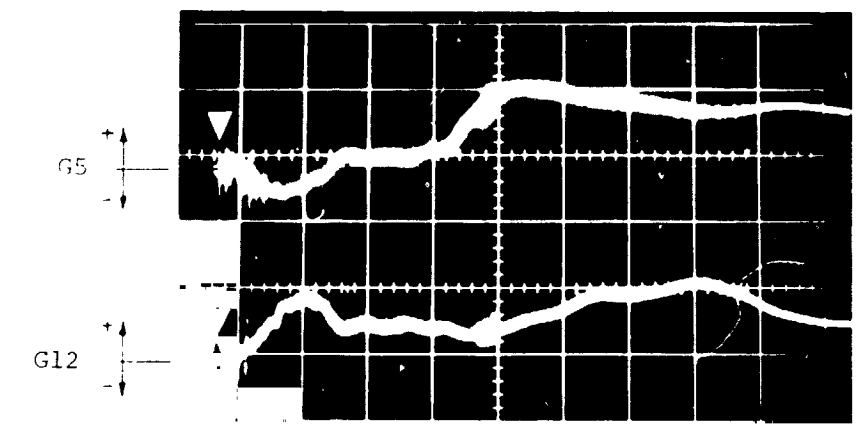

GAGE 5
E_x: 1.5%/DIV
100 μSEC/DIV

GAGE 12
E_x: 1%/DIV
100 μSEC/DIV

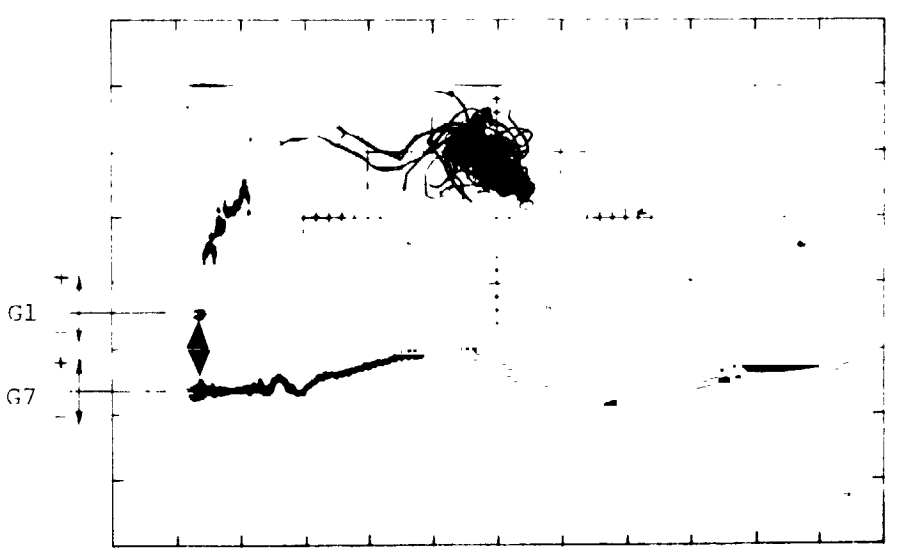

GAGE 1
E_x: 3%/DIV
50 μSEC/DIV

GAGE 7
E_x: 1%/DIV
50 μSEC/DIV

FIG. 22 CONCLUDED (CB-13)

ABSCISSA: TIME
ORDINATE: UNCORRECTED RELATIVE ELONGATION E_x IN PER CENT
+ = TENSION
- = COMPRESSION
∇: INSTANT OF IMPACT

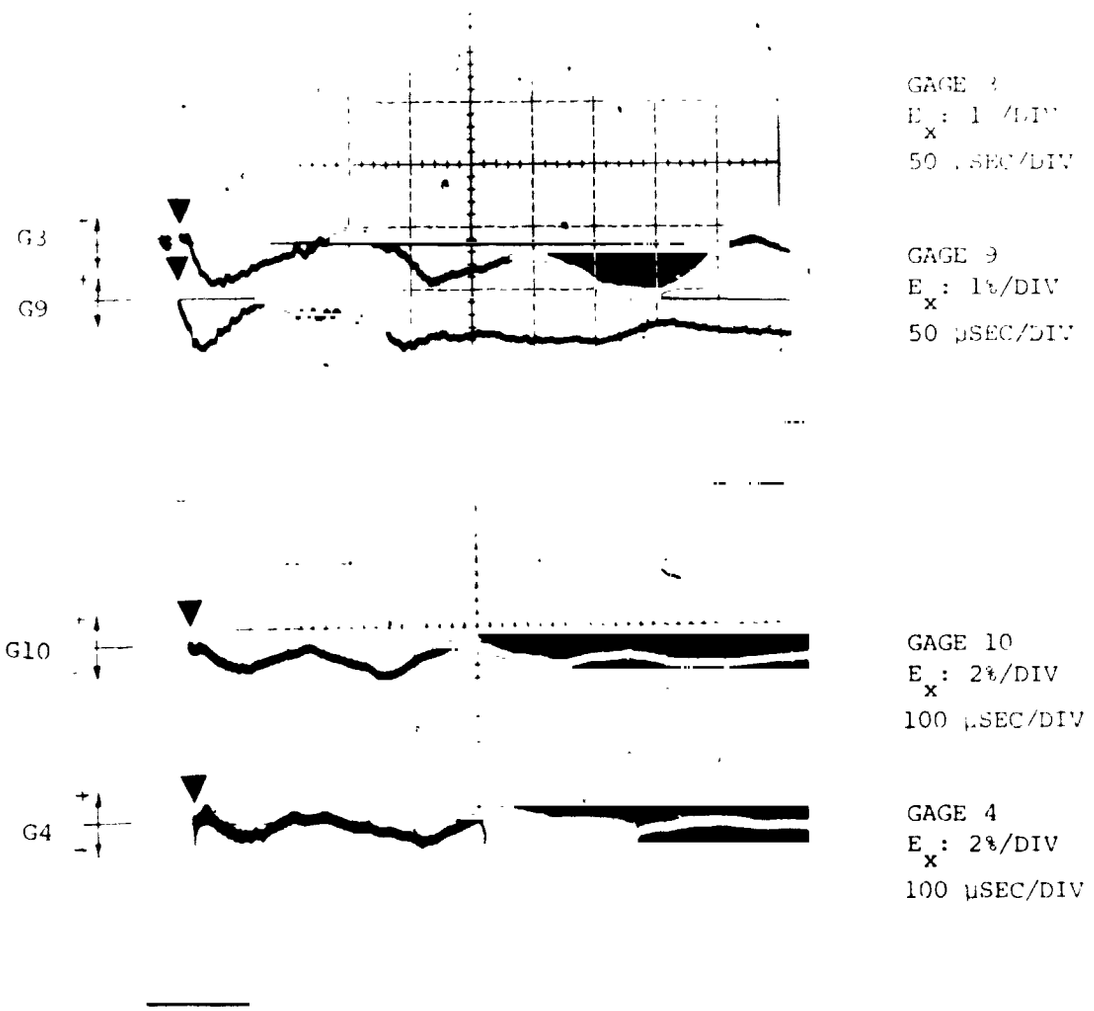

FIG. 23 UNCORRECTED TRANSIENT STRAIN RECORDS FOR STEEL-SPHERE IMPACTED 6061-T651 ALUMINUM BEAM MODEL CB-14

ABSCISSA: TIME, 100 μSEC/DIV
ORDINATE: UNCORRECTED RELATIVE ELONGATION E_x IN PER CENT
+ = TENSION
- = COMPRESSION
V: INSTANT OF IMPACT

GAGE 5
E_x: 2%/DIV

GAGE 12
E_x: 2%/DIV

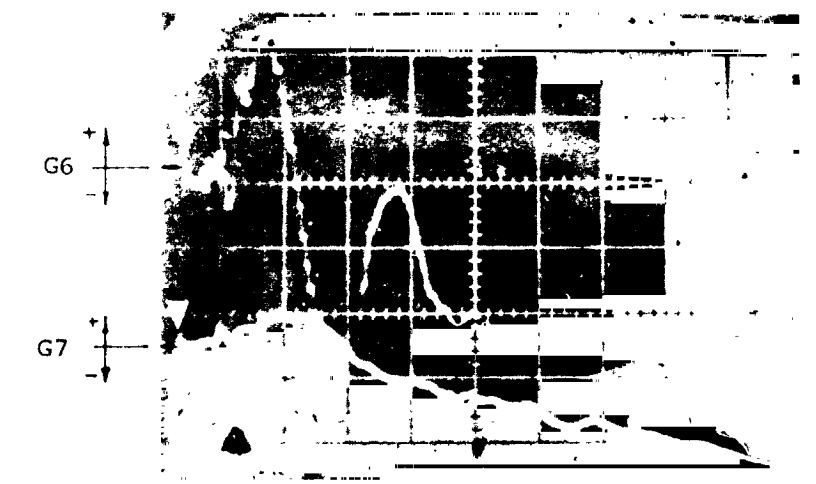

GAGE 6
E_x: 1%/DIV

GAGE 7
E_x: 1%/DIV

FIG. 23 CONCLUDED (CB-14)

ABSCISSA: TIME
ORDINATE: UNCORRECTED RELATIVE ELONGATION E_x IN PER CENT
+ = TENSION
- = COMPRESSION
V: INSTANT OF IMPACT

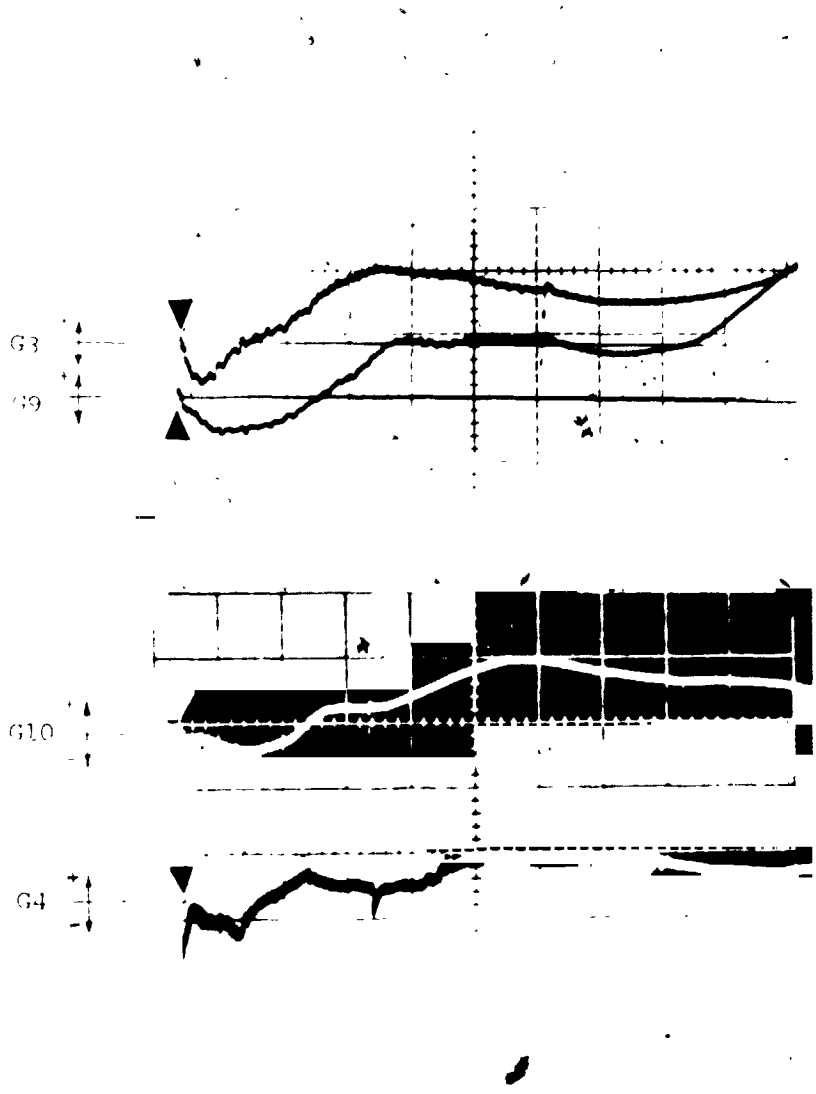

GAGE 3
E_x: 1%/DIV
50 µSEC/DIV

GAGE 9
E_x: 1%/DIV
50 µSEC/DIV

GAGE 10
E_x: 2%/DIV
100 µSEC/DIV

GAGE 4
E_x: 2%/DIV
100 µSEC/DIV

FIG. 24 UNCORRECTED TRANSIENT STRAIN RECORDS FOR STEEL-SPHERE IMPACTED 6061-T651 ALUMINUM BEAM MODEL CB-15

ABSCISSA: TIME, 100 μSEC/DIV
ORDINATE: UNCORRECTED RELATIVE ELONGATION E_x IN PER CENT
+ = TENSION
- = COMPRESSION
V: INSTANT OF IMPACT

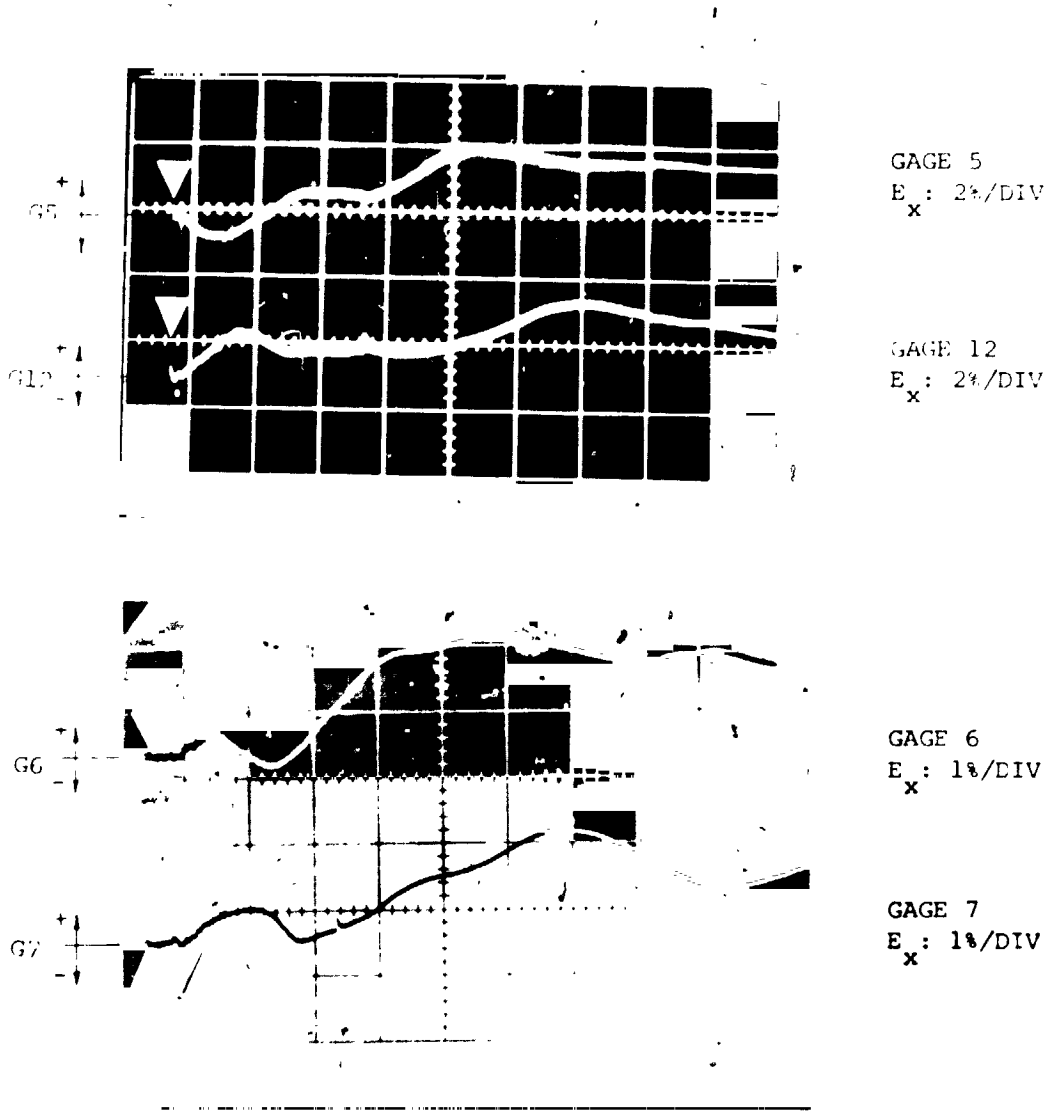

FIG. 24 CONCLUDED (CB-15)

ABSCISSA: TIME
ORDINATE: UNCORRECTED RELATIVE ELONGATION E_x IN PER CENT
+ = TENSION
- = COMPRESSION
∇: INSTANT OF IMPACT

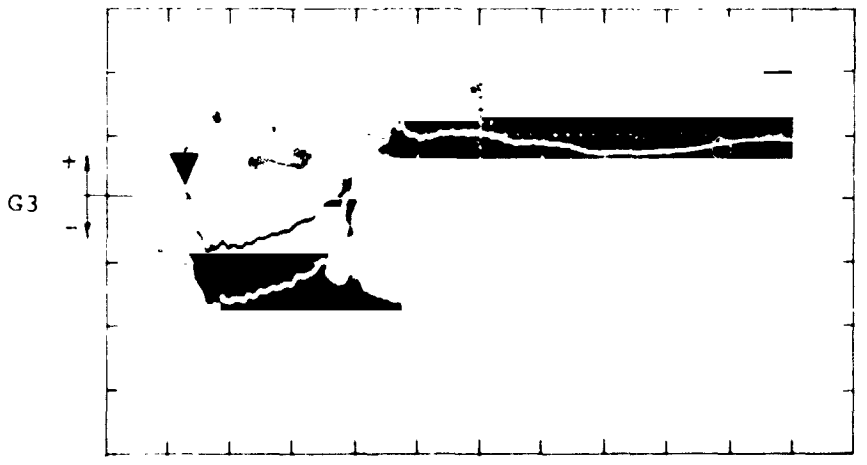

GAGE 3
E_x: 1%/DIV
50 μSEC/DIV

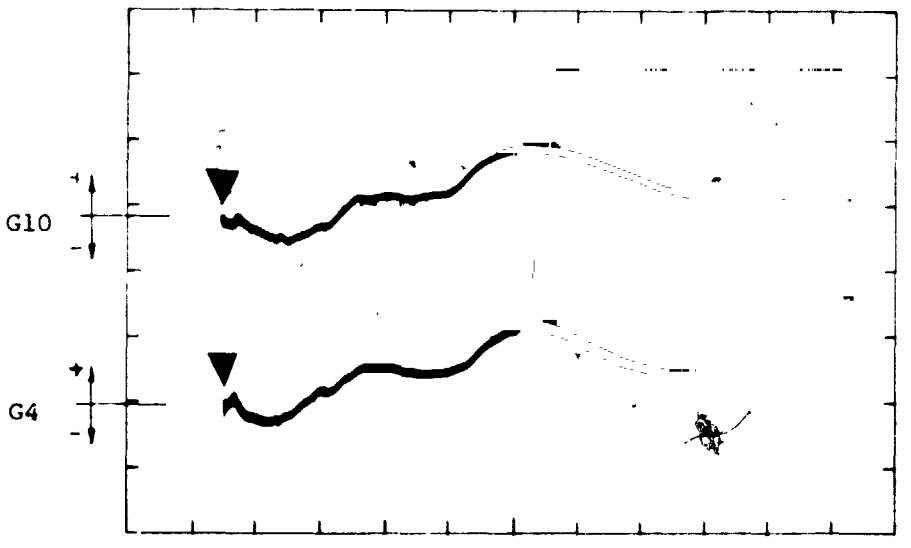

GAGE 10
E_x: 2%/DIV
100 μSEC/DIV

GAGE 4
E_x: 2%/DIV
100 μSEC/DIV

FIG. 25 UNCORRECTED TRANSIENT STRAIN RECORDS FOR STEEL-SPHERE IMPACTED 6061-T651 ALUMINUM BEAM MODEL CB-16

ABSCISSA: TIME, 100 μSEC/DIV
ORDINATE: UNCORRECTED RELATIVE ELONGATION E_x IN PER CENT
+ = TENSION
- = COMPRESSION
▽: INSTANT OF IMPACT

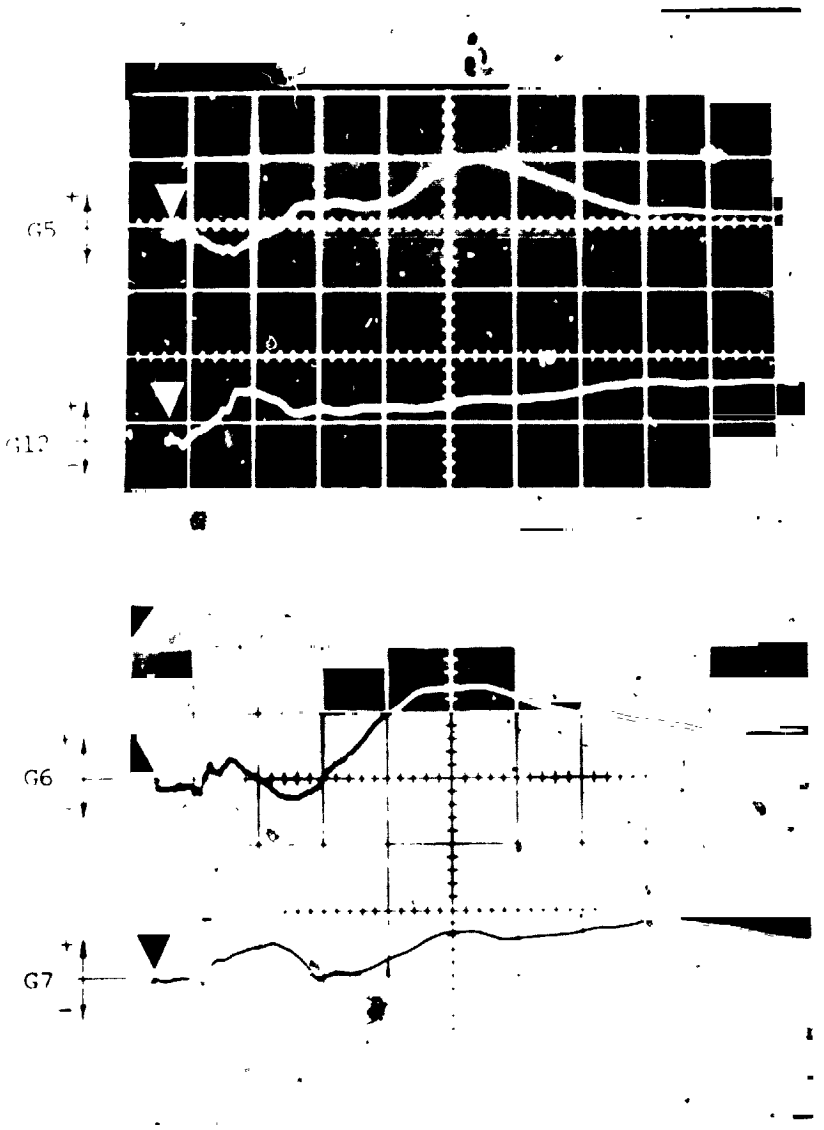

FIG. 25 CONCLUDED (CB-16)

ABSCISSA: TIME
ORDINATE: UNCORRECTED RELATIVE
ELONGATION E_x IN PER CENT
+ = TENSION
- = COMPRESSION
↓: INSTANT OF IMPACT

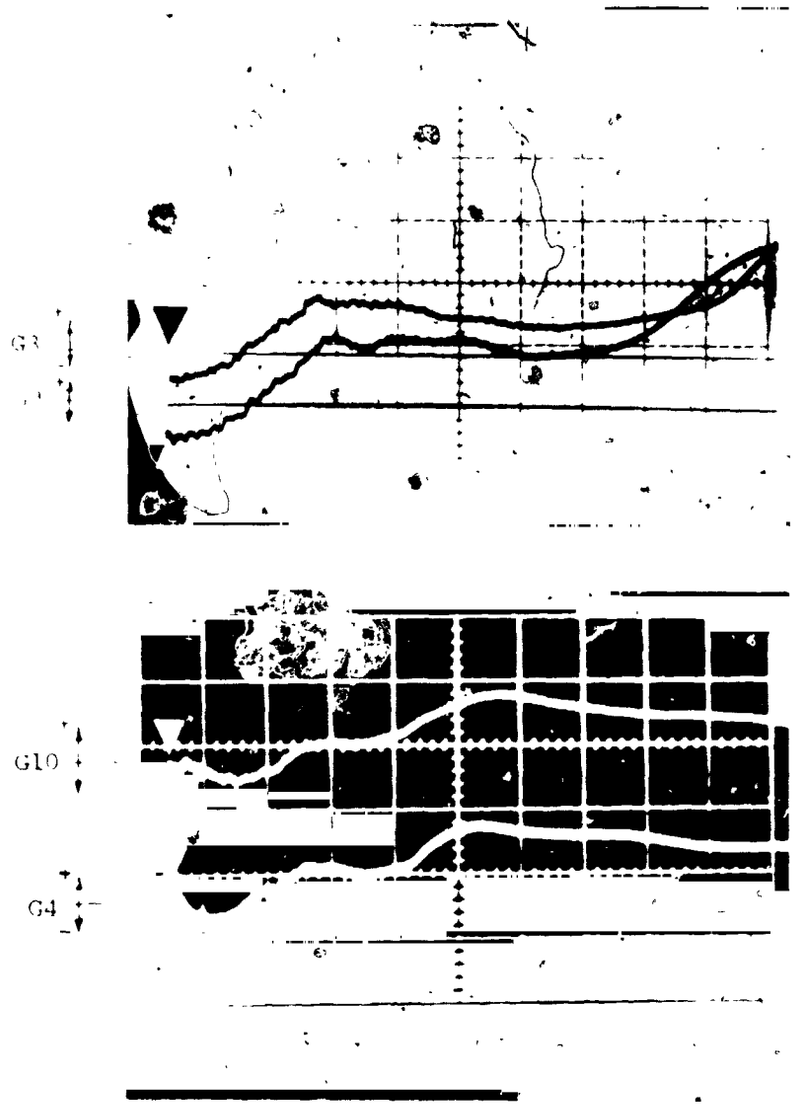

GAGE 3
E_x: 1 %/DIV
5 μSEC/DIV

Gage 9
E_x: 1%/DIV
50 μSEC/DIV

GAGE 10
E_x: 2%/DIV
100 μSEC/DIV

GAGE 4
E_x: 2 %/DIV
100 μSEC/DIV

FIG. 26 UNCORRECTED TRANSIENT STRAIN RECORDS FOR STEEL-SPHERE IMPACTED 6061-T651 ALUMINUM BEAM MODEL CB-17

ABSCISSA: TIME, 100 μSEC/DIV
ORDINATE: UNCORRECTED RELATIVE ELONGATION E_x IN PER CENT
+ = TENSION
- = COMPRESSION
∇: INSTANT OF IMPACT

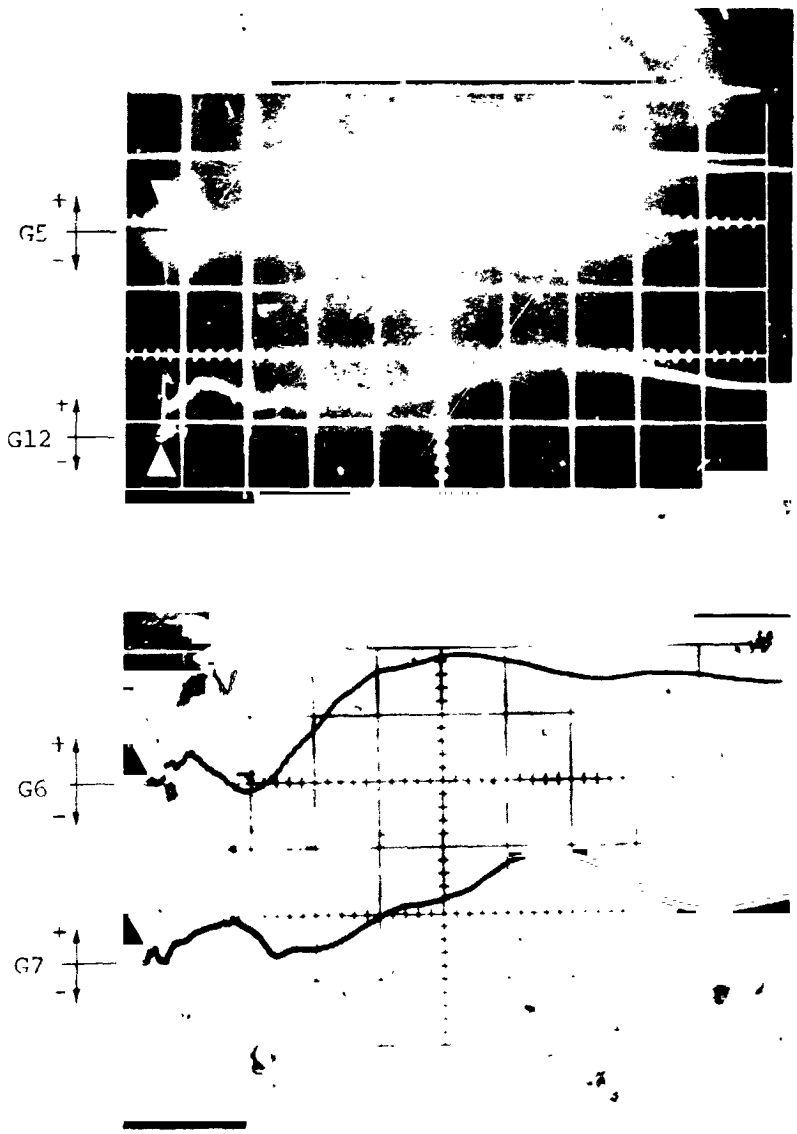

GAGE 5
E_x: 2%/DIV

GAGE 12
E_x: 2%/DIV

GAGE 6
E_x: 1%/DIV

GAGE 7
E_x: 1%/DIV

FIG. 26 CONCLUDED (CB-17)

ABSCISSA: TIME
ORDINATE: UNCORRECTED RELATIVE ELONGATION E_x IN PER CENT
+ = TENSION
- = COMPRESSION
▽: INSTANT OF IMPACT

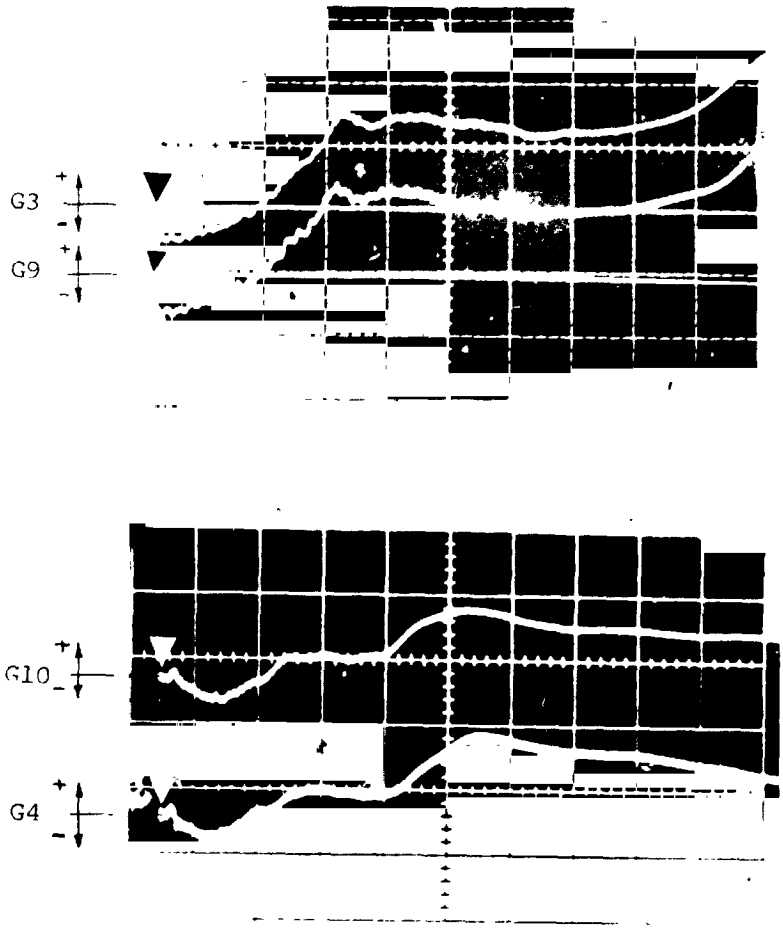

GAGE 3
E_x: 1%/DIV
50 μSEC/DIV

GAGE 9
E_x: 1%/DIV
50 μSEC/DIV

GAGE 10
E_x: 2%/DIV
100 μSEC/DIV

Gage 4
E_x: 2%/DIV
100 μSEC/DIV

FIG. 27 UNCORRECTED TRANSIENT STRAIN RECORDS FOR STEEL-SPHERE IMPACTED 6061-T651 ALUMINUM BEAM MODEL CB-18

ABSCISSA: TIME, 100 μSEC/DIV
ORDINATE: UNCORRECTED RELATIVE ELONGATION E_x IN PER CENT
+ = TENSION
- = COMPRESSION
▽: INSTANT OF IMPACT

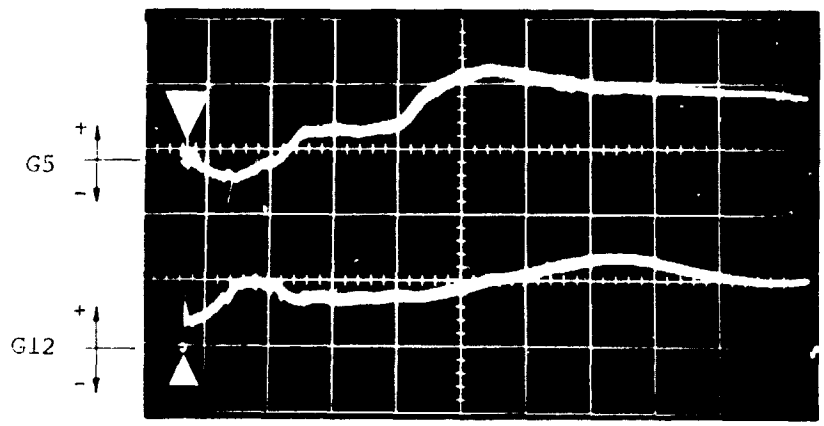

GAGE 5
E_x: 2%/DIV

GAGE 12
E_x: 2%/DIV

FIG. 27 CONCLUDED (CB-18)

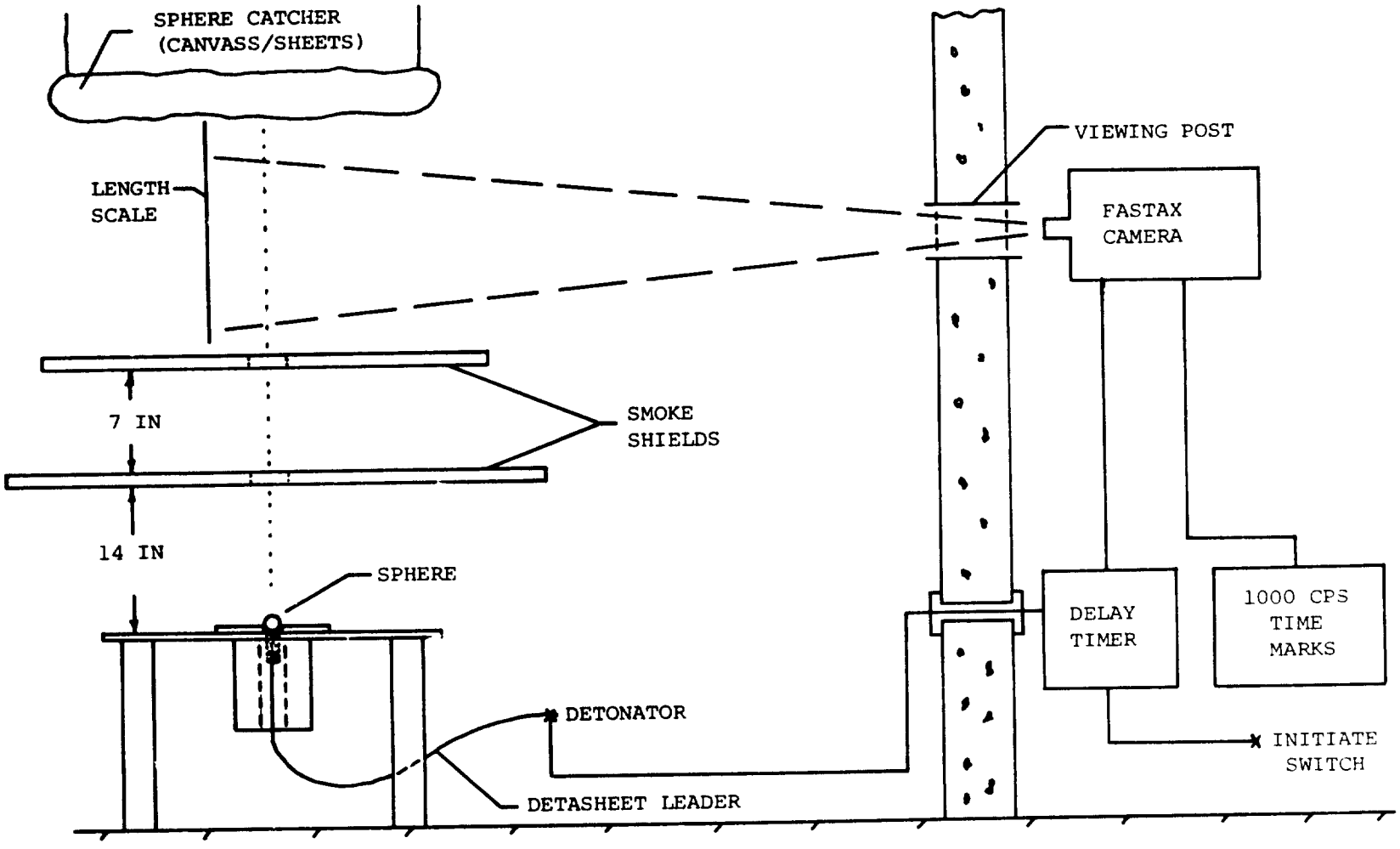

(a) Overall Schematic

FIG. 28 TEST SCHEMATIC FOR STEEL SPHERE POSITION VERSUS TIME MEASUREMENTS

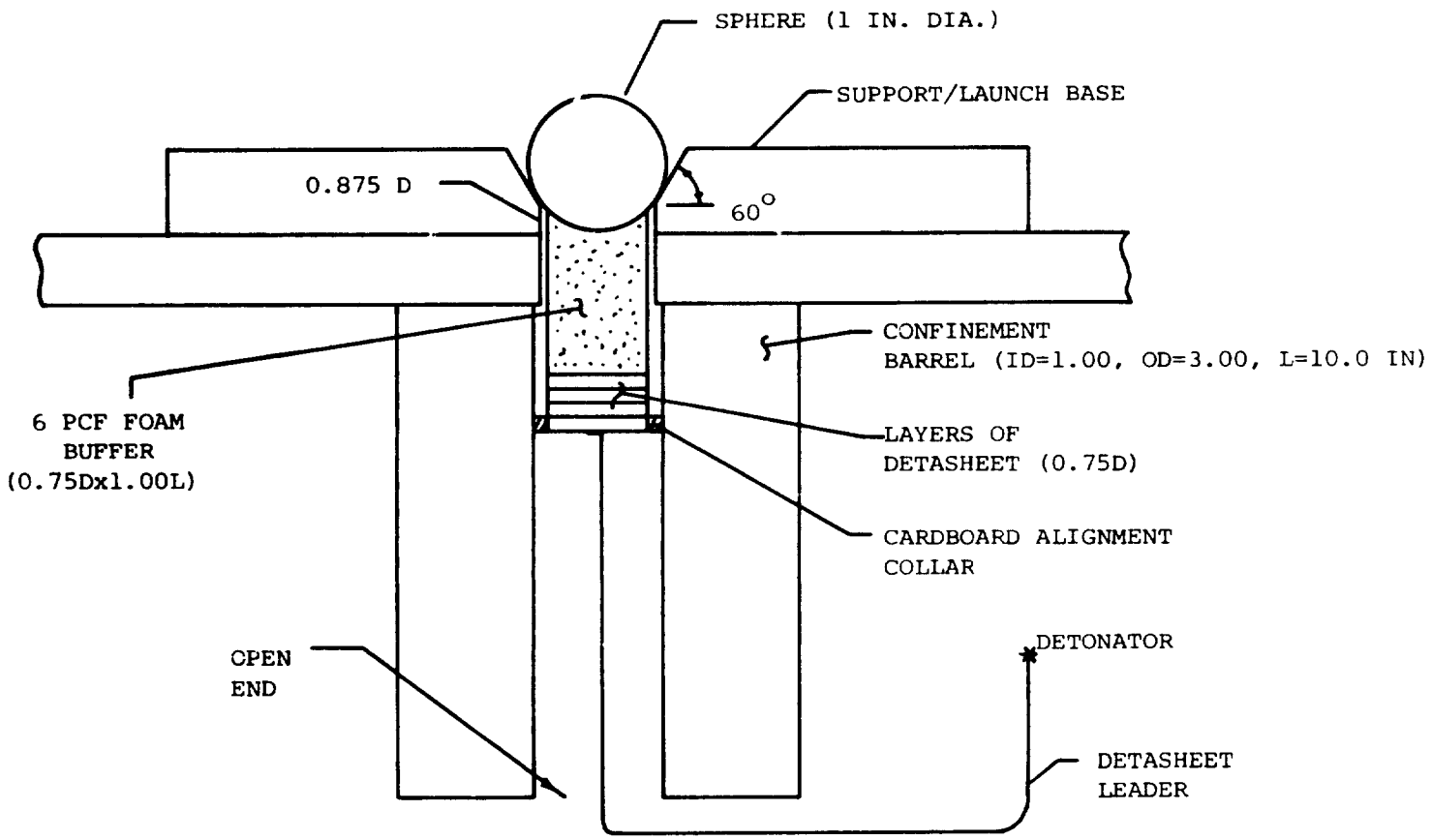

(b) Cross-Section Schematic of Sphere-Launching Arrangement

FIG. 28 CONCLUDED

APPENDIX A

STATIC UNIAXIAL STRESS-STRAIN PROPERTIES OF

6061-T651 ALUMINUM

A.1 Procedure

Static uniaxial stress-strain tests were conducted on samples of the aluminum material from which the present models were prepared; those data are given in Ref. 7 but are repeated here for the reader's convenience. Test specimens nominally of 0.36-inch diameter and 0.75-inch long "working section" were prepared and instrumented with Micro-Measurements, Inc. precision-type high-elongation strain gages (Type EP-08-210DA-350); the outputs from strain gages on opposite sides of each specimen were combined in a Wheatstone bridge to cancel out inadvertent bending effects. The resulting outputs were either read from an SR-4 strain indicator or were recorded on a Hewlett-Packard Model Moseley 7005B x,y recorder. These specimens were tested using a calibrated Baldwin Model FGT Testing Machine (screw driven) operating at its slowest rate.

The output from the strain gage bridge, accounting for the changing gage factor as a function of the strain level at high strains (Refs. 8 and 10) provides a measure of the axial-direction relative elongation E_1:

$$E_1 = \frac{\ell - \ell_o}{\ell_o} \tag{A.1}$$

where $\ell(\ell_o)$ represents the current (original) gage length. In turn, the axial Cartesian tensor strain component γ_{11} is related to E_1 by

$$E_1 = \sqrt{1 + 2\gamma_{11}} - 1 \tag{A.2}$$

Hence,

$$\gamma_{11} = E_1 + \frac{1}{2}E_1^2 \tag{A.3}$$

where, in usual tensor notation

$$\gamma_{mn} = \frac{1}{2}\left[\frac{\partial u_n}{\partial y_m} + \frac{\partial u_m}{\partial y_n} + \frac{\partial u_k}{\partial y_m}\frac{\partial u_k}{\partial y_n} \right] \tag{A.4}$$

In Eq. A.4, the y_m are rectangular Cartesian coordinates which serve to define the "undeformed location" of material particles in the body, and the u_m represent the displacement components for any given material point in the body.

From the measured axial load P (in the y_1 direction) applied to the specimen, one can determine the engineering stress $(\sigma_{11})_E$ -- or simply σ_E -- from

$$(\sigma_{11})_E \equiv \sigma_E = \frac{P}{A_o} \tag{A.5}$$

where A_o represents the measured (known) cross-sectional area of the specimen before the load was applied. Thus, if desired, one can depict the uniaxial stress-strain behavior of these specimens in terms of σ_E versus γ_{11}.

An alternative means of presenting such stress-strain data is to display the true stress $(\sigma_{11})_T$ -- or simply σ_T versus γ_{11}, where

$$(\sigma_{11})_T \equiv \sigma_T = \frac{P}{A} = \frac{P}{A_o}\frac{A_o}{A} = \sigma_E \frac{A_o}{A} \tag{A.6}$$

In Eq. A.6, A represents the current cross-sectional area of the deformed specimen. In terms of the Poisson ratio ν, one may write the area ratio A/A_o as

$$\frac{A}{A_o} = [1 - \nu E_1][1 - \nu E_1] \tag{A.7}$$

Hence, Eq. A.6 becomes:

$$\sigma_T = \frac{\sigma_E}{[1 - \nu E_1][1 - \nu E_1]} \tag{A.8}$$

Noting that for the elastic range of aluminum behavior $\nu \doteq 1/3$ while in the "fully plastic" range ν becomes 1/2, one can make a reasonably accurate estimate of σ_T for the entire range of the measured behavior of stress versus γ_{11}. An example of each of these limiting cases is displayed in Fig. A.1 for 6061-T6 aluminum. One can choose a plausible faired transition curve which is reasonable for engineering purposes.

For the reader's convenience, plots of true stress σ_T vs. γ_{11} and engineering stress σ_E vs. γ_{11} are included in this report. Since yield, flow, and plastic deformation are handled conveniently via appropriate yield criteria and flow rules in terms of true stress, the σ_T vs. γ_{11} data are approximated herein by straight-line segment fitting for possible use in the mechanical sublayer model (see Refs. 1-5, for example, and Subsection A.3). The resulting data plots and the selected straight-line-segment approximations for each of these materials are given in Subsection A.2.

A.2 Data for 6061-T651 Aluminum

The 6061-T651 uniaxial test specimens were prepared from samples taken from the thick flat plate stock from which the beam models described in Sections 2 and 3 were machined. The axis of these test specimens were either parallel to or perpendicular to the roll direction of the plate stock, respectively; these specimens are denoted as longitudinal (L) or transverse (T). Seven specimens of each type were tested; some in monotonic tension, some in monotonic compression, one in tension to well beyond yielding and then "cycled", and one first in compression to well beyond yielding and then "cycled".

True stress σ_T versus γ_{11} is shown for uniaxial monotonic stress-strain tests for tension in Fig. A.2 and for compression in Fig. A.3 for 6061-T651 material. Note that the longitudinal and the transverse specimens of the 6061-T651 material show almost identical stress-strain behavior; hence, this material appears to be essentially isotropic, at least initially.

Figures A.4 and A.5 show σ_T vs. γ_{11} for 6061-T651 specimens loaded to beyond yielding first, respectively, in tension or compression and then "cycled". Here again the longitudinal specimens and the transverse specimens

exhibit nearly identical behavior. Plots of σ_E vs. γ_{11} are given in Figs. A.6 and A.7.

The monotonic loading data of Figs. A.2 and A.3 and the "cyclic" data of Figs. A.4 and A.5 have been employed in a trial-and-error process to select straight-line-segment approximations for possible use in the mechanical-sublayer model. For most practical purposes, yield stress magnitudes selected for representing these two materials by the mechanical sublayer model can be the same in compression as in tension. Shown in Table A.1 are the resulting selected 1-sublayer, 2-sublayer, and 3-sublayer approximations to these data. Of course, other fits would be selected if one desired to emphasize either the tension or the compression behavior.

A.3 Mechanical Sublayer Model Representation of Uniaxial Stress-Strain Data

Included for the reader's convenience is the following terse description of a straight-line-segment approximation of uniaxial stress-strain data by a scheme known as the mechanical-sublayer model. In this model the material is conceived of as behaving like a collection of n "sublayers" of elastic, perfectly-plastic material with all sublayers experiencing identical strain and having an identical elastic modulus, E, but having appropriately different yield stresses. For the static case, the yield stress σ_{ok} of the kth sublayer is given by $E\gamma_K$, where γ_k is the strain at the kth "corner" σ_k, γ_k of the straight-line-segment approximation of the stress-strain curve. The stress σ in the material is then expressed as the weighted sum of the contributions from each sublayer as given by

$$\sigma = \sum_{k=1}^{n} C_k \sigma_k(\gamma) \tag{A.9}$$

where C_k is a weighting factor for the kth sublayer and is given by

$$C_k = \frac{E_k - E_{k+1}}{E} \tag{A.10}$$

where

$$E_1 \equiv E \; ; \; E_k = \frac{\sigma_k - \sigma_{k-1}}{\gamma_k - \gamma_{k-1}} \text{ for } k = 1, 2, \ldots n$$
$$\text{and } E_{n+1} = 0 \tag{A.11}$$

The following steps indicate how the stress is computed for a given sequence of strain values:

1. To begin, assume that at strain state γ_j all of the $(\sigma_k)_j$ are known ($k = 1, 2, \ldots, n$).
2. Next, consider a prescribed strain increment $\Delta\gamma_{j+1}$ such that $\gamma_{j+1} = \gamma_j + \Delta\gamma_{j+1}$. Then proceed to determine $(\sigma_k)_{j+1}$ by:

$$\left(\overset{t}{\sigma_k}\right)_{j+1} = (\sigma_k)_j + E\,\Delta\gamma_{j+1} \qquad \text{"trial value"} \tag{A.12}$$

$$\Delta\gamma_{j+1}\begin{cases} > 0 \rightarrow \left(\overset{t}{\sigma_k}\right)_{j+1} \begin{cases} > \sigma_{ok} \rightarrow (\sigma_k)_{j+1} = \sigma_{ok} \\ \leq \sigma_{ok} \rightarrow (\sigma_k)_{j+1} = \left(\overset{t}{\sigma_k}\right)_{j+1} \end{cases} \\ = 0 \rightarrow \left(\overset{t}{\sigma_k}\right)_{j+1} = (\sigma_k)_j = (\sigma_k)_{j+1} \\ < 0 \rightarrow \left(\overset{t}{\sigma_k}\right)_{j+1} \begin{cases} \geq -\sigma_{ok} \rightarrow (\sigma_k)_{j+1} = \left(\overset{t}{\sigma_k}\right)_{j+1} \\ < -\sigma_{ok} \rightarrow (\sigma_k)_{j+1} = -\sigma_{ok} \end{cases} \end{cases} \tag{A.13}$$

This procedure is applied to all sublayers $k = 1, 2, \ldots, n$; then eq. A.9 is employed to compute $\sigma(\gamma_{j+1})$.

The described procedure applies to cases in which the tension and compressive behaviors are "symmetric".

TABLE A.1

COORDINATES FOR STRAIGHT-LINE-SEGMENT FITTING* OF 6061-T651

UNIAXIAL STATIC DATA FOR TRUE STRESS σ_T VERSUS γ_{11}

1-SUBLAYER FIT		2-SUBLAYER FIT		3-SUBLAYER FIT	
σ_T (psi)	γ_{11} (in/in)	σ_T (psi)	γ_{11} (in/in)	σ_T (psi)	γ_{11} (in/in)
$\pm$ 50,000	$\pm$ .0050	$\pm$ 46,000	$\pm$ .0046	$\pm$ 44,000	$\pm$ .0044
		$\pm$ 58,000	$\pm$ .1800	$\pm$ 47,800	$\pm$ .0280
				$\pm$ 58,000	$\pm$ .1800

σ_T = true stress = (load)/(current area)

γ_{11} --- see Eqs. A.3 and A.4

Elastic Modulus = E = 10×10^6 psi

*This is a "balanced fitting" for both tension and compression. Different fits would be chosen if one wished to emphasize either the tension or the compression behavior.

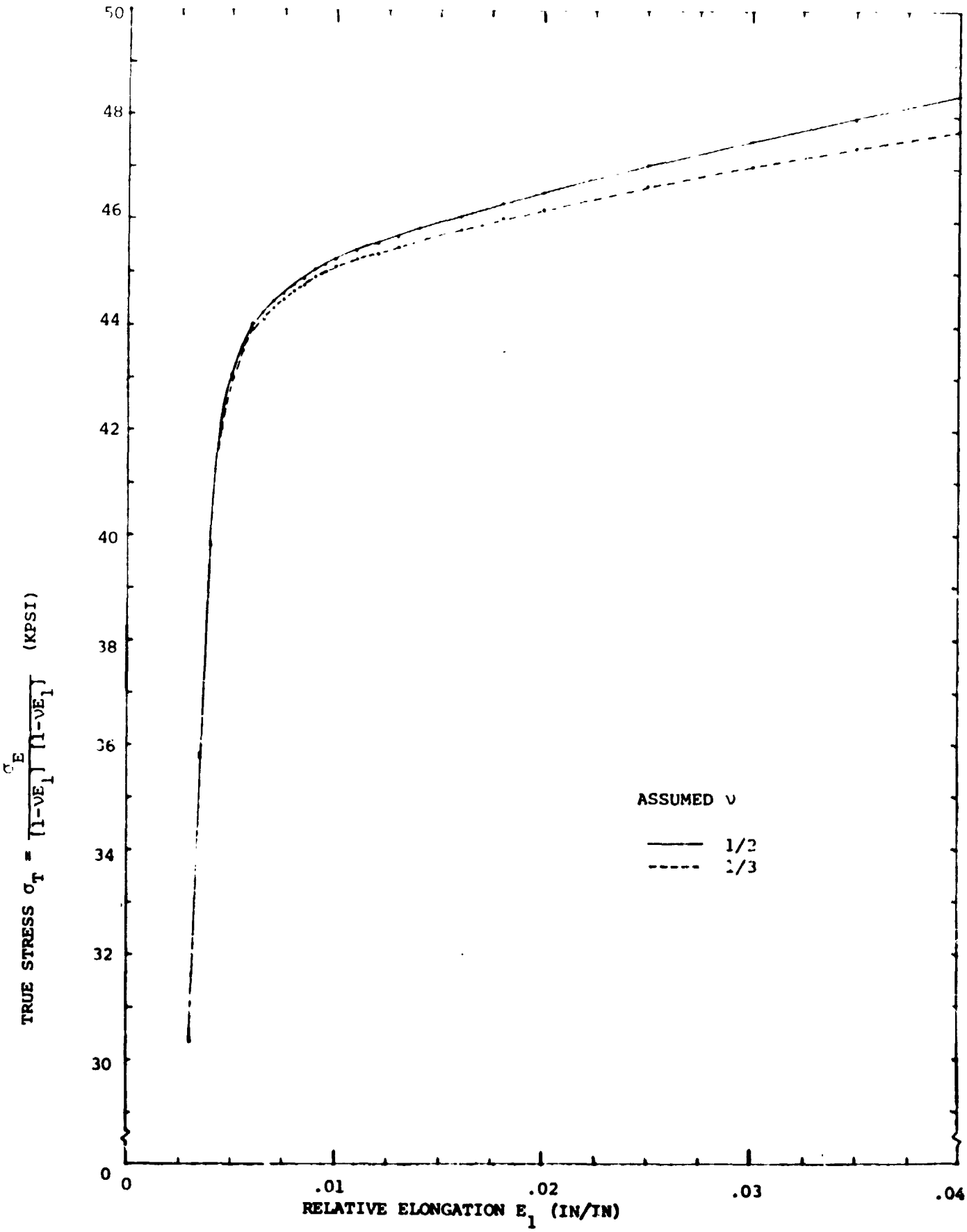

FIG. A.1 EFFECT OF POISSON'S RATIO ν ON CALCULATED TRUE STRESS FOR 6061-T651 TENSILE UNIAXIAL STATIC STRESS-STRAIN DATA

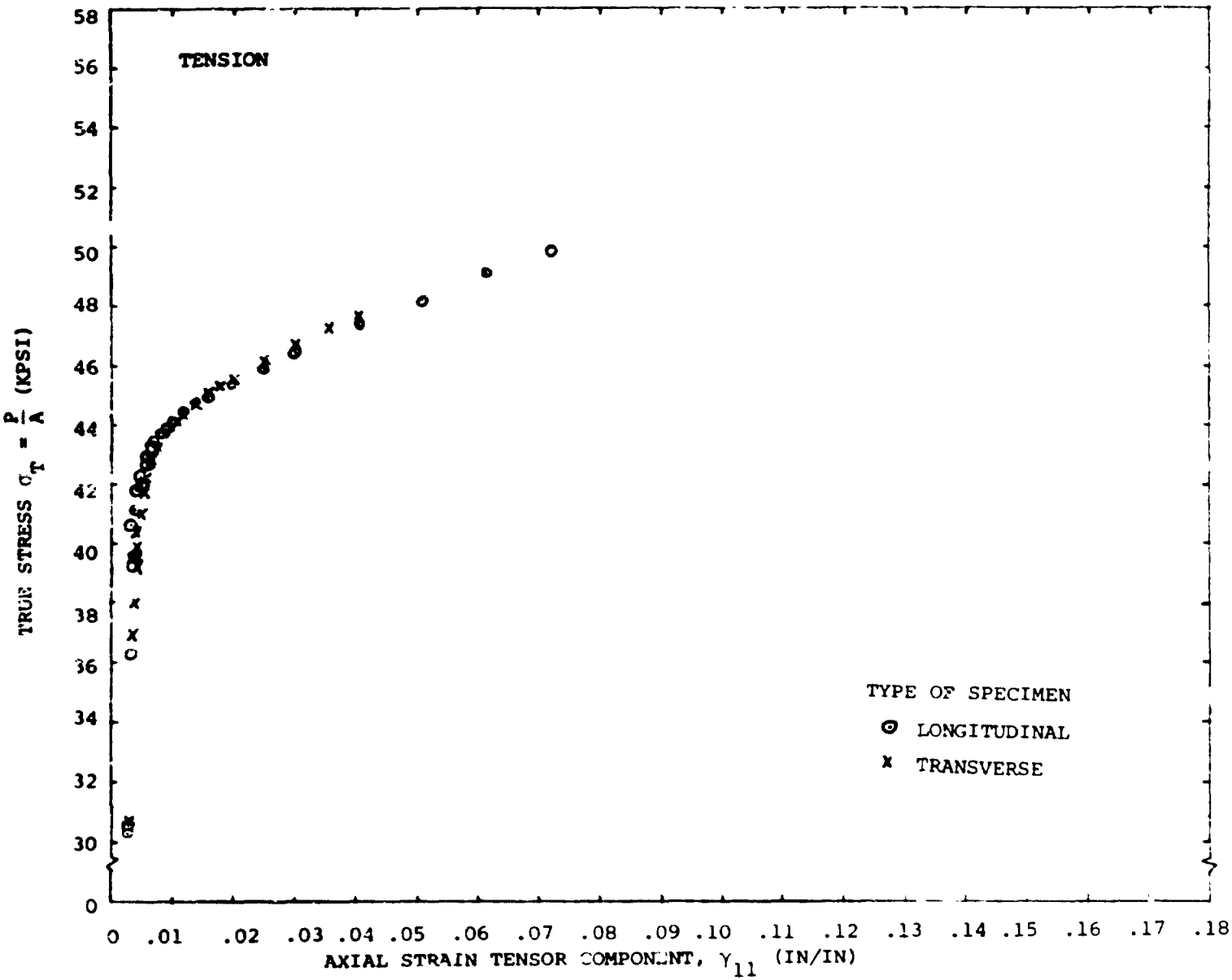

FIG. A.2 TENSILE UNIAXIAL STATIC STRESS-STRAIN DATA FOR 6061-T651 PLATE STOCK: σ_T VS. γ_{11}

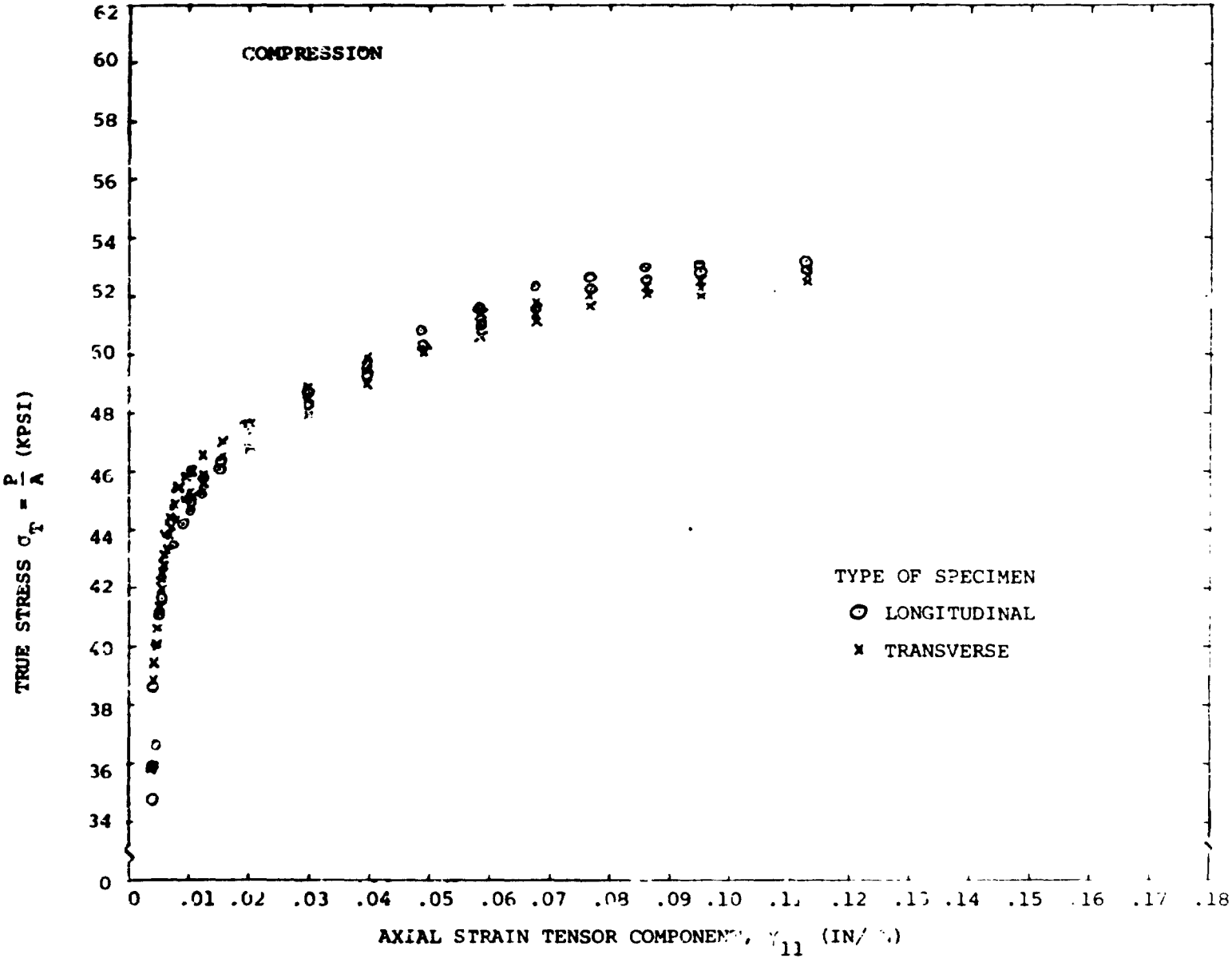

FIG. A.3 COMPRESSION UNIAXIAL STATIC STRESS-STRAIN DATA FOR 6061-T651 PLATE STOCK: σ_T VS. γ_{11}

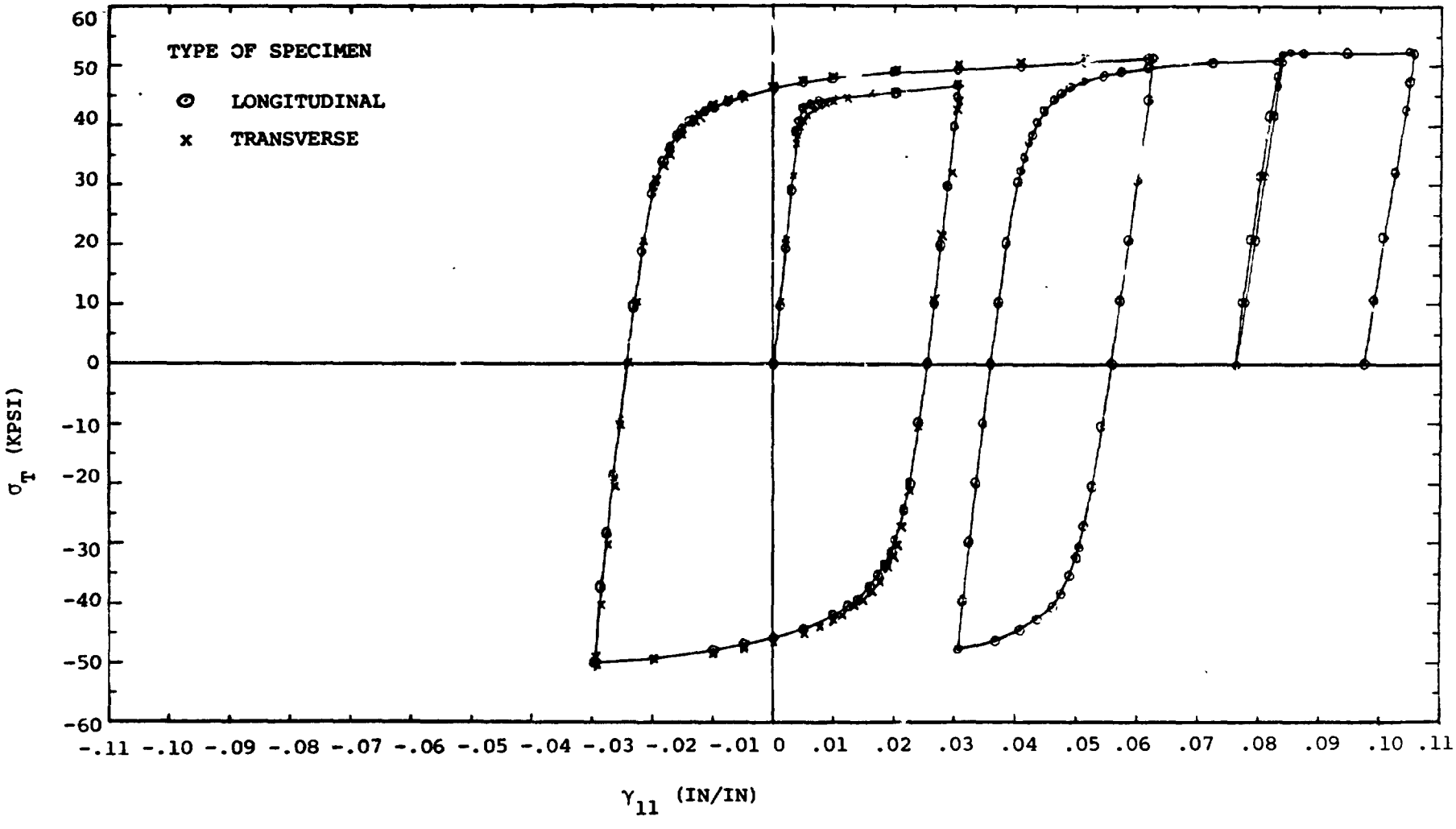

FIG. A.4 UNIAXIAL STATIC STRESS-STRAIN DATA FOR 6061-T651 PLATE MATERIAL, LOADED FIRST IN TENSION AND THEN "CYCLED": σ_T VS. γ_{11}

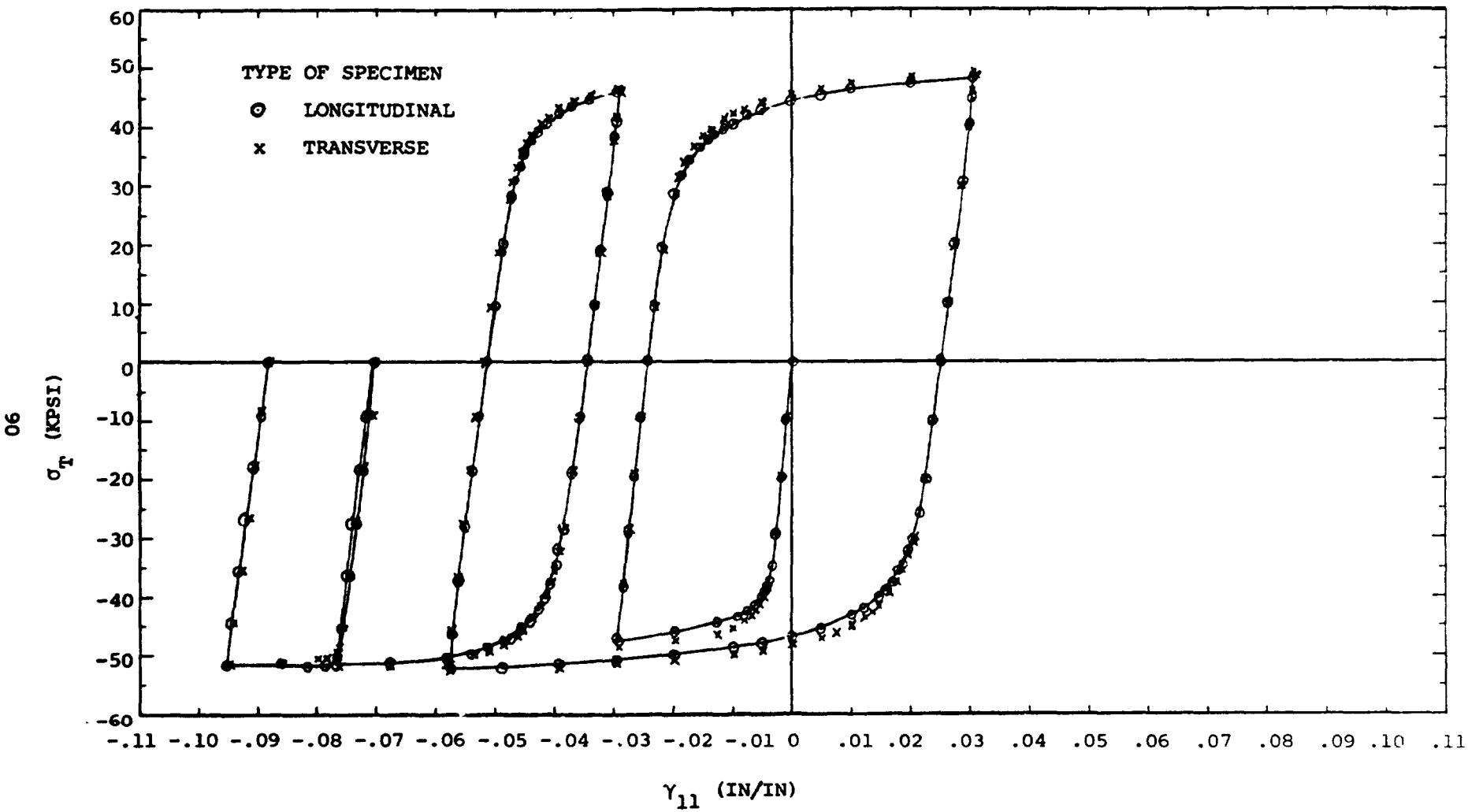

FIG. A.5 UNIAXIAL STATIC STRESS-STRAIN DATA FOR 6061-T651 PLATE MATERIAL, LOADED FIRST IN COMPRESSION AND THEN "CYCLED": σ_T VS. γ_{11}

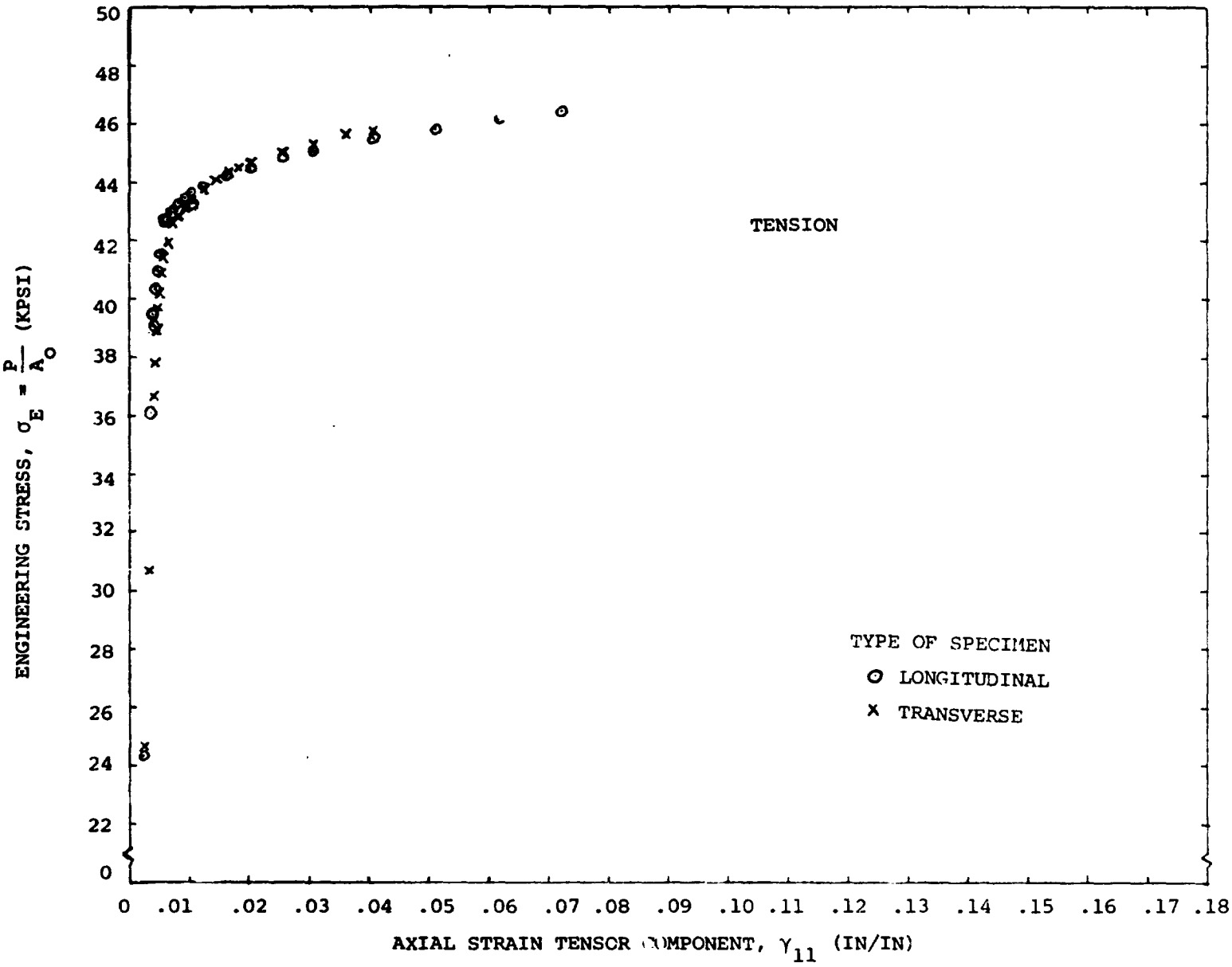

FIG. A.6 TENSILE UNIAXIAL STATIC STRESS-STRAIN DATA FOR 6061-T651 PLATE STOCK: σ_E VS. γ_{11}

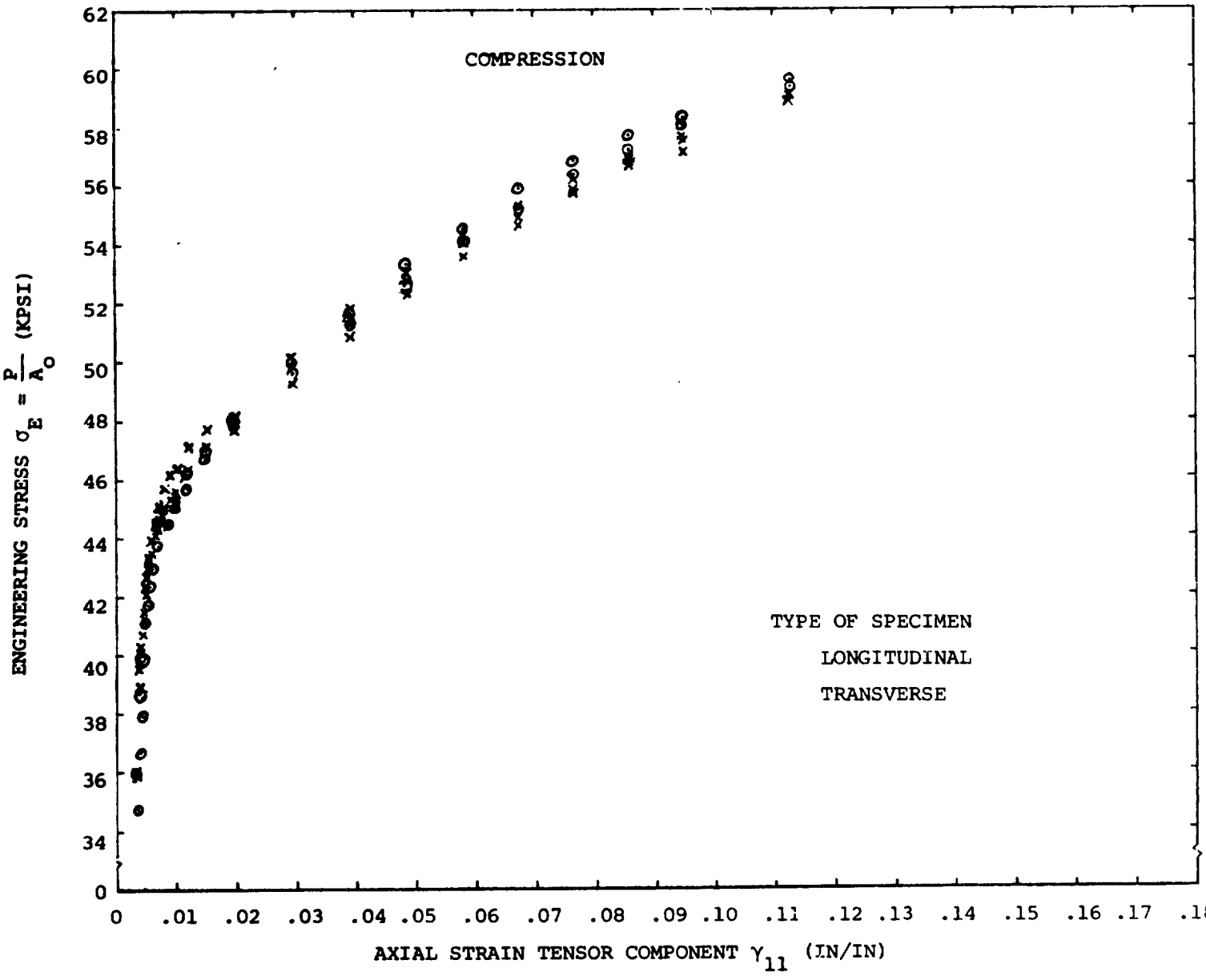

FIG. A.7 COMPRESSION UNIAXIAL STRESS-STRAIN DATA FOR 6061-T651 PLATE MATERIAL: σ_E VS. γ_{11}

APPENDIX B

STRAIN-GAGE INSTALLATION AND WIRING TECHNIQUES

During the study reported in Ref. 9, attempts were made to measure much larger transient strains than, to the author's knowledge, had been obtained successfully and reported heretofore for impulsively-loaded structures. Hence, a succession of strain-gage installation techniques, strain-gage cements, types of lead wires and lead wire attachments, etc., were investigated. Reported concisely in the following, therefore, are the most successful of the techniques tried. Although the basic recommendations of the strain-gage manufacturers were followed, some modifications in procedure, arrangement, and technique were employed.

For purposes of discussion, let it be assumed that one of the following two high elongation strain gages[+] (used in the present study) is to be installed on an aluminum test specimen such as the beams discussed in Sections 2 and 3:

Gage	Active Element Size		Overall Size		Size of Polyimide Backing	
	Length (in)	Width (in)	Length with Tabs (in)	Width (in)	Length (in)	Width (in)
EP-08-031DE-120	.031	.032	.140	.032	.27	.12
EP-08-125AD-120	.125	.125	.250	.125	.40	.22

The polyimide backing is of nominal one-mil thickness (.001 inch).

The following terse "installation steps" involve the following four groups of operations:

(1) Surface preparation,

(2) Gage installation and curing,

(3) Lead wires and attachments, and

(4) An "enhanced survival" measure.

The step-by-step procedure follows:

SURFACE PREPARATION

Step 1. Degrease specimen surface with a solvent such as chlorothene or

[+] Manufactured by Micro-Measurements Co., Romulus, Michigan.

toluene. Apply a liberal amount on and surrounding the surface on which the gage is to be mounted; wipe off with a clean gauze pad.

Step 2. Roughen specimen surface gage area with 320 grit siliconcarbide paper. Apply a few drops of Conditioner A*, and wet-lap with the carbide paper. Remove residue by gently wiping with a gauze pad. If the Conditioner has dried up before all residue has been wiped off, repeat the process with more Conditioner.

Step 3. Apply alignment marks to the surface to assist in properly locating and properly orienting the gage during attachment (see Fig. B.1). If very fine alignment marks are needed, these may be produced by using a metal scribe; very light (barely visible) lines should be made -- avoid making "deep gouge marks". If scribe marks cannot be tolerated, alignment marks could be applied by using a sharp 4H drafting pencil.

After application of the alignment marks on the specimen surface where the gage is to be positioned, clean this surface again with Conditioner A -- repeating until a clean gauze pad does not become discolored when wiping through the "gage area".

Step 4. Apply a liberal amount of Neutralizer 5* (N5) to the "gage area" of the specimen. Keeping the surface wet, scrub with a cotton-tipped applicator. Do not let the neutralizer evaporate on the surface. Wipe through the gage area with a sterile gauze pad, slowly enough to absorb all of the neutralizer; wipe in one direction only so that contaminants will not be redeposited on the cleaned area.

GAGE INSTALLATION AND CURING

Step 5. Remove the strain gage from its container; if gage becomes contaminated, clean it with a cotton applicator moistened with N5. Place this gage on a pre-cleaned (with N5) glass plate, with the side to be bonded facing down.

With a sharp razor blade, cut out a 3/8 in. by 3/8 in. square of 0.001-inch thick polyimide sheet to be installed as an electrical

*Supplied by Micro-Measurements Co., Romulus, Michigan.

insulator on the specimen surface next to the strain-gage tabs as indicated in Fig. B.2. Roughen the surface of this polyimide insulator patch with 400 grit silicon-carbide paper and clean with N5. Place this polyimide insulator patch on the glass plate butted against the end of the strain gage as indicated in Fig. B.2. The purpose of this insulator patch is to prevent the lead wires from shorting to the surface of the test specimen. The use of this patch is optional; however, if not used, one must take extreme care in removing the insulation at the gage end of the lead wires and also apply an extra amount of adhesive on the specimen surface (for insulation) near the end of the gage where the lead wires are attached. Do not overlap this insulator patch over the polyimide backing upon which the strain gage has been mounted by the manufacturer. Center a 4-inch long by 3/4-inch wide strip of cellophane tape such as Permacel 404 (supplied by the M-M Co.) on the polyimide-backed gage and the polyimide insulator patch (see Fig. B.3); then slowly lift the tape from the glass plate with the now-attached strain gage and insulator patch (G/P) assembly.

Step 6. Position the G/P assembly onto the (aluminum) test specimen surface where the alignment marks have already been provided (See Fig. B.1). If the gage turns out to be misaligned on the first attempt, the tape with the attached G/P assembly may be lifted and repositioned. The tape can be moved without fear of contaminating the clean surface by the adhesive on the Permacel 404 tape (if this particular recommended type of tape is used). After the G/P assembly has been aligned satisfactorily, lift one end of the tape until the G/P assembly is off the surface. Tuck the "loose end" of the tape under and press to the surface as depicted in Fig. B.4.

Step 7. Prepare a batch of AE-15 cement according to Micro-Measurements Instruction Bulletin B-137, Oct. 1970. Apply a thin layer of this cement to the bottom of the G/P assembly and on the surface of the test specimen where the G/P assembly is to be cemented. Lift the tucked-over end of the tape and "bridge" over the cement-covered

alignment-mark region on the surface at approximately a 45° angle. With a piece of gauze, slowly make a single wiping stroke over the tape, bringing the G/P assembly down properly over the alignment marks and cement already on the surface.

Step 8. Curing of the cemented G/P assembly on the surface with proper pressure and heat comes next. Place a 3/32-inch thick silicone gum pad provided by the M-M Co. over the G/P assembly and tape it down onto the surface with cellophane tape. Place a hardwood back-up block over the pad; pressure will be applied to the G/P assembly by placing appropriate weight on or clamping onto the hardwood block (see Fig. B.5). Apply weights or Hargrave clamps (supplied by the M-M Co.) until a "clamping pressure" of 8 to 10 psi is obtained. Place the entire assemblage into an oven and cure the cement for 2 hours at 175°F. The oven temperature should be increased slowly after the specimen is placed inside; after the 2-hour curing period, the oven should be cooled down slowly before the model is removed. After removing the model from the oven, remove the back-up block, the silicone-gum pad, and the cellophane tape.

LEAD WIRES AND ATTACHMENTS

Since strains are to be measured on structural test specimens which undergo violent transient response, the lead wires and attachment scheme must be "nearly massless". Hence, very fine varnish-covered copper lead wires (AWG36 or 40) are used. To minimize the forces on the lead wire and on the wire/gage junction, these lead wires are installed in a "soft coil" configuration adjacent to the test specimen for those gages to be used for transient strain measurements. Only permanent strains are to be measured from other gages; for those gages, only small solder beads need to be applied to the strain gage tabs. The following description pertains to those gages which are to be used for measuring transient strains.

Step 9. Select a suitable length(s) of varnish-covered AWG copper wire. Coil this length by wrapping it around a small-diameter mandrel such as an ordinary wooden pencil or wooden dowel stock. Along about a 1/16-in.

length at each end, remove the varnish insulating layer with Strip-X (General Cement No. 26-2). Coat these stripped ends with solder and attach by soldering to the strain-gage tabs as described in the following. For ease of soldering, the leads may be held down temporarily with a small strip of drafting tape (see Fig. B.6). Apply a small drop of AR flux (supplied by M-M Co.) on the lead wire ends and on the gage tabs; simultaneously apply a temperature-controlled soldering iron and Kester Co. No 44 solder to the tab/lead junction, forming a solder bead not exceeding 1/32 inch in either diameter or height. Carefully remove the drafting tape, clearn off the soldering flux residue with M-M Co. supplied rosin solvent, and reclean the entire gage/connection/insulator patch area with N5.

ENHANCED-SURVIVAL COVERING

Experience demonstrated that strain gages installed and wired as just described would survive intact and provide plausible transient and permanent strain data under moderately severe impulsive loading conditions. However, under more severe conditions, the gages became detached from the surface. It was found that gage survival could be increased significantly by cementing a covering patch of polyimide sheet over the entire gage and a portion of the lead wires as shown in Fig. B.7 and described in the following.

Step 10. From a 0.001-inch thick sheet of polyimide, cut a "cover patch" of the size indicated in Fig. A.7. Roughen and clean this patch as in Step 5. Apply a thin coat of AE-15 cement to (a) the gage area, (b) the polyimide insulator patch, and (c) both sides of the polyimide cover patch. Position as shown in Fig. B.7 and cover the entire region with a strip of 0.003 x 1 x 1 inch Teflon film. Secure the Teflon in place with cellophane tape. Repeat Step 8 to complete the cementing/curing process. The Teflon cover does not adhere, and is hence then removed. The result is a multilayer cover of cement/polyimide/cement, with an exterior layer of cured AE-15 cement.

The test specimen is now ready for installation in the impulse-loading test area. Let the test specimen, for example, be a circular ring freely

hanging from a light webbing support strap as indicated in Fig. B.8. Impulse loading is to be applied by detonating a uniform-thickness, full-ring-width, sheet of Detasheet-D explosive (HE) which is centered at the bottom of the ring and spans a selected circumferential sector of the ring's outer surface. The ring is separated from the sheet HE by a suitable layer of buffer material. Since this impulsive loading will induce a severe radially inward initial velocity, the lead wires to each strain gage need to be arranged in such a fashion that they will experience a minimum stress for a maximum length of time. Accordingly, the lead wires coming from the gages are suspended in the "soft coil" arrangement and orientation indicated in Fig. B.8. This coiled wire is then attached to terminal blocks which are taped to the model support strap at some distance from the test specimen. Heavier lead wires then run from said terminal block to the strain recording equipment.

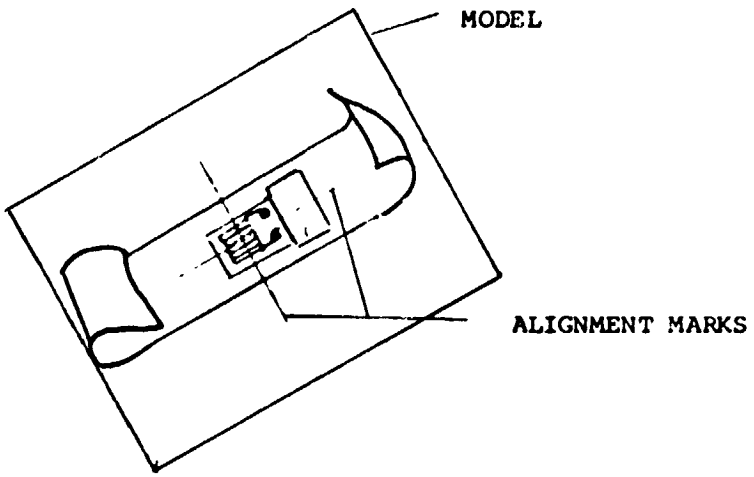

FIG. B.1 ALIGNMENT MARKS AND GAGE-POLYIMIDE ASSEMBLY ON SPECIMEN SURFACE

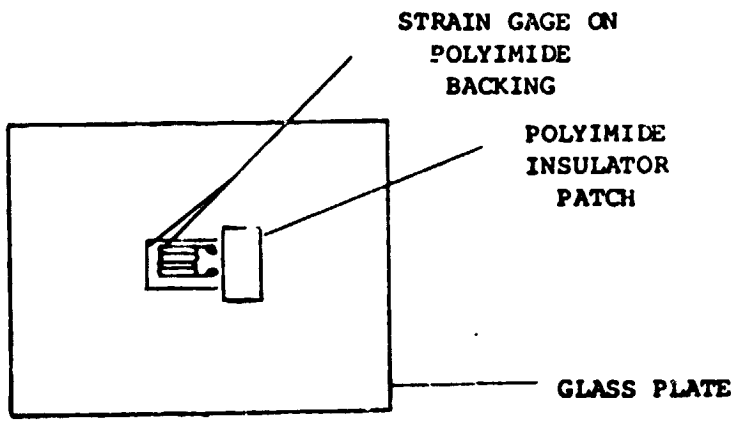

FIG. B.2 STRAIN GAGE-POLYIMIDE BASE LAYER ALIGNED ON GLASS PLATE

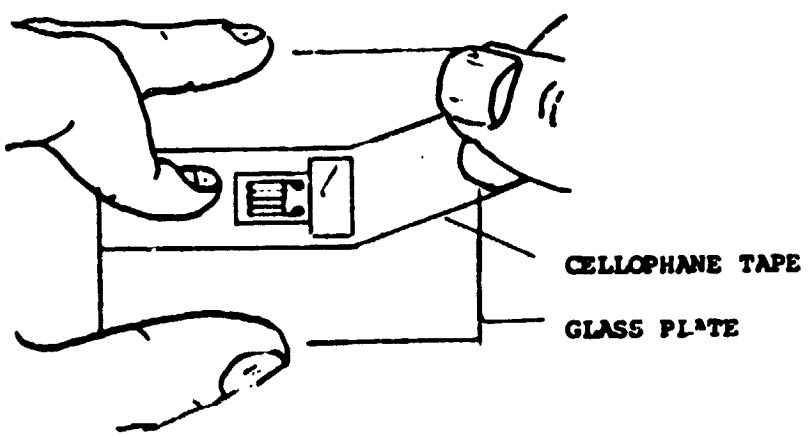

FIG. B.3 GAGE-POLYIMIDE ASSEMBLY ON CELLOPHANE TAPE

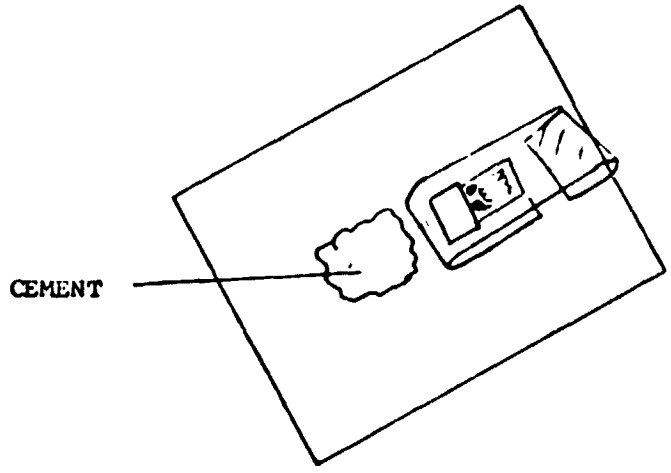

FIG. B.4 ASSEMBLY IN POSITION FOR CEMENT APPLICATION

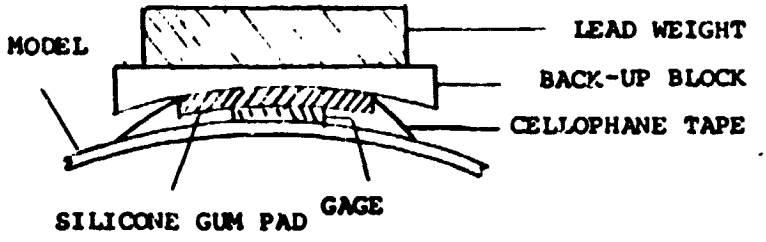

FIG. B.5 CLAMPING ARRANGEMENT

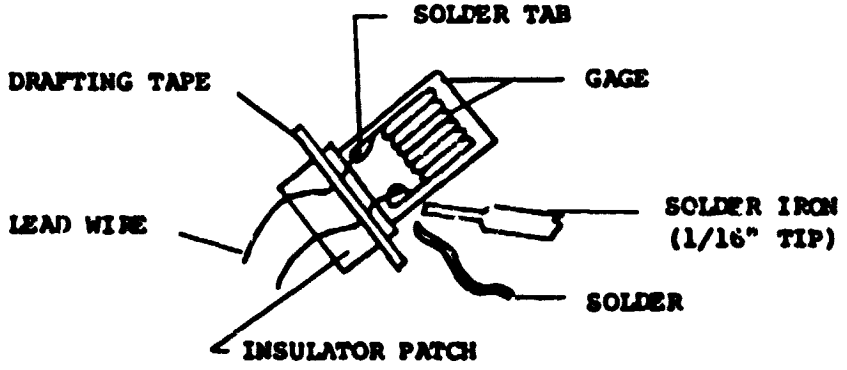

FIG. B.6 ATTACHMENT OF LEAD WIRES TO SOLDER TABS OF GAGE

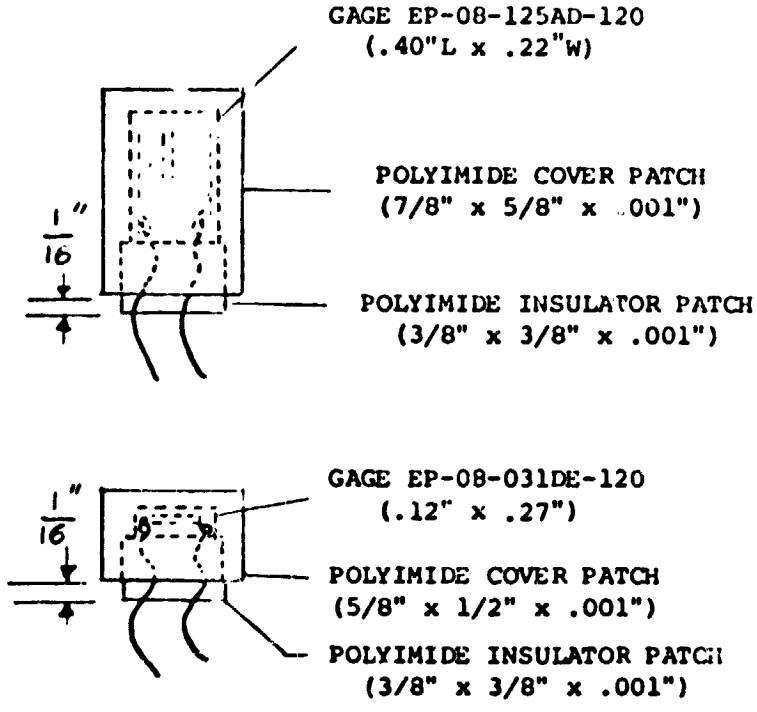

FIG. B.7 POLYIMIDE COVER PATCH DIMENSIONS AND LOCATION

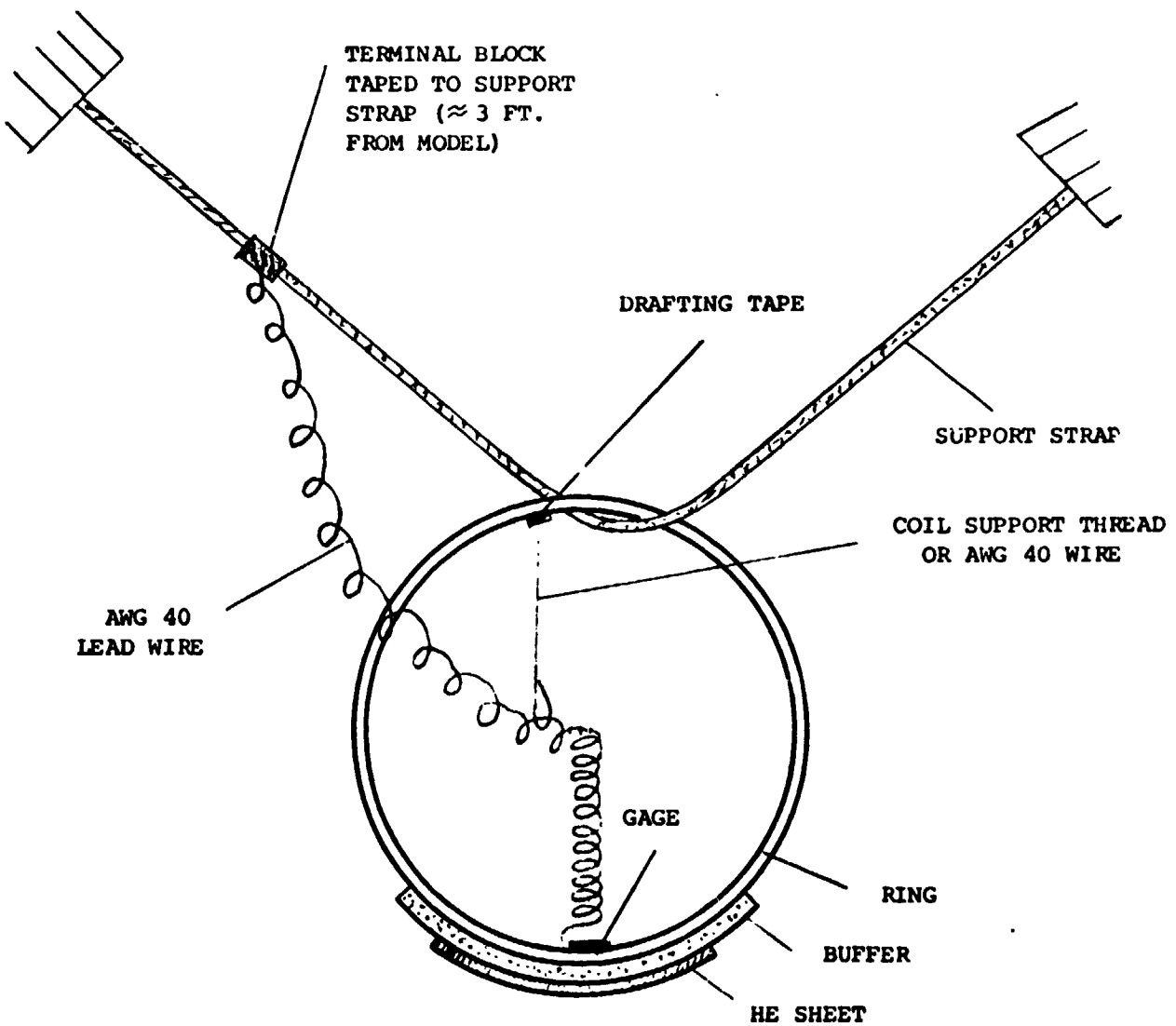

FIG. B.8 SCHEMATIC OF STRAIN-GAGE LEADS AND SPECIMEN READY FOR TESTING